Neutral Polymeric Micelles for RNA Delivery

Brittany Bradshaw Lundy

A dissertation submitted in partial fulfillment of the requirements for the degree of

Doctor of Philosophy

University of Washington

2013

Reading Committee:

Patrick Stayton, Chair

Suzie Pun

Oliver Press

Program Authorized to Offer Degree:

Bioengineering

University of Washington

Abstract

Neutral Polymeric Micelles for RNA Delivery

Brittany Bradshaw Lundy

Chair of the Supervisory Committee:

Patrick Stayton

Department of Bioengineering

Small interfering RNA (siRNA) is a therapeutic gene silencing strategy that has generated substantial interest in the scientific community, but it remains a challenge to produce a robust and nontoxic systemic delivery system capable of efficient *in vivo* intracellular siRNA delivery. Due to the complexity of this problem, an efficient delivery system requires multiple functional components including a cell targeting moiety, siRNA binding region, and an endosomal escape component, all of which must be independently functional when combined. Based upon these requirements, we developed a rationally designed siRNA carrier possessing the above properties that form the basis for successful siRNA-polymer conjugates systemic delivery *in vivo*. We engineered a biocompatible, neutral, pH-responsive multifunctional micellar system using reversible addition fragmentation chain transfer (RAFT) polymerization. By incorporating biotin and pyridyl disulfide functionalities into the polymer, we were able to directly link streptavidin antibody conjugates and conjugate thiolated siRNA for multi-functional delivery platform. In this work, we explored several advanced cell targeting moieties including antibody and carbohydrate strategies, and furthermore we demonstrated that this modular siRNA delivery

platform has the capability to overcome various delivery limitations on both cellular and systemic levels. Finally, we demonstrated proof-of-principle therapeutic efficacy by sensitizing ovarian cancer cells to carboplatin after Bcl-xL gene silencing with the trastuzumab-targeted siRNA conjugates. The polymer-siRNA conjugates developed in this work may prove to a useful approach for future clinical delivery of siRNA therapeutics in a variety of disease states.

Table of Contents

List of Figures

List of Schemes

List of Tables

List of Supporting Figures

Glossary

ANS: 1-Anilino-8-Naphthalene Sulfonate
Bcl-2: B-cell lymphoma-2
Bcl-xL: B-cell lymphoma-extra large
BHV1: non-targeting isotype-matched IgG1 human anti-bovine herpes virus-1 antibody
BMA: butyl methacrylate
CTA: chain transfer agent
DMAEMA: dimethylaminoethyl methacrylate
DTT: dithiothreitol
GAPDH: glyceraldehyde 3-phosphate dehydrogenase
HPMA: N-(2-hydroxypropyl) methacrylamide
LDH: lactate dehydrogenase
MAA: methyl methacrylate
NT: No treatment
PAA: propyl acrylic acid
PDS: pyridyl disulfide
PDSMA: pyridyl disulfide methacrylamide
RAFT: Reversible Addition-Fragmentation chain Transfer
RNAi: RNA interference
SA: streptavidin
SCR: scrambled
SDS: sodium dodecyl sulfate
siRNA: short interfering RNA
TCEP: tris(2-carboxyethyl)phosphine
Trast: Trastuzumab

Acknowledgements

I would like to express my deepest appreciation for my mentor Pat Stayton. Without his guidance and expertise, my journey through graduate school would have been far less productive both scientifically and personally. His willingness to give me independence to develop my own solutions to difficult problems has made me a far better independent researcher and scientist. I would also like to thank my thesis committee members Suzie Pun, Oliver Press, Kim Woodrow, Christine Luscombe. They have challenged me, encouraged me, and developed my ability to think critically, and because of their guidance and critical thinking, my thesis is far stronger. I would especially like to acknowledge Tony Convertine, who has proven to be an invaluable mentor, especially in the area of polymer chemistry. His support has been instrumental in the development of this project. I would like to thank Corinna Palanca-Wessels for her mentorship and assistance in the development of the Trastuzumab targeted siRNA conjugates. I also sincerely appreciated the assistance provided by her technician Garrett Booth. I would like to thank my collaborator Yu-Hua Chow in the Lynn Schnapp Laboratory for all her hard work and patience with the animals in our acute lung injury studies. Furthermore, I would not be able to complete this work with out the help and support of my labmates Geoffrey Berguig, Emily Crownover, Jessica Garbern, Bilal Ghosn, Matthew Manganiello, Salka Keller, and John Wilson. I have enjoyed our lively scientific discussions and working with each and everyone one of you for the past six years. And finally to my friends and family, I would like to thank you all. You have made Seattle my home and I will be forever grateful to you all.

Dedication

The following work is dedicated to my family, whose love and support have allowed me to become the person I am today. To my husband Scott, who encouraged me to pursue my dreams and never give up, and to my parents, whose unconditional love and faith allowed me explore different facets of life. Finally, to my son Jacob, who brings me happiness and joy every day.

Chapter 1. siRNA-Polymer Conjugates for the Treatment of Disease

Small interfering RNA (siRNA) has been hailed as a revolutionary approach for disrupting gene expression and treating a diverse array of diseases. Despite its unequivocal potential to treat disease, siRNA has one major limitation that must first be addressed; it must be delivered intact to the cytoplasm of target cells. This delivery challenge has spurred research efforts in a variety of fields, including polymer science, to produce a nontoxic carrier vehicle capable of crossing the cell membrane and delivering functional siRNA. Recent advances in controlled polymerization techniques, cell-specific targeting strategies, and clinically relevant disease models have enabled researchers to begin rationally designing siRNA carriers for therapeutic use. Here we describe the development of next-generation polymeric materials for cell-specific targeting for *in vivo* siRNA delivery.

1.1 Introduction

Modern medicine's knowledge of disease pathology continues to grow exponentially, and the identification of new cellular and molecular pathways and targets that play a role in disease progression has raised our knowledge of biology immensely. Despite these advances, often a significant delay occurs between our understanding of a disease and our ability to treat it. Until relatively recently, for example, most drugs were limited to small hydrophobic compounds capable of crossing the cell membrane or to compounds with an extracellular site of action[1]. This has drastically limited the number of "druggable" targets to a fraction (less than 20 %) of

identified human genes, with the remainder of drug targets considered "undruggable" with current technology[2]. Recent advances in drug design, however, have opened up a world of new opportunities, including novel intracellular drug targets, antibodies, proteins, peptides, DNA, and RNA interference molecules. The immense potential of these new targets and strategies is now limited only by the comparatively outdated approaches currently used clinically to deliver biological drugs to these targets[2].

1.2 siRNA

First reported by Fire *et al*. in 1998, RNA interference (RNAi) is the process of sequence-specific mRNA transcript degradation prior to translation[3]. This degradation is triggered by the presence of double-stranded silencing RNA (siRNA) in the cytosol, which activates intracellular degradation machinery and effectively silences gene expression. While the first reports of RNAi were conducted in C. elegans, more recent work has extended this work to mammals and suggests that this pathway is highly conserved[4]. The Nobel prize-winning discovery of RNAi clearly has promising therapeutic potential, especially for conditions where silencing of a single upregulated pathological gene may ameliorate the disease phenotype[5]. siRNA is typically 21-23 nucleotides in length and has approximately 40 negatively-charged phosphates, rendering the molecule rather large, anionic, and difficult to deliver across cell membranes effectively. The development of a robust siRNA delivery platform capable of targeting specific cell populations in the body following systemic administration is the main challenge for therapeutic use of siRNA in a clinical setting[6].

1.2.1 RNAi Mechanism

RNAi is a naturally occurring phenomenon that can be exploited for therapeutic purposes (**Figure 1.1**). The pathway is activated when double-stranded RNA (dsRNA) of approximately 100 or more nucleotides in length is detected in the cytosol of the cell. Upon recognition, the dsRNA is degraded into siRNA fragments by the ribonuclease (RNAse) III-type enzyme Dicer[7]. These fragments enter the RNA-induced silencing complex (RISC), which becomes activated after unwinding and selecting the guide (antisense) strand. Determination of the guide stand is performed by a multifunctional protein, Argonaute 2, within the RISC and is based on the less thermodynamically stable 5' end of the duplex[6]. The guide stand then selectively targets complementary mRNA for degradation through the RNAse activity of the Argonaute 2 protein[8]. Following transcript destruction, the guide strand is then free to interact with another transcript.

1.2.2 siRNA Delivery

Delivery of dsRNA greater than 30 nucleotides in the length activates the innate immune response by antagonizing the antiviral interferon (IFN) response[9]. *In vivo* therapeutic strategies for RNAi thus must rely on the delivery of synthetically generated shorter (21-23nt) siRNA to bypass this unsolicited immune response yet still activate this potent and highly specific gene silencing machinery. Naked siRNA is polyanionic in nature and has a large molecular weight, which prevents it from readily crossing the cell membrane[10]. To overcome these obstacles, several nonviral delivery strategies including cationic lipoplexes, liposomes, and cationic polymers have been developed for delivery siRNA *in vivo*. Unmodified siRNAs are highly susceptible to degradation by endo- and exonucleases; however, chemical modifications to the backbone, base, or sugar of the RNA can be employed to enhance potency and stability[11]. In

addition, siRNA sequences must be investigated to ensure assessable hybridization with target mRNA and to avoid unintended (off-target) effects often caused by partial sequence homology or stimulation of the innate immune response with GU-rich sequences antagonizing the toll-like receptor 3[6,12]. It is important to note that in order to achieve 90% suppression of target gene product, the siRNA must remain active inside the cell for more than 3 half-lives of the protein. This is an important consideration when designing a gene targeting strategy, and some targets may require multiple dosing to achieve this effect[6].

1.2.3 Delivery Challenges and Approaches

The hurdles with siRNA delivery are diverse and exist on multiple scales, including extracellular and intracellular transport, circulation, and biodistribution after systemic *in vivo* delivery (**Figure 1.2**). Depending on the route of administration, endothelium penetration (extravasation) may be the initial extracellular transport challenge[13]. Following escape from the circulatory system, the siRNA delivery system must then diffuse though the extracellular matrix network and bind specifically to target cells. Once identified, target cells must internalize the siRNA complex via endocytosis. Once internalized, however, endocytic vesicles rapidly become highly acidic and fuse with the lysosome to allow for thorough degradation of the vesicular contents. To prevent degradation and facilitate gene silencing, siRNA must escape this endosomal environment. Finally, the siRNA must dissociate for the carrier in order to activate the cellular machinery enabling RNAi[14]. As discussed previously, off-target RNAi and enzymatic degradation are two more challenges inherent to siRNA sequences. Rapid clearance of siRNA after administration or non-specific accumulation in tissues leading to systemic toxicity are also potential challenges to consider when designing a siRNA delivery system for *in vivo* delivery[15].

Several approaches have been utilized to overcome these challenges using non-viral delivery systems. Computer algorithms and empirical testing have lead to the identification of active siRNA sequences with chemically-modified structures to increase stability in blood[16]. Cationic carriers shield siRNA from endonuclease activity, and biocompatible or PEGylated carriers reduce toxicity as well as rapid clearance by the renal system[17]. Direct conjugation of siRNA molecules to small molecules, peptides, cholesterol, fatty acids, and bile salts have been evaluated and shown *in vivo* efficacy by increasing circulation and cell uptake[18,19]. Increased cell uptake has also been exploited via targeting moieties to facilitate receptor-mediate endocytosis[20]. Optimization of delivery route or use of leaky vasculature (tumor targeting) can relieve unwanted systemic effects and extravasation into tissues[21]. Fusogenic and endosome-destabilizing peptides/polymers have been used to facilitate endosomal escape and stimuli-cleavable polymers have also been shown to release siRNA in the cytosplasm[22,23,24,25].

In particular, our laboratory has great interest in the polymer poly(propylacrylic acid) (PPAA) to facilitate endosomal escape by undergoing a process similar to that of viruses, which have evolved efficient ways to evade degradation by the lyosomal pathway[26]. Viruses display fuscogenic proteins on their viral coat that undergo a conformational change under the acidic conditions found in the endosomal compartments[27]. These newly hydrophobic regions allow the viral coat to perturb the endosomal membranes and allow for cytosolic release. Carboxylic acid residues along PPAA are partially ionized under physiological pH (pH 7.4), creating a hydrophilic and aqueous soluble polymer. However, as the pH decreases to endosomal pH levels (less than 6.6) the carboxylic acids residues become protonated, causing a pH-responsive

conformational change resulting in a hydrophobic, membrane destabilizing switch[28,29,30]. Because of these advantageous characteristics, we have chosen to incorporate propylacrylic acid as part of the membrane-destabilizing component of the siRNA delivery system.

1.3 Polymers for siRNA Delivery

Polymers for siRNA delivery can be classified into two categories based on siRNA binding mechanism; those that are positively charged (cationic) and those that are neutral. Linear or branched cationic polymers rely on electrostatic interactions to condense negatively charged siRNA and form polyplexes. Endosomal escape is achieved by the high charge density in the cationic polymer, which acts a sponge and buffers endosomal pH. This buffering enhances the influx of protons and water and results in the rupture of the endosome, which delivers the siRNA cargo via "proton-sponge" effect[16]. One of the most highly studied cationic polymers for the delivery of siRNA is polyethyleneimine (PEI). PEI, like many other cationic polymers, tends to be cytotoxic, and polycations in general are associated with systemic toxicity and thus are of limited clinical significance[31,32].

Without a highly charged makeup to drive siRNA complexation, neutral polymers must employ functional groups to covalently attach siRNA. The most common attachment species is a disulfide linkage, which is reducible by the cytoplasmic protein glutathione[19]. The literature is sparse on the topic of neutral polymers directly conjugated to siRNA; however, a few recent studies have directly conjugated poly(ethylene glycol) (PEG) to siRNA[33,34,35]. This particular system required the addition of complexation to a polycation after siRNA-PEG conjugation to see any efficacy *in vivo*. Acid-responsive polymers synthesized of amphipathic poly(vinyl ether)

composed of butyl and amino vinyl ether and contained PEG along with a hepatocyte targeting ligand were directly conjugated to siRNA making a 'Dynamic PolyConjugate'[36]. This system demonstrated successful multifunction *in vivo* delivery by suppressing both apolipoprotein B and peroxisome proliferator-activated receptor alpha in a murine model. York, *et al*. demonstrated the feasibility of multiconjugation of folate and cleavable siRNA to a well-defined N-(2-hydroxypropyl) methacrylamide-s-N-(3-aminopropyl)methacrylamide (HPMA-s-APMA) copolymer synthesized via reversible addition-fragmentation chain transfer (RAFT) polymerization; however, no *in vitro* or *in vivo* characterization of this siRNA delivery system was performed[37].

1.3.1 Reversible Addition Fragmentation Chain Transfer (RAFT)

To rationally design polymers for biological applications, we must employ a polymerization technique capable of tight synthetic control to insure homogeneity and reproducibility. In 1998, the CSIRO group reported the invention of a control "living" radical polymerization technique called Reversible Addition Fragmentation Chain Transfer (RAFT), which is an extremely versatile polymerization process with respect to the type of monomer and reaction conditions[38]. This technique is characterized by the formation of polymers with controlled molecular weight, low polydispersity, and complex polymeric microstructure[39]. The primary difference between RAFT and traditional free radical polymer is a reagent called the chain transfer agent (CTA), which forms intermediate radicals with two propagating polymer chains to facilitate uniform propagation of the polymer chains. The overall RAFT mechanism can be described in two parts. The first phase is the "pre-equilibrium" set of reactions and involves the initial RAFT agent and the initiation of the living process. The second phase, or "main equilibrium" set of reactions,

occurs between growing and dormant polymer chains[40]. This process is advantageous because it reduces the amount of free radicals in solution and thereby limits termination and uncontrolled polymerization. In addition, the CTA provides a "living" functionality on isolated polymer chains, which can subsequently act as a macroCTA for future block polymerizations. Modifications of the CTA prior to polymerization can provide multiple functionalities on either terminus[41]. Polymers prepared with RAFT exhibit precise molecular weights and narrow polydispersities, with a variety of architectures and chemical modality of either terminus. Taken together, these advantageous characteristics make RAFT uniquely suited to future potential use as pharmaceutical carriers.

1.3.2 Block Copolymers for siRNA Delivery

The RAFT polymerization technique enables the control synthesis of polymers with discrete regions (blocks) with separate functionalities. Amphiphilic block copolymers are polymers with one hydrophilic block and one hydrophobic block which self-assemble to form core-shell micelles under aqueous environments[42]. The micelle structure is driven by the entropic sequestration of hydrophobic regions and stabilized by the solubility of the hydrophilic regions. Amphiphilic micelles have been previously successful in the delivery of hydrophobic chemotherapy drugs by providing a hydrophobic core for encapsulation purposes[43,44]. Cationic micelles are a subset of amphiphilic block copolymers that use electrostatic interactions to drive the complexation of negatively charged molecules and can incorporate pH-responsive activity in the core[45]. Potent mRNA knockdown, illustrated in **Figure 1.3**, has been shown with siRNA delivery carriers composed of a positively charged block of dimethylaminoethyl methacrylate

(DMAEMA) to mediate siRNA binding and a second pH-responsive endosome releasing block composed of DMAEMA, PAA, and butyl methacylate (BMA)[46].

1.4 Cell Targeting Agents

Cell targeting can greatly improve efficacy and specificity of therapeutic delivery in clinical applications[47]. This targeting takes advantage of the intrinsic cell surface receptors or biochemical characteristics unique to the tissue of interest. Various ligands including folate, transferrin, antibodies, oligosaccharides, peptides, and polysaccharides have been utilized to facilitate advances in siRNA delivery[48,49,50,51,52,53].

1.4.1 Human Epidermal Growth Factor Receptor 2 (HER2)

HER2 is a tyrosine kinase receptor of the epidermal growth factor receptor family[54]. Though thought to be an orphan receptor, HER2 does form heterodimers with other HER2 members, and heterodimerization results in the activation of signaling pathways involving mitogen-activated protein kinase (MAPK) and phosphatidylinositol 3-kinase (PI3K) pathways[55]. When activated, HER2 stimulates a signal cascade that drives cellular proliferation, migration, differentiation, angiogenesis, and cell survival. Several cancers including breast, ovarian, gastric, and prostate cancers overexpress wild-type HER2, which leads to enhanced and prolonged signals triggering transformation, which is directly associated with poor clinical outcomes[56].

There are several reasons HER2 has been historically chosen as a useful target for cancer therapies. Most importantly, HER2 upregulation leads to tumorigenesis and expression levels are much higher in malignant cells than in healthy cells[57]. Furthermore, HER2 overexpression is

found in both primary malignant cells as well as metastases[58]. Finally, inhibition of HER2 heterodimerization with other HER family members impedes signal propagation through P13K and MAPK pathways[55].

The extracellular domain of HER2 in particular has provided an ideal target for cancer therapies. Artificial ligands, such as affibodies and peptides, have been generated and linked directly to cytotoxic agents or attached to nanoparticles encapsulation therapeutic drugs[55]. A humanized monoclonal antibody directed against HER2, trastuzumab, has been used a both as drug and a cell-targeting agent of drug conjugates for cells overexpressing HER2. Trastuzumab is FDA approved to treat HER2+ breast cancer as both a standalone therapy and as an adjuvant therapy. Its ability to provide targeting for nanoparticles and immunoliposomes has been employed in numerous studies to delivery small molecule drugs or nucleic acid. In the current work, we have investigated Trastuzumab as an ovarian cell targeting agent to facilitate cell uptake of our neutral micellar siRNA delivery system and provide synergism with existing approved drug therapies.

1.4.2 Mannose Receptor

Sugar modalities are also often used to enhance cell-specific uptake and targeting. Macrophages have mannose-specific membrane receptors, which can mediate phagocytosis of saccharide-coated carriers and pinocytosis of soluble glycoconjugates[59,60,61]. A mannosylated liposome appears to be a promising approach for the delivery of chemotherapeutics[62] as well as the antituberculosis drug rifabutin in targeting alveolar macrophages[63]. We have investigated mannosylated diblock copolymers to target alveolar macrophages in a murine lung injury model to enhance the neutral siRNA conjugates delivery.

1.5 CONCLUSIONS

The therapeutic promise of siRNA to treat a dizzying array of illnesses has challenged the drug delivery field to invest in strategies to overcome the inherent obstacles associated with its functional delivery. For siRNA to become a viable clinical therapy, a robust non-toxic delivery system must be developed. The work discussed in the following chapters addresses the rational design of a novel RAFT synthesized copolymer for the delivery of siRNA in respect to the challenges associated with systemic delivery of siRNA to cell-specific targets.

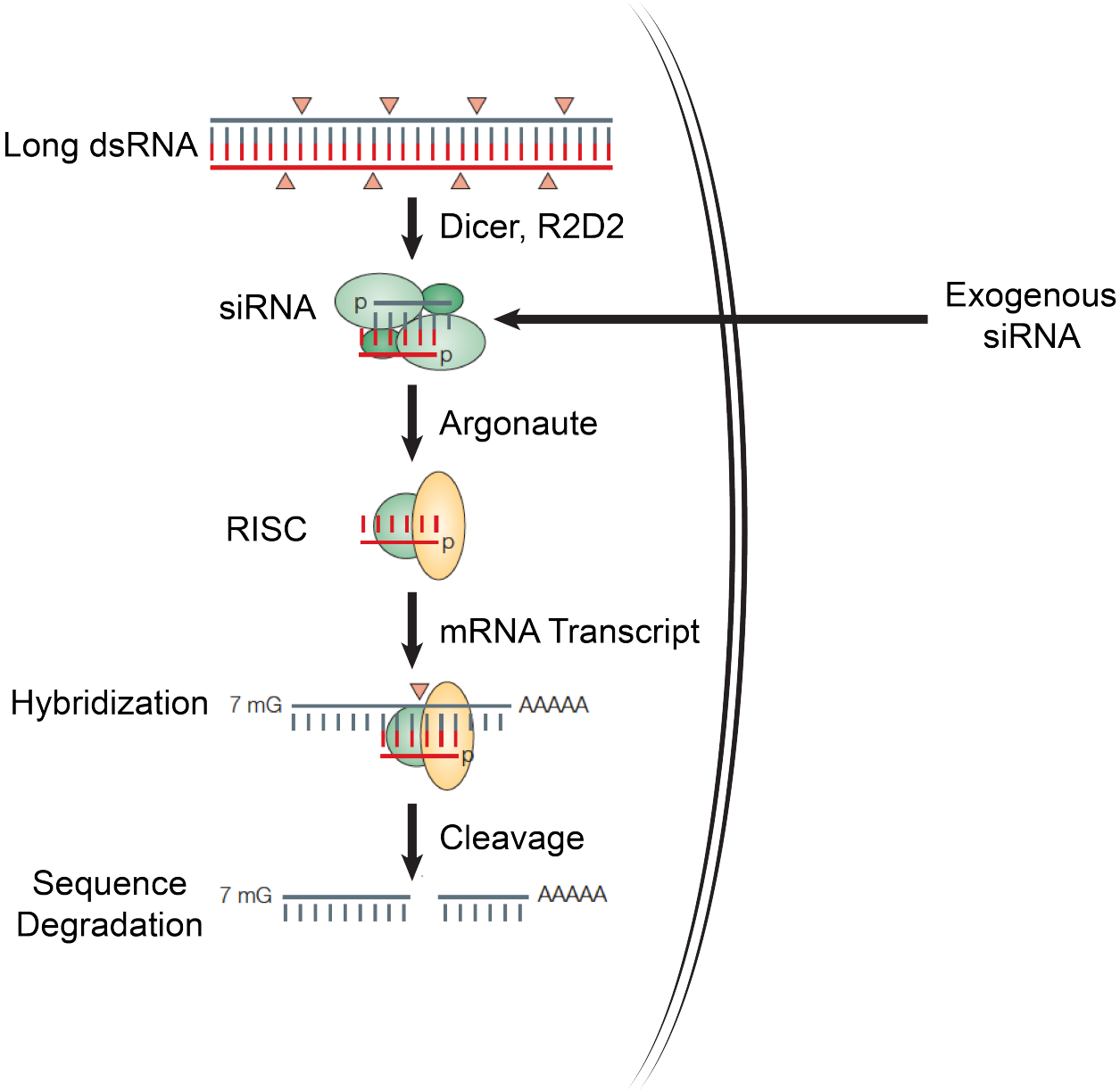

Figure 1.1 RNAi mechanism

RNA interference (RNAi) is activated when double-stranded RNA (dsRNA) is detected in the cytosol of the cell. Ribonuclease (RNAse) III-type enzyme Dicer degrades dsRNA into short fragments called siRNA. These fragments enter the RNA-induced silencing complex (RISC), which becomes activated after unwinding and selecting the guide (antisense) strand. Determination of the guide stand is performed by a multifunctional protein, Argonaute 2, within the RISC and is based on the less thermodynamically stable 5' end of the duplex. Complementary mRNA binds to the guide strand and is then cleaved and degraded. The guide strand is then free to interact with another transcript.

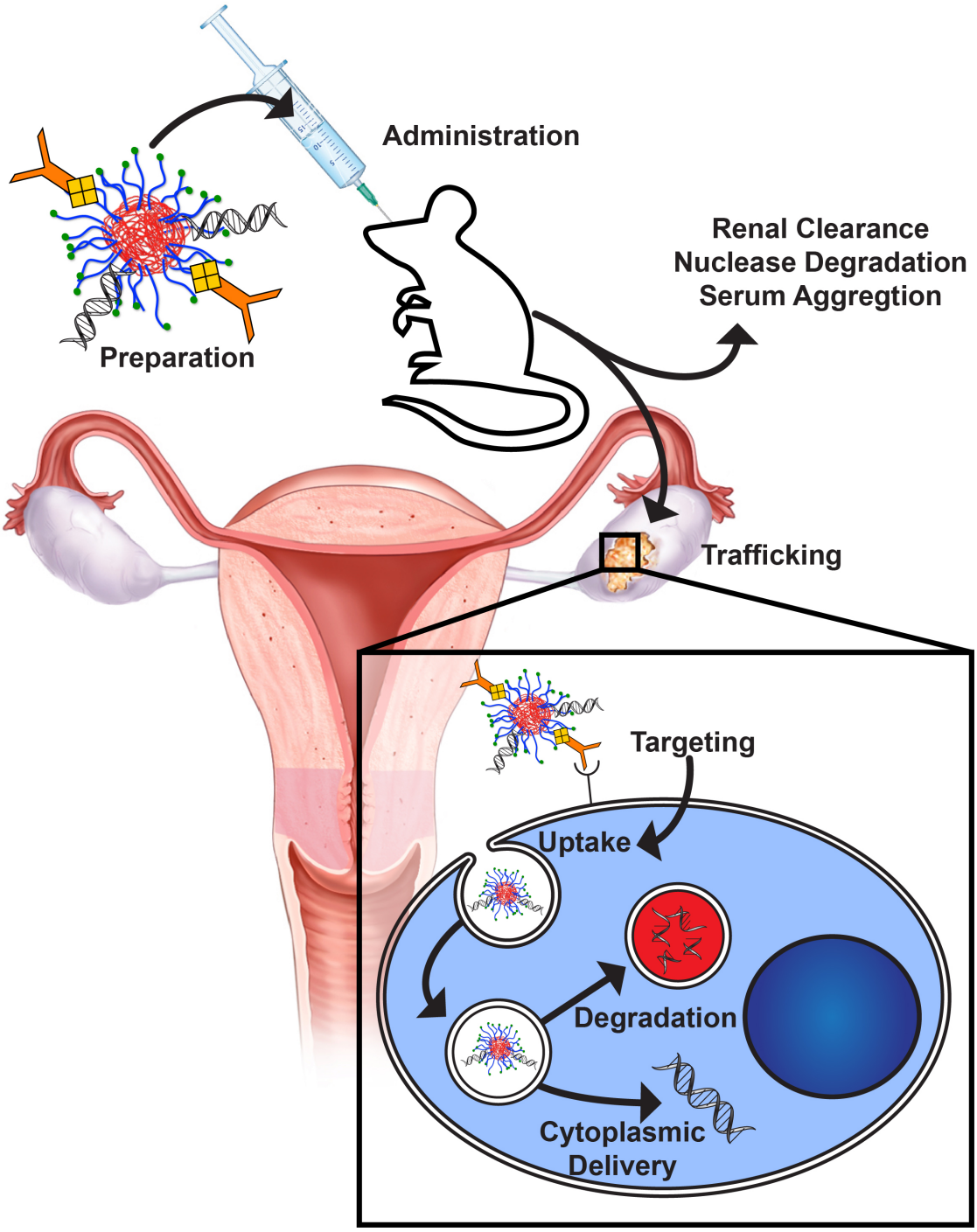

Figure 1.2 Challenges associated systemic delivery of siRNA.

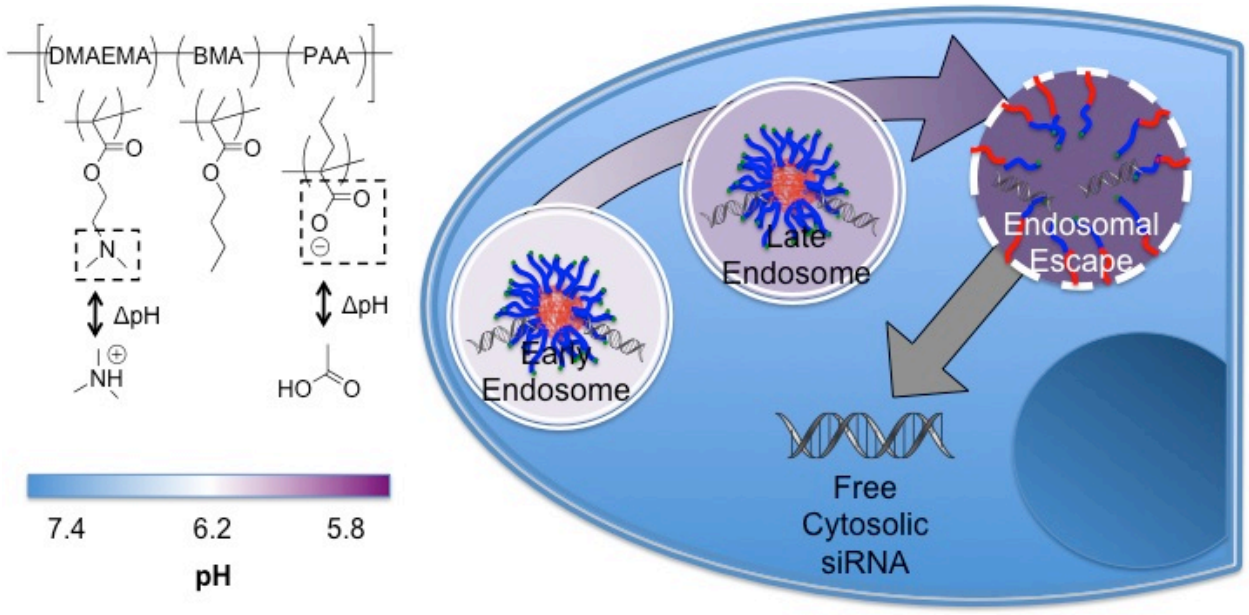

Figure 1.3 Polymer based endosomal escape strategy.

Synthetic polymer poly(PAA-co-DMAEMA-co-BMA) is designed to mimick viral mechanisms for intracellular biologic transport and exploits endosomal acidification for pH-responsive membrane destabilization.

Chapter 2. NEUTRAL POLYMERIC MICELLES FOR RNA DELIVERY

RNA interference (RNAi) drugs have significant therapeutic potential but delivery systems with appropriate efficacy and toxicity profiles are still needed. Here, we describe a neutral, ampholytic polymeric delivery system based on conjugatable diblock polymer micelles. The diblock copolymer contains a hydrophilic poly[*N*-(2-hydroxypropyl) methacrylamide-co-*N*-(2-(pyridin-2-yldisulfanyl)ethyl)methacrylamide) (poly[HPMA-co-PDSMA]) segment to promote aqueous stability and facilitate thiol-disulfide exchange reactions, and a second ampholytic block composed of propyl acrylic acid (PAA), dimethylaminoethyl methacrylate (DMAEMA), and butyl methacrylate (BMA). The poly[(HPMA-co-PDSMA)-b-(PAA-co-DMAEMA-co-BMA)] was synthesized using Reversible Addition-Fragmentation chain Transfer (RAFT) polymerization with an overall molecular weight of 22,000 g/mol and a PDI of 1.88. Dynamic light scattering and fluorescence measurements indicated that the diblock copolymers self-assemble under aqueous conditions to form polymeric micelles with a hydrodynamic radius and critical micelle concentration of 25 nm and 25 μg/mL respectively. Red blood cell hemolysis experiments show that the neutral hydrophilic micelles have potent membrane destabilizing activity at endosomal pH values. Thiolated siRNA targeting glyceraldehyde 3-phosphate dehydrogenase (GAPDH) was directly conjugated to the polymeric micelles via thiol exchange reactions with the pyridal disulfide groups present in the micelle corona. Maximum silencing activity in HeLa cells was observed at a 1:10 molar ratio of siRNA to polymer following a 48 h incubation period. Under these conditions 90 % mRNA knockdown and 65 % and protein knockdown of at 48 h was achieved with negligible toxicity. In contrast the polymeric micelles lacking a pH-responsive endosomalytic segment demonstrated negligible mRNA and protein

knockdown under these conditions. The potent mRNA knockdown and excellent biocompatibility of the neutral siRNA conjugates demonstrate the potential utility if this carrier design for delivering therapeutic siRNA drugs.

2.1 INTRODUCTION

Short interfering RNA (siRNA) technology has the potential to revolutionize the treatment of serious diseases by allowing selective silencing of oncogenic or therapeutic mRNAs and their corresponding proteins. Despite this immense therapeutic potential of this technology the effective systemic and intracellular delivery of siRNA remains a significant challenge. The delivery of siRNA typically yields low levels of mRNA silencing due to barriers that include degradation by endo- and exo-nucleases, poor cellular uptake, and intracellular trafficking[10].

To overcome these obstacles, delivery systems including liposomes, cationic lipoplexes, and cationic polymers, have been developed to enhance the effectiveness of siRNA[10,64,65]. Due to their small size (~100 nm), biocompatibility, and activity, liposomes have been used to successfully knock down the expression of proteins associated with a variety of disease targets[66-71]. Both cationic and neutral lipoplexes have exhibited good efficacy[72-77], with different toxicity and protein adsorption/targeting properties that affect the choice of target tissue and medical application[78,79]. Cationic polymers, such as chitosan[80-83] and other natural polymers[81,84], polyethylenimine (PEI)[85], dendrimers[86,87], and other synthetic polymers[88,89] have also shown promise although the toxicity of polycation carriers remains problematic.

Conjugation strategies have also been developed with a variety of non-viral delivery carrier systems. Lipophilic siRNA conjugates to cholesterol[90], bile acids[19,91], lipids[92], and α-tocopherol (vitamin E)[93] have been shown to moderately increase target cell uptake. Cell-penetrating peptides such as TAT trans-activator protein[94,95], Penetratin[95,96], and Transportan[96] have also been conjugated to the antisense strand of siRNA to increase cellular uptake and enhance gene

silencing. PEG-siRNA conjugates exhibit high levels of serum stability and have been shown to increase gene silencing efficiency[97]. Additionally, PEG-siRNA conjugates complexed with a cationic polymers or peptides to form polyelectroplyte complex micelles, further enhancing circulation time, uptake, and efficacy[35,36,98,99]. Recently, Heredia, *et al*. employed reversible addition-fragmentation chain transfer (RAFT) to prepare poly(ethylene glycol acrylate) with telechelic pyridyl disulfide functionality[34]. Covalent siRNA conjugates have also been prepared by Xu, *et al*. who conjugated siRNA to a pyridyl disulfide end-capped poly(HPMA)-dendritic carbohydrate scaffold[100].

Previously, we described the synthesis of a new family of diblock copolymer siRNA carriers[23,45,46,101]. These carriers are composed of a positively charged block of dimethylaminoethyl methacrylate (DMAEMA) to mediate siRNA binding and a second pH-responsive endosomal-releasing block composed of DMAEMA, propylacrylic acid (PAA), and butyl methacylate (BMA) monomers. This carrier system displays excellent delivery activity but the cationic segment could have adverse toxicity profiles. Here, we describe the development of a neutral, ampholytic diblock copolymer that replaces the cationic DMAEMA segment with a hydrophilic block of N-(2-hydroxypropyl) methacrylamide (HPMA) and a disulfide-conjugatable monomer *N*-(2-(pyridin-2-yldisulfanyl)ethyl)methacrylamide. This system provides a starting foundation for future targeted siRNA delivery schemes using pH-responsive polymeric micelle conjugates for therapeutic use.

2.2 METHODS

2.2.1 Materials

All reagents were purchased from Sigma-Aldrich and Wako Chemicals and used without further purification unless specified otherwise. The trithiocarbonate CTAs ethyl cyanovaleric trithiocarbonate (ECT) and PEG3 Biotin ECT were synthesized as previously described[101,102]. Pyridyl disulfide methacrylamide (PDSMA) was synthesized as described previously[103]. N,N-dimethylacrylamide was distilled under reduced pressure. Propylacrylic acid (PAA) was synthesized as previously reported. Radical initiator (V70) was purchased from Wako chemicals. 2,2-azobisisobutyronitrile (AIBN) was recrystallized from methanol.

2.2.2 Synthesis of poly(N-(2-hydroxypropyl)methacrylamide (HPMA)-co-PDSMA) macro chain transfer agent (macroCTA)

Poly(HPMA-co-PDSMA) was synthesized using a mixed aqueous-organic solvent system. Polymerizations were conducted with an initial molar HPMA to PDSMA ratio of 9:1. HPMA (1.134 g, 7.9 mmol) was dissolved in ultra pure water (5.87 g). Biotinylated-4-Cyano-4-(ethylsulfanylthiocarbonyl) sulfanylvpentanoic acid (Biotin-ECT) (93.8 mg, 0.106 mmol) was dissolved in ethanol (1 g). The initiator solution was prepared by dissolving V501 (1.23 mg/g ethanol solution, 4.38 μmol) in ethanol. PDSMA (0.225 g, 0.89 mmol) was dissolved in ethanol (1 g). The ethanol solutions were combined and added to the aqueous HPMA solution in a 25 mL round bottom flask. The final solvent concentration was a ratio of 2:1 (water to ethanol). The solution was purged with nitrogen for 30 min on ice and then allowed to react at 70 °C for 4 h. Ultra pure water (35 g) was added to the reaction solution and frozen under liquid nitrogen. Water was removed from the reaction via lyphilization after 48 h. The resultant polymer was isolated by repeated precipitation from ethanol into an excess of ether. The polymer was rinsed

after final precipitation with pentane to remove excess ether and dried overnight in vacuum oven. The macroCTA was characterized by SEC to be 9,300 g/mol with a PDI of 1.07 from the measured dn/dc of 0.091. ^{1}H NMR was used to determine the composition of 94 % HPMA and 6 % PDSMA, by evaluating the peak at 3.9 ppm and aromatic peaks at resonances between 7-8.5 ppm for HPMA and PDSMA, respectively.

2.2.3 Synthesis of poly[(HPMA-co-PDSMA)-b-(BMA-co-DMAEMA-co-PAA)]

Poly[(HPMA-co-PDSMA)-b-(BMA-co-DMAEMA-co-PAA)] was prepared by adding the poly(HPMA-co-PDSMA) macroCTA (0.239 g, 28.5 μmol) to a solution of BMA (0.486 g, 3.42 mmol), DMAEMA (0.403 g, 2.56 mmol) and PAA (0.292 g, 2.56 mmol) (40:30:30 mol %) in dimethyl acidimid (DMAc) (2.4 g) such that the final solvent concentration was 66 % by weight. The initial macroCTA to V70 initiator (3.5 mg, 11.4 μmol) ratio ([macroCTA]o/[I]o) and initial monomer to macroCTA ([M]o/[macroCTA]o) was 2.5:1 and 300:1 respectively. The polymerization solution was purged with nitrogen for 30 min before being allowed to react at 30 °C for 24 h. The final polymers were isolated by precipitation from ethanol into a 50x excess of pentane:ether (3:1 v/v). The polymer precipitant was rinsed with neat pentane and dried under vacuum overnight. The polymers were dissolved in deionized water and further purified by passing them through PD10 desalting columns. The final dry polymers were obtained via lyophilization. The diblock copolymer was characterized by SEC to be 22,000 g/mol with a PDI of 1.88 from the measured dn/dc of 0.081. ^{1}H NMR was used to determine the composition of the second block to be 27 % PAA, 24 % DMAEMA, and 49 % BMA, by evaluating the peaks between 3.9-4.2 ppm (representing HPMA, BMA, and DMAEMA), peak at 2.4 ppm (resonance peak of DAEMA) and the backbone peaks. The proportion of PAA was back-calculated from

integrating the entire backbone peak and subtracting the protons associated with the other protons from HPMA, PDSMA, DMAEMA, and BMA.

2.2.4 Synthesis of poly[(HPMA-co-PDSMA)-b-(methyl methacrylate) (MAA)] non-pH responsive Control Polymer

The control polymer was prepared by adding the poly(HPMA-co-PDSMA) macroCTA (0.066 g, 7.92 μmol) to a solution of MAA (0.278 g, 2.77 mmol) in dimethylformamide (DMF) (0.416 g) such that the final solvent concentration was 55 % by weight. The initial macroCTA to AIBN initiator (0.125 mg) ratio ([macroCTA]o/[I]o) and initial monomer to macroCTA ([M]o/[macroCTA]o) was 10:1 and 350:1 respectively. The polymerization solution was purged with nitrogen for 30 min before being allowed to react at 30 °C for 6 h. The final polymers were isolated by precipitation from DMF into a 50x excess of ether. The polymer precipitant was rinsed with neat ether and dried under vacuum overnight. The polymers were dissolved in deionized water and further purified by passing them through PD10 desalting columns. The final dry polymers were obtained via lyophilization. The diblock copolymer was characterized by SEC to be 17,300 g/mol with a PDI of 1.04 from the measure dn/dc of 0.0963.

2.2.5 Polymer Characterization

Absolute molecular weights and polydispersities (PDI) were determined via SEC laser light scattering (LLS) using a Optimlab T-rEX (Wyatt) equipped with miniDAWN TREOS (Wyatt) for light scattering, refractive index, and UV. HPLC-grade DMF containing 0.1 wt. % LiBr at 60 °C was used as the mobile phase at a flow rate of 1 mL/min. Copolymer composition was determined via ^{1}H NMR spectra were recorded on a Bruker AV301 in deuterated methanol

(CD_3OD) at 25 ºC. A deuterium lock (CD_3OD) was used and chemical shifts were determined in ppm at 3.35 and 4.78 (CD_3OD). Polymer concentration was 7.5 mg/mL. Copolymer morphology was determined via ^1H NMR spectra and was recorded on a Bruker AV500 in CD_3OD and deuterated oxide (D_2O) at 25 ºC. Polymer concentration was 12.5 mg/mL.

2.2.6 Critical Micelle Concentration (CMC) via ANS fluorescence

The CMC for the diblock copolymer was determined using a fluorescent probe, 1-Anilino-8-Naphthalene Sulfonate (ANS). The ANS was dissolved in ethanol to form a 100 uM stock solution. Polymer concentration was varied from 1 to 100 μg/mL with a set ANS concentration of 5 μM. The various polymer solution (95 μL) was incubated with ANS stock solution (5 μL) for 1 h in a black 96-well Nunc plate. The fluorescence spectra (ex 390/ em 550 nm) were recorded using a Tecan Safire 2 microplate reader. The CMC was estimated to be the concentration corresponding to the half-width intensity at 550 nm between low and high plateau regions.

2.2.7 Transmission Electron Microscopy (TEM)

A 1.0 mg/mL solution of poly[(HPMA-co-PDSMA)-b-(BMA-co-DMAEMA-co-PAA)] in PBS was applied to a carbon-coated copper grid for 30 min and fixed in Karnovsky's solution, washed in cacodylate buffer and water. The grid was stained with a 6% solution of uranyl acetate for 15 min and then dried until analysis. Transmission electron microscopy was carried out on a Tecnai G2 F20, 200 kV scanning transmission electron microscope (S/TEM).

2.2.8 Dynamic Light Scattering

Particle sizes of polymer alone or polymer-siRNA conjugates were measured by dynamic light scattering (DLS) using a Malvern Zetasizer Nano ZS. Lyophilized polymer was dissolved in 100 % ethanol at 10-50 mg/mL, then diluted 10-fold into phosphate buffer, pH 7.4. Polymers were analyzed in phosphate buffered saline, pH 7.4 (PBS) at 0.1 mg/mL for polymer alone and polymer-siRNA conjugates. Polymers and polymer-siRNA conjugates were filtered with a 200 nm filter prior to measurement.

2.2.9 siRNA Conjugation via thiol-exchange

The number of thiol reactive pyridyl disulfide groups on the diblock copolymer was determined by following the release of pyridine-2-thione at 343 nm following a 60 min incubation period in pH 7.4 phosphate buffered saline (PBS) (137 mM NaCl, 2.7 mM KCl, 8 mM Na_2HPO_4, and 2 mM KH_2PO_4). The thiolated siRNA was reduced (GAPDH and SCR sequences) by combining 20 μL thiolated siRNA stock solution (500 μM) with 45 μL RNAse-DNAse free water and 50 μL of DTT (0.1 M) with 3 μL of triethylamine (TEA) (All values are per number of reactions)[100]. Reactions incubated for 30 min, and the thiolated siRNA was isolated by precipitation into water saturated with ethyl acetate. The lyophilized diblock polymer was predissolved in 100 % ethanol then diluted 10-fold into phosphate buffer (RNAse-DNAse free), pH 7.4 at a final concentration of 2.5 mg/mL. Varying molar ratios of reactive PDS groups on polymer determined via TCEP reduction (1, 2, 5, 10, 20) were immediately added to siRNA solution (10 nmol siRNA). Sterile phosphate buffer (RNAse-DNAse free), pH 7.4, was added to the final reaction have siRNA concentration of 11 μM and reacted at 37 °C for 12 h. The degree of siRNA conjugation to the

block copolymer was determined by measuring the release of pyridine-2-thione at 343 nm using an extinction coefficient of 8.08×10^3 M^{-1} cm^{-1}.

2.2.10 Gel Shift Assay

To determine the polymer to thiol ratio at which complete siRNA conjugation occurs, gel retardation assays were conducted at varying molar ratios of polymeric PDS groups to thiolated siRNA. Ratios of 1:1, 2:1, 5:1, 10:1, and 20:1 (polymer reactive PDS groups to siRNA) were evaluated. A 2 % agarose gel was loaded with each lane containing 1 μg of free siRNA or siRNA conjugated with varying quantities of diblock copolymer. 2 μL of a 0.1 M DTT solution were reacted with the conjugates for 1 h prior to loading on gel to evaluate the reversibility of the siRNA conjugation. 5 μL of 2.5 % SDS solution were combined to siRNA-conjugates to determine if electrostatic interactions were driving complexation rather than conjugation. Non-thiolated siRNA and the same polymer to siRNA ratios were also evaluated as controls. The gels were run at 100 volts for 1 h and then stained with SYBR Safe dye diluted 1:5000 for 30 min for UV visualization.

2.2.11 Red blood cell hemolysis assay

pH responsive membrane destabilizing activity was assayed by titrating polymer alone or polymer-siRNA conjugates into preparations of human red blood cells (RBCs) and determining membrane-lytic activity by hemoglobin release (determined by measuring absorbance at 540 nm) under 5 different pH conditions. RBCs were isolated by centrifugation from whole blood collected in vaccutainers containing EDTA. RBCs were washed 3 times in normal saline and brought to a final concentration of 2 % RBCs in PBS at a specific pH (5.8, 6.2, 6.6, 7.0, or 7.4).

Polymer alone or polymer-siRNA conjugates were evaluated at 20 and 40 μg in triplicate at each pH. RBCs with polymer alone or polymer-siRNA conjugates were incubated at 37 °C for 60 min and centrifuged to remove intact RBCs. Supernatants were transferred to a transparent 96-well plate and absorbance determined at 540 nm. Percent hemolysis is expressed as A540 sample/A540 of 1 % Triton X-100 treated RBCs (control for 100 % lysis).

2.2.12 Cytotoxicity Measurements

Free diblock copolymer toxicity was evaluated in HeLa cells using the CellTiter 96AQueous One Solution Cell Proliferation Assay (MTS) (Promega Corp., Madison, WI). HeLa cells were seeded in 96-well plates at a density of 3,000 cells/cm^2 and allowed to adhere overnight. The media was then replaced with 200 μL of fresh media containing the diblock copolymer at the appropriate concentrations. Polymer cytotoxicity was evaluated in triplicate after 12 h using the CellTiter MTS assay according to the manufactures instructions. The absorbance at 490 nm was evaluated using Tecan Safire 2 microplate reader, and untreated cells in media were used as a negative control.

The cytotoxicity of diblock copolymer and siRNA-polymer conjugates for normalization in the GAPDH protein assay was determined by assaying for cell metabolic activity. HeLa cells were seeded in 96-well plates at a density of 3,000 cells/cm^2 and allowed to adhere overnight. Conjugates were formed with GAPDH siRNA at concentrations up to 100 nM siRNA/well (200 μL volume). Samples were added to wells in triplicate. After cells had been incubated for 24 h or 48 h with the polymer or polymer-siRNA conjugates, the cells were lysed with KDalert Lysis buffer and incubated at 4 ºC for 20 min. 40 μL of cell lysate from each sample was then

transferred to a fresh transparent 96-well plate and diluted with 60 μL of PBS buffer (pH 7.4). 100 μL of Lactate Dehydrogenase (LDH) reagent mix was then added to each well (Roche). The coupled enzymatic reaction occurred within 5 min at 25 °C, and fluorescence (490/650 nm) was determined according to the manufacturer's instructions. Percent viability is expressed as function of 1 % Triton X-100 treated cells (control for 0 % viability).

2.2.13 Measurement of siRNA knockdown activity using quantitative PCR

Knockdown activity of siRNA-poly[(HPMA-co-PDSMA)-b-(BMA-co-DMAEMA-co-PAA)] complexes was assayed in 96-well format by measuring specific gene expression after 24 h and 48 h of treatment with polymer-siRNA conjugates. Polymer and GAPDH targeting siRNA or negative control siRNA were mixed as described above and allowed to conjugate overnight before the addition to HeLa cells in 200 μL normal media containing 10 % FBS. Final siRNA concentration was evaluated at 50 nM. Total RNA was isolated 24 and 48 h post treatment and GAPDH expression was measured relative to the internal normalizer gene, B-actin, by quantitative PCR.

2.2.14 Measurement of siRNA knockdown activity by measuring GAPDH protein

HeLa cells were seeded in 96-well plates at a density of 3,000 cells/cm^2 and allowed to adhere overnight. Conjugates were formed with GAPDH siRNA or negative control siRNA to attain concentrations up to 50 nM siRNA (200 μL volume). Ratios of 1:1, 2:1, 5:1, 10:1, and 20:1 (polymer PDS groups to siRNA) were evaluated. Samples were added to wells in triplicate. After cells had been incubated for 24 h or 48 h with the polymer or polymer-siRNA conjugates, the cells were lysed and incubated at 4 ºC for 20 min. The KDalert GAPDH assay kit (Ambion)

was used to determine GAPDH protein levels. 10 μL of cell lysate from each sample was then transferred to a fresh black 96-well plate and 90 μL of KDalert master mix was then added to each well. Fluorescence levels for each well were then read immediately after addition of the master mix (λExc. = 560 nm and λEmm. = 590 nm). Identical measurements were then repeated after 4 min. GAPDH activity was determined by the difference of the two readings. Values were then normalized to total Lactate Dehydrogenase (LDH) protein content via lysate analysis with LDH cytotoxicity kit (Roche) as previously described.

2.2.15 Polymer siRNA Conjugate Internalization by Fluorescence Microscopy

Internalization of diblock siRNA conjugates was visualized by fluorescence live-cell microscopy. Helas were seeded in 96-well plates at a density of 15,000 cells/cm^2 and allowed to adhere overnight in Lab-Tek II Chambered Coverglass Slides (NUNC, Rochester, NY). Polymer and polymer-siRNA conjugates were bound to Alexa-488-label streptavidin (4:1 M polymer to streptavidin) through the biotin RAFT agent after 1 h incubation. Cells were treated with a 30 min incubation of polymer, polymer siRNA conjugate, or streptavidin alone to look at internalization of the carrier at 1 h. 25 nM steptavidin dose was administered in all sample groups. Chamber slides were placed on a Live-Cell Fluorescence Microscope (Nikon Ti-E) equipped with an environmental control chamber at 37 °C. Cells were imaged with a mercury lamp and a 100X objective using the following filter sets for AF488 and DAPI. Z-sections of the cells (step size 0.4 μm) were acquired and after image acquisition image stacks were deconvolved using object-based measurement software, Volocity (Perkin Elmer), to focus fluorescence. To deconvolve image stacks, point spread functions were calculated for the green and blue channel and applied using 25 iterations to reach a near 100 % confidence interval.

2.3 RESULTS

2.3.1 Polymer Synthesis and Characterization

RAFT polymerization methodology was employed in order to prepare the macro chain transfer agent (macroCTA) composed predominately of the hydrophilic HPMA with 10 mol % (feed) of a thiol-reactive PDSMA comonomer as shown in **Scheme 2.1**. Aqueous conditions were selected for the copolymerization of the methacrylamido-based comonomers as they have been shown to provide excellent control over the molecular weight and polydispersity at lower initiator concentrations leading to materials high chain end retention of the thiocarbonylthio groups[104,105]. In order to facilitate solubilization of the poorly water soluble PDSMA comonomer, 33 % ethanol by volume was added to the aqueous polymerization solution. These conditions provided excellent control over the copolymerization as evidenced by the narrow and symmetric molecular weight distribution (**Supporting Figure S 2.1**) and yielded a copolymer with a molecular weight and polydispersity of 9,300 g/mol and 1.07 respectively. Incorporation of both comonomers in the copolymer as well as retention of PDS functionality was determined by ^{1}H NMR spectroscopy in CD_3OD. Comparison of the HPMA methyne resonance at 3.78 ppm to the PDSMA aromatic resonances at 8.45 ppm suggests that approximately 6 % PDSMA was incorporated into the polymer as compared to 10 % in the feed (**Table 2.1**).

The resultant copolymer was subsequently employed as a macroCTA for block copolymerization of PAA, DMAEMA, and BMA. The polymerization was conducted in DMAc at 30 °C for 24 h. Although broadening of the molecular weight distribution was observed for the diblock

copolymer, a clear shift to lower elution volumes is observed (**Supporting Figure S 2.1**). Evaluation of the copolymer composition via ^{1}H NMR spectroscopy indicates approximately 49 mol % BMA content in the second block with approximately equimolar quantities of of PAA and DMAEMA making up the remainder (**Figure 2.1**). Also evident from the ^{1}H NMR spectrum is the presence of aromatic resonances asociated with the PDS pyridine ring. Because the absolute concentration of PDSMA residues in the block copolymer are critically important for conjugation of thiolated siRNA, a TCEP reduction assay was also conducted to corroborate the values determined by ^{1}H NMR. In this assay the copolymer was dissolved in PBS buffer and incubated with 50 mM TCEP for 1 h in order to reduce disulfide bonds. It was determined that the number of PDS groups retained on the polymer was approximatey 1.9 as compared to 2 PDS groups per polymer by NMR. A non pH-reponsive control polymer containing a methyl methacrylate (MMA) based core (poly[(HPMA-co-PDSMA)-b-(MAA)]) was also synthesized via RAFT polymerization and had an overall molecular weight of 17,300 g/mol with a PDI of 1.04.

2.3.2 Diblock copolymer morphology

Spectroscopic confirmation of the anticipated micellar morphology with a poly(HPMA-co-PDSMA) segment making up the corona and the poly(PAA-co-DMAEMA-co-BMA) segment making up the core was provided by ^{1}H NMR. Analysis of copolymer in deuterated methanol, which acts as a solvent for both block copolymer segments, shows resonances associated comonomer residues present in both blocks. This is clearly shown in Figure 2 where resonances associated with HPMA residues (iii, iv) as well as DMAEMA (i v) and BMA (ii, vi, vii) are observed together. In contrast NMR analysis of the diblock copolymer in D_2O NMR shows a

strong attenuation of resonances associated with the poly(PAA-co-DMAEMA-co-BMA) segment. This is illustrated in **Figure 2.2** most notably by the disappearance ester resonances (DMAEMA and BMA; i, ii) at 4.2 ppm and 4.0 ppm respectively as well as an almost complete disappearance of the strong DMAEMA dimethyl resonance (v) at 2.4 ppm. These results, taken together, strongly suggest the association of the diblock copolymers under aqueous conditions to from core shell particles. The peaks corresponding to the proton adjacent from the hydroxyl on HPMA (3.8 ppm) (iii) and the protons adjacent from the amide of HPMA (3.0 ppm) (iv) retain their intensity.

Self-assembly of the diblock copolymers into a micelle-like morphology under aqueous conditions was further supported by conducting dynamic light scattering measurements as a function of solution pH. Polymer and polymer siRNA conjugates were prepared in 1x PBS solutions (0.1 mg/mL) at pH 7.4, 6.6, and 5.8. Under physiological conditions, a hydrodynamic diameter from 25 to 27 nm was observed for polymer and siRNA-polymer conjugates (ratio of 20:1 PDS to siRNA); this is indicative of the expected micelle morphology. Under more acidic environments representative of the endocytosis pathway, a reduction in the hydrodynamic diameter was observed to below 10 nm, which is consistent with unimers and micelle disruption. This transition occurs when DMAEMA residues in the core-forming block become increasingly protonated, building up an excess cationic charge as PAA is protonated and becomes neutral. No significant size difference was observed with the addition of a reducing agent, TCEP, in solution under these conditions.

The critical micelle concentration (CMC) for the diblock copolymer was determined by following the change in fluorescence intensity of 8-Anilino-1-naphthalenesulfonic acid (ANS) as a function of block copolymer concentration. ANS shows a significant increase in fluorescence intensity as well as a blue shift upon translocation from an aqueous solution to a nonpolar environment. By evaluating the fluorescence intensity of ANS at 550 nm (370 nm excitation) it was possible to follow the transition of the diblock copolymer from an associated micellar state to unimers. Low ANS fluorescence is observed below a diblock copolymer concentration of approximately 10 μg/mL, while above this concentration a sharp increase in fluorescence occurs indicating a transition from unimers to micelles (**Supporting Figure S 2.2A**). Measurements of the half-width intensity between low and high plateau regions indicate a CMC of ca. 25 μg/mL for the diblock copolymer derived micelles. Additional evidence that the diblock copolymer exists in particle morphology was evaluated by electron microscopy (**Supporting Figure S 2.2B**) From the electron micrograph the average diameter of the particles, which appear spherical, are sub-50 nm.

2.3.3 Polymer-siRNA conjugation and characterization by gel electrophoresis

To conjugate polymer and siRNA via reducible disulfide linkages, thiolated siRNA molecules were first reduced with DTT for 30 min and then reacted with the PDS-functional diblock copolymer overnight at 37 °C. Polymer-siRNA conjugation efficiency was determined via agarose gel electrophoresis and by analysis of pyridine-2-thione release. Thiol to PDS ratios of 1:1, 1:2, and 1:10 (thiol to polymer ~1:0.5, 1:1, and 1:5) were evaluated in order to determine the minimum ratio necessary to achieve complete siRNA conjugation. This value was determined to be 1:10 (thiol to polymer ~ 1:5) as evidenced by gel electrophoresis where a complete

disappearance of the free siRNA band is observed at this ratio (**Supporting Figure S 2.3**). As expected, siRNA conjugations conducted at a thiol to PDS ratio of 1:20 also showed complete siRNA conjugation (**Figure 2.3**). Following incubation with DTT, a disulfide reducing agent that cleaves the siRNA-polymer linkage, electrophoresis of the conjugates resulted in a reappearance of the free siRNA band. Following incubation with SDS, which disrupts micelle formulation, electrophoresis of the conjugates indicated no band corresponding to free siRNA, suggesting that the siRNA molecules remained conjugated to the unimer form of the polymer. Complete siRNA reduction from the polymeric system was observed under the presence of DTT and SDS, perhaps because the DTT was allowed access to the bond without steric hindrance from the micelle formation. Control experiments in which non-thiolated siRNA was incubated in the presence of the diblock copolymer did not result in any visible associations with the polymer. Comparison of thiolated GAPDH siRNA to the corresponding scrambled sequence showed negligible differences in the pyridine-2-thione release, particle sizes, and conjugation reversibility assays. In addition, siRNA conjugation was successful at this ratio to the non-pH-responsive control polymer (data not shown).

2.3.4 pH-responsive Membrane Destabilizing Activity

The pH-responsive membrane destabilizing activity of diblock copolymer was assayed using a red blood cell hemolysis assay. Five different pH conditions were used to mimic the transitions within the endosomal pH environments ranging from extracellular pH = 7.4 to late endosome pH = 5.8. Membrane destabilization is thought to occur through a combination of ionic localization of the polymer on the membrane surface and hydrophobic interaction of the nonpolar butyl methacrylate with the membrane lipids. To test whether conjugation of the diblock copolymer to

a hydrophilic nucleic acid interfered with the intrinsic membrane disruptive properties of the polymer, hemolysis experiments were conducted on both the polymer alone and the polymer-siRNA conjugates for both the GAPDH and SCR siRNA sequences with a final polymer concentration at 40 μg/mL (**Figure 2.4**). No significant hemolytic activity was observed at pH 7.4 for polymer and polymer-siRNA conjugates. Significant increases in red blood cell lysis were observed as pH was reduced to 6.2. Under these conditions, similar hemolytic properties were observed between the both GAPDH and SCR sequence siRNA-polymer conjugates. The maximum hemolytic activity was approximately one-third of the value for free polymer alone, suggesting that the RNA does attenuate the membrane-destabilizing activity when conjugated. Attenuation of the polymers intrinsic membrane disruptive properties, as shown by the red blood cell hemolysis assay, is generally proposed to be a result of altering the individual polymer chains hydrophilic-hydrophobic balance. The pH-responsive segment becomes sharply membrane destabilizing as the propyl acrylic acid is protonated to neutrality, where the alkyl segment can destabilize membrane packing together with the butylmethacrylate alkyl segments. More specifically, there could also be activity reducing effects of ionic interactions between the negatively charge siRNA and the endosomolytic segment as the pH drop increases the net positive charge of this block. The non-pH-responsive control polymer and siRNA-polymer conjugates exhibited no hemolytic activity at all pH ranges.

2.3.5 Polymer-siRNA conjugate internalization

In order to evaluate the presence of polymer-siRNA conjugates within the HeLa cells, nanoparticles were incubated for 1 h at room temperature with an Alexa-488 labeled streptavidin (SA) to bind the biotin on the RAFT chain transfer agent. The SA-polymer-siRNA conjugates

were then added to the cell media at a dose of 25 nM. After 30 min incubation with the SA-polymer-siRNA conjugates and a media wash, cells demonstrated robust intracellular fluorescence, suggesting that internalization had occurred. Free SA alone was not visualized within the cells (**Supporting Figure S 2.4**).

2.3.6 siRNA conjugates are active in vitro

The knockdown activity of the pH-responsive siRNA-polymer conjugate was evaluated in HeLa cells. siRNA directed against GAPDH (or a scrambled negative control) was conjugated to the polymer carrier and added directly to HeLa cells in media containing 10 % FBS for a 48 h continuous incubation. The final siRNA concentration was evaluated at 50 nM for the polymer-siRNA conjugates and 25 nM for the commercially available siRNA delivery agent Hiperfect. The high intrinsic toxicity of Hiperfect limited the maximum siRNA dose for the control to 25 nM. Above this concentration a substantial loss in cell viability was observed. Specific gene knockdown activity was then measured 24 and 48 h post transfection via real-time quantitative PCR (**Figure 2.5A**). GAPDH-polymer conjugates successfully reduced GAPDH mRNA to 17 % and 11 % control at 24 and 48 h, respectively. Negative control SCR-polymer conjugates did not show any knockdown GAPDH mRNA activity at either time point. Cell toxicity was evaluated with an MTS assay and verified the polymer and polymer-siRNA conjugates up to 3 orders of magnitude above reasonable siRNA doses are non-toxic in Helas cells (**Supporting Figure S 2.5**).

The ability of the siRNA-polymeric conjugates to deliver active siRNA was further evaluated by assaying the amount of GAPDH protein in HeLa cells (**Figure 2.5B**). GAPDH protein

knockdown activity was then measured 24 and 48 h post transfection via KDalert GAPDH assay kit. GAPDH-polymer conjugates successfully reduced GAPDH protein levels to 50 % of controls at 24 h incubation and 35 % of controls at 48 h incubation at 50 nM siRNA dose in HeLas. Negative control SCR-polymer conjugates failed to exhibit GAPDH protein knockdown. To evaluate with effect of the polymer on the ability to effect siRNA knockdown, various ratios of conjugated siRNA to polymer were tested at a fixed siRNA dose of 50 nM. A higher dose of polymer (lower siRNA to polymer ratio during conjugation) in the siRNA-polymer conjugates resulted in a greater ability to knockdown GAPDH without increasing toxicity in this concentration range (**Figure 2.6**). Physical mixtures of non-thiolated siRNA and polymers showed negligible protein knockdown activity (**Supporting Figure S 2.6**).

2.4 DISCUSSION

Delivery challenges still limit the therapeutic potential of siRNA[106]. Considerable progress has been made in siRNA drug development with liposomal carriers for liver applications[107,108]. These carriers can have excellent therapeutic indices due to both passive and intrinsic targeting to the liver. They can also be designed to enhance endosomal release via proton sponge and/or lipid phase effects directly on the endosomal membrane. While lipid-based systems have led the way in the siRNA delivery field, a critical need exists for better carriers that work in other disease target tissues and with good toxicity profiles. In this work have described an endosomal-releasing siRNA delivery system that retains delivery activity within a neutral, ampholytic diblock copolymer micelle system. The carrier exploits a reducible disulfide conjugation strategy for linking the siRNA to the micelle carrier. This approach allows for direct conjugation

of thiolated siRNA drugs directly to the polymeric scaffold without the need for a polycation segment.

The cytotoxicity of our neutral corona nanocarrier is strikingly reduced compared to the polycation corona composition with negligible toxicity observed in HeLa cells even after 24 hours continuous exposure at 500 mg/mL polymer[46]. Successful disulfide formation between thiolated siRNA and the PDS functional polymer was quantitated via pyridine-2-thione release and agarose gel electrophoresis. These studies suggest that greater than 95 % siRNA conjugation was observed at a siRNA to PDS ratio of 1:20. GAPDH-polymer conjugates at 50 nM doses successfully reduced GAPDH mRNA to 17 % and 11 % of the untreated control levels at 24 and 48 h, respectively. No reduction in GAPDH levels was observed for physical mixture of the diblock copolymer micelles with siRNA lacking thiol-functionality. This finding supports the conclusion that reversible covalent association of the siRNA to the micelle is necessary to achieve cytoplasmic delivery. Control experiments conducted with micelle carriers containing an inert micelle core lacking any pH-responsive membrane destabilizing behavior (ie. poly(methyl methacrylate)) also showed negligible mRNA knockdown. The strong correlation between the hemolytic activity of the siRNA conjugates and the ability to knockdown GAPDH protein indicate that an endosomal releasing core provides a significant intracellular delivery advantage in this carrier system.

2.5 Conclusions

Here, we have reported the development of a neutral, ampholytic polymer micelle carrier for siRNA delivery that exploits direct disulfide drug conjugation. Using RAFT polymerization, an

[(HPMA-co-PDSMA)-b-(DMAEMA-co-PAA-co-BMA)] diblock copolymer was synthesized with 2 mol % PDS groups per polymer chain. Thiolated siRNA was reacted with the pyridyl disulfide moieties incorporated into the hydrophilic block to achieve approximately 1 to 2 siRNA molecules per micelle with an average diameter of 25 nm. The siRNA conjugates retain the pH-responsive membrane-destabilizing activity of the parent polymer, although the absolute activity is attenuated by conjugation. The siRNA-polymer linkages are reducible by glutathione and conjugation is required for the knockdown of GAPDH mRNA and protein. These carriers exhibit maximum mRNA and protein knockdown at 50 nM siRNA doses in Helas with a siRNA linear dose response curve. The effectiveness and low cytotoxicity of this new carrier make it a promising candidate for future *in vivo* siRNA delivery studies in disease models.

2.6 Acknowledgements

We acknowledge Scott Braswell at University of Washington's 697 NanoTech User Facility for his assistance with electron 698 microscopy. This work was funded by the National Institutes 699 of Health (Grant R01EB002991 and Grant 1R21EB014572-01A1), The Life Science Discovery 700 Fund (Grant 2496490), and the National Science Foundation 701 Graduate Fellowship.

2.7 Conflict of Interest

Professor Stayton has a financial interest in the company PhaseRx Inc. that has licensed some of the drug delivery technology described in this work. However, this work was entirely conducted at the University of Washington without funding or scientific connections to PhaseRx Inc.

2.8 SUPPORTING INFORMATION

Size exclusion chromatograph for p(HPMA-co-PDSMA), p[(HPMA-co-PDSMA)-b-(PAA-co-DMAEMA-co-BMA)], and p[(HPMA-co-PDSMA)-b-(MAA)]; CMC of diblock copolymer via ANS fluorescence; Polymer-siRNA conjugation at various ratios via gel retardation assay; Polymer-siRNA uptake via fluorescent microscopy; Polymer toxicity via MTS assay in HeLa cells after 24 hour incubation; GAPDH protein knockdown with non-thiolated siRNA and polymer. This material is available free of charge via the Internet at http://pubs.acs.org.

Table 2.1 Polymer characterization.

Molecular weight and chemical composition of the diblock copolymer for siRNA conjugations employed in these studies.

Polymer	Composition (Feed)	Composition[a] (Exp.)	M_n[b] (g/mol)	PDI[b] (M_w/M_n)
($HPMA_{61}PDSMA_2$)	90:10	94:6	9,300	1.07
($HPMA_{61}PDSMA_2$)-b-($PAA_{30}DMAEMA_{19}BMA_{44}$)	30:30:40	27:24:49	22,000	1.88

[a] As determined by ^1H NMR (CD_3OD) spectroscopy (Bruker AV 500) (Fig. 1)
[b] As determined and size exclusion chromatography.

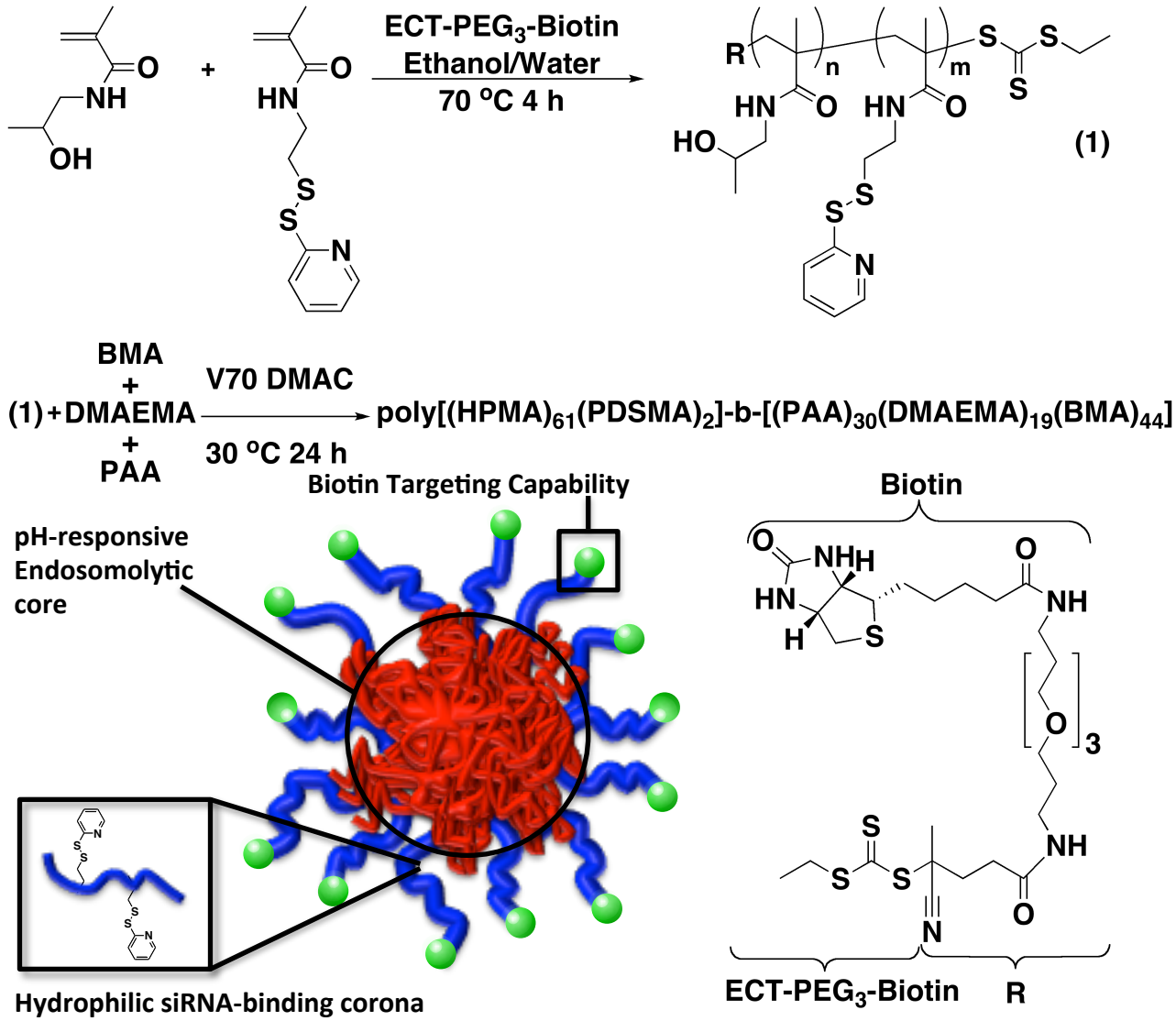

Scheme 2.1 Polymer synthesis strategy.

Synthetic structure, molecular weight, and chemical composition of the diblock copolymer for siRNA conjugations employed in these studies.

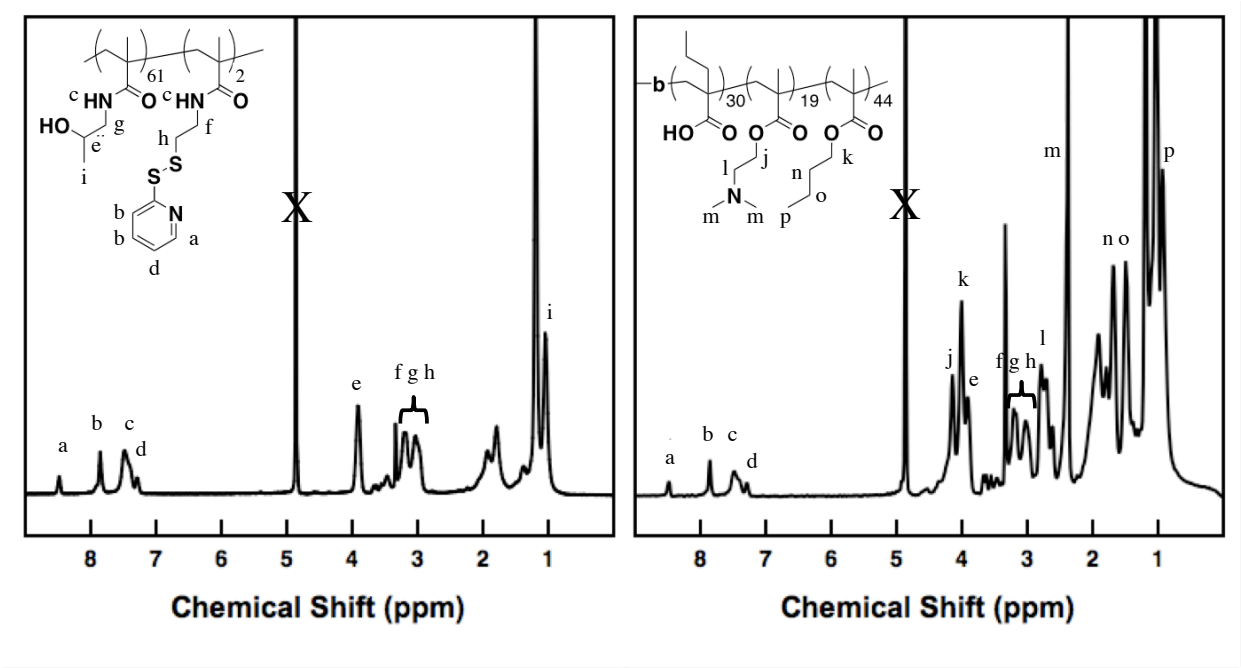

Figure 2.1 Polymer composition via ^{1}H NMR.

^{1}H NMR spectra of the macroCTA and diblock copolymer in deuterated methanol (CD_3OD) at 25 ºC. (a) is one proton from PDSMA, (e) is one proton from HPMA, (j) is two protons from DMAEMA, (k) is two protons from BMA, (m) is 6 protons from DMAEMA and the sum of protons from 0.5-3.1 ppm are from HPMA (10), DMAEMA (13), PDSMA (9), PAA (9), and BMA (12).

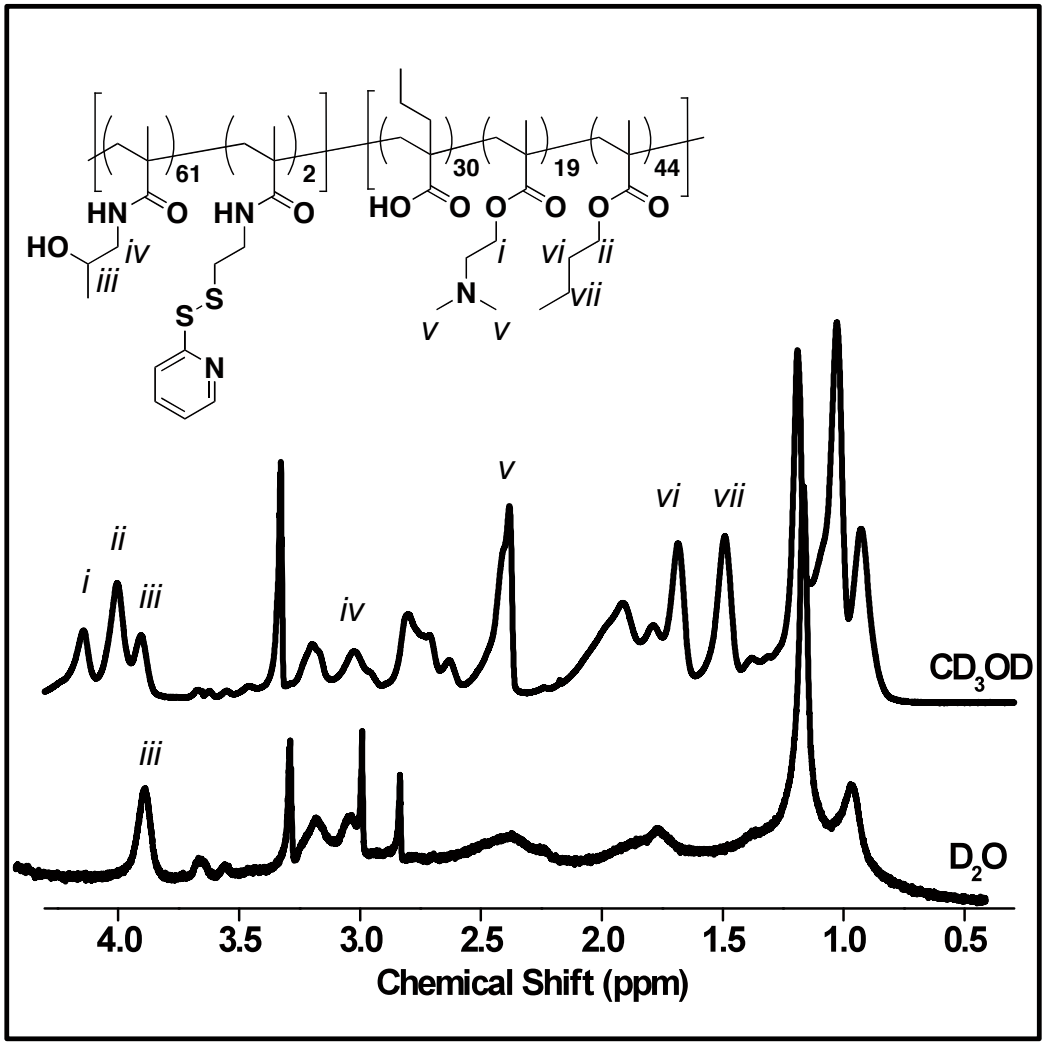

Figure 2.2 Polymer morphology via ^{1}H NMR.

^{1}H NMR spectra of the poly [(HPMA-co-PDSMA)-b-(PAA-co-DMAEMA-co-BMA)] in deuterated methanol (CD_3OD) and deuterated oxide (D_2O) at 25 ºC represents polymer morphology based on environment. Resonances associated with HPMA residues (iii, iv) as well as DMAEMA (i v) and BMA (ii, vi, vii) are fully solvated in CD_3OD, while a strong attenuation of resonances associated with DMAEMA (i, v) and BMA (ii) at 4.2 ppm, 2.4 ppm, and 4.0 ppm respectively, is observed in D_2O.

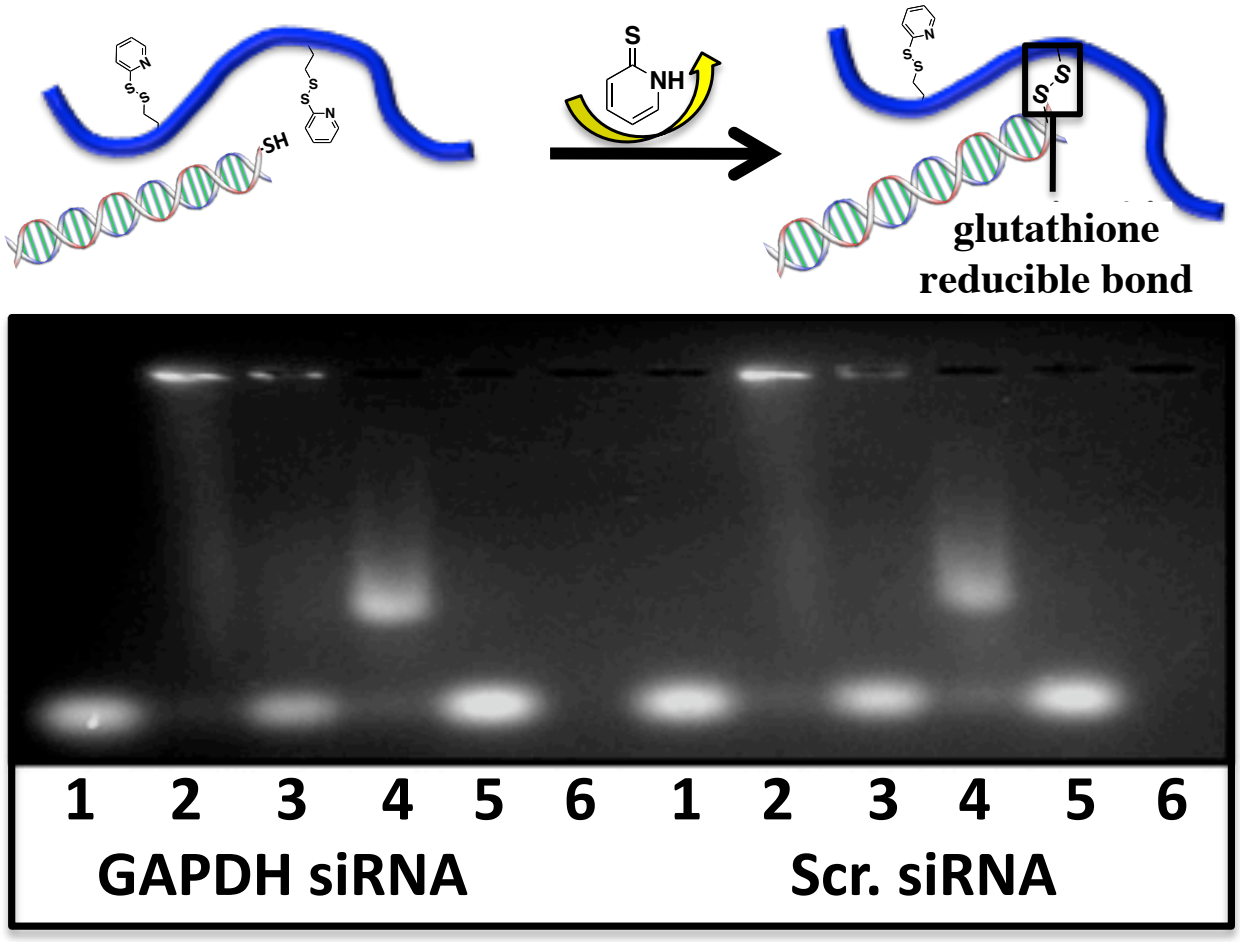

Figure 2.3 Polymer-siRNA conjugation validation.

Gel Retardation Assay validating polymer-siRNA conjugation via a reducible disulfide bond. 1 µg siRNA/lane. Lane: Free thiolated siRNA (1), 20:1 (Reactive PDS-groups on polymer to thiolated siRNA) polymer-siRNA conjugate (2), polymer-siRNA conjugate and 0.1 M DTT (3), polymer-siRNA conjugate and 1 % SDS (4), polymer-siRNA conjugate, 0.1 M DTT and 1 % SDS (5), free polymer (6).

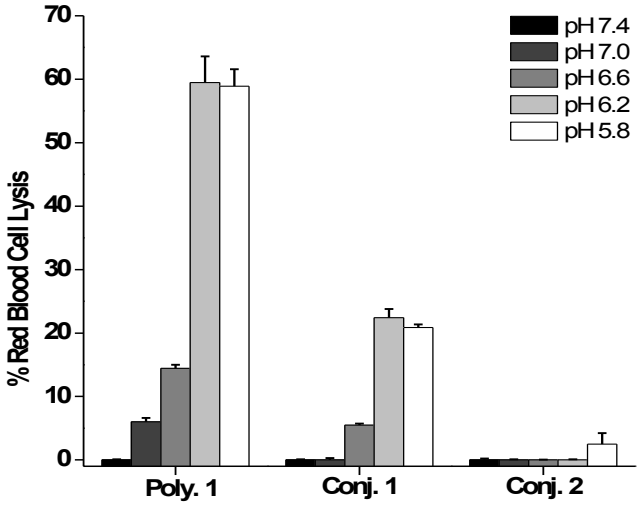

Figure 2.4 pH-responsive membrane lytic profile of polymer.

Hemolysis of the poly [(HPMA-co-PDSMA)-b-(PAA-co-DMAEMA-co-BMA)] diblock copolymer, poly [(HPMA-co-PDSMA)-b-(PAA-co-DMAEMA-co-BMA)] diblock copolymer-siRNA conjugates (Conj. 1), and poly [(HPMA-co-PDSMA)-b-(MMA)] diblock copolymer-siRNA conjugates (Conj. 2) both at a 20:1 of the reactive PDS groups on the polymer to thiolated siRNA at pH concentrations of 5.8, 6.2, 6.6 and 7.4 of 40 μg polymer/mL. Hemolytic activity is normalized relative to a positive control, 1 % v/v Triton X-100, and the data represent a single experiment conducted in triplicate ± standard deviation.

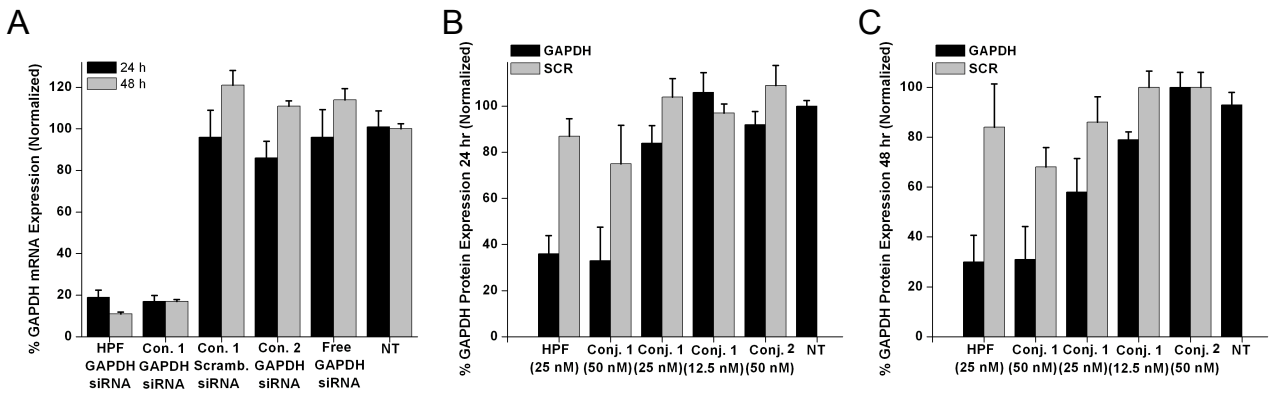

Figure 2.5 siRNA dose dependent RNA and protein knockdown.

(A) GAPDH mRNA knockdown in HeLa cells was measured using real time RT-PCR following a 24 and 48 h incubation with the poly [(HPMA-co-PDSMA)-b-(PAA-co-DMAEMA-co-BMA)] diblock copolymer-siRNA conjugates (Con. 1) and poly [(HPMA-co-PDSMA)-b-(MMA)] diblock copolymer-siRNA conjugates (Con. 2) both at a 20:1 of the reactive PDS groups on the polymer to thiolated siRNA at 50 nM doses. Scrambled siRNA conjugates and a commercially available transfection reagent, Hiperfect, were used as negative and positive controls, respectively. The data is represented with a N= 6 ± standard error. (B and C) GAPDH protein knockdown in HeLa cells was measured using KDalert GAPDH Assay following 24 and 48 h incubation period with poly [(HPMA-co-PDSMA)-b-(PAA-co-DMAEMA-co-BMA)] diblock copolymer-siRNA conjugates (12.5, 25, and 50 nM siRNA dose). Data was normalized with an LDH toxicity assay. Scrambled siRNA conjugates and a commercially available transfection reagent, Hiperfect, were used as negative and positive controls, respectively. The data is represented with a N= 6 ± standard deviation.

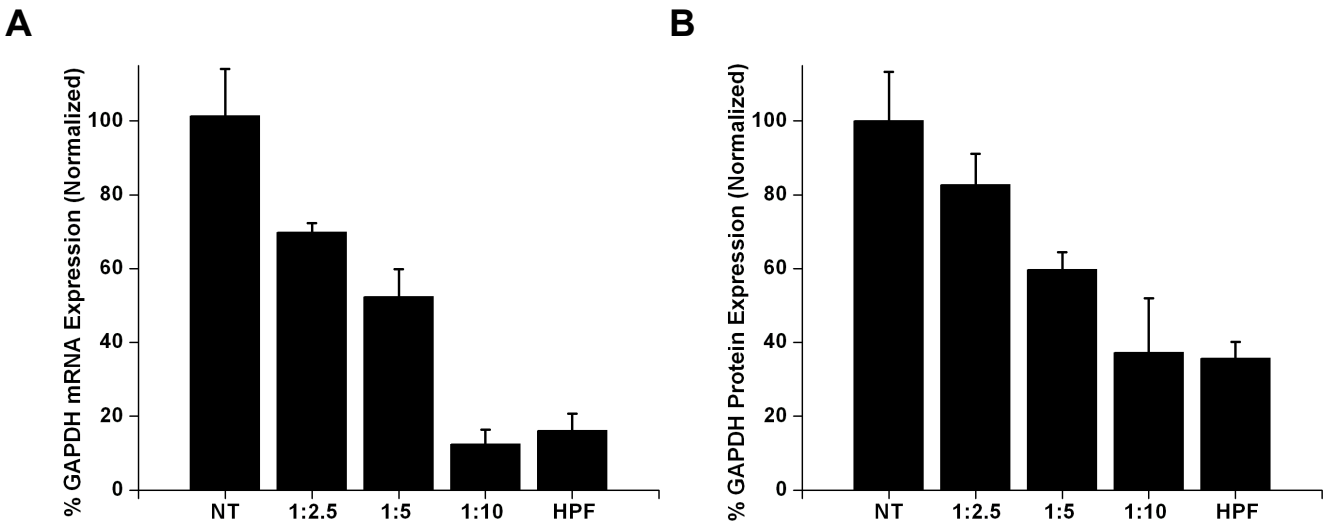

Figure 2.6 Polymer-dependent RNA and protein knockdown.

(A) GAPDH mRNA knockdown in HeLa cells was measured using real time RT-PCR following a 24 h incubation with the poly [(HPMA-co-PDSMA)-b-(PAA-co-DMAEMA-co-BMA)] diblock copolymer-siRNA conjugates at a 1:2.5, 1:5 and 1:10 of the thiolated siRNA to the diblock copolymer at a 50 nM siRNA dose. A commercially available transfection reagent, Hiperfect, was used as a positive control. The data is represented with a N= 6 ± standard error. (B) GAPDH protein knockdown in HeLa cells was measured using KDalert GAPDH Assay following 48 h incubation period with poly [(HPMA-co-PDSMA)-b-(PAA-co-DMAEMA-co-BMA)] diblock copolymer-siRNA conjugates (50 nM GAPDH siRNA dose) with a range of siRNA to diblock copolymer ratios. Data was normalized with an LDH toxicity assay. A commercially available transfection reagent, Hiperfect, was used as a positive control. The data is represented with a N= 6 ± standard deviation.

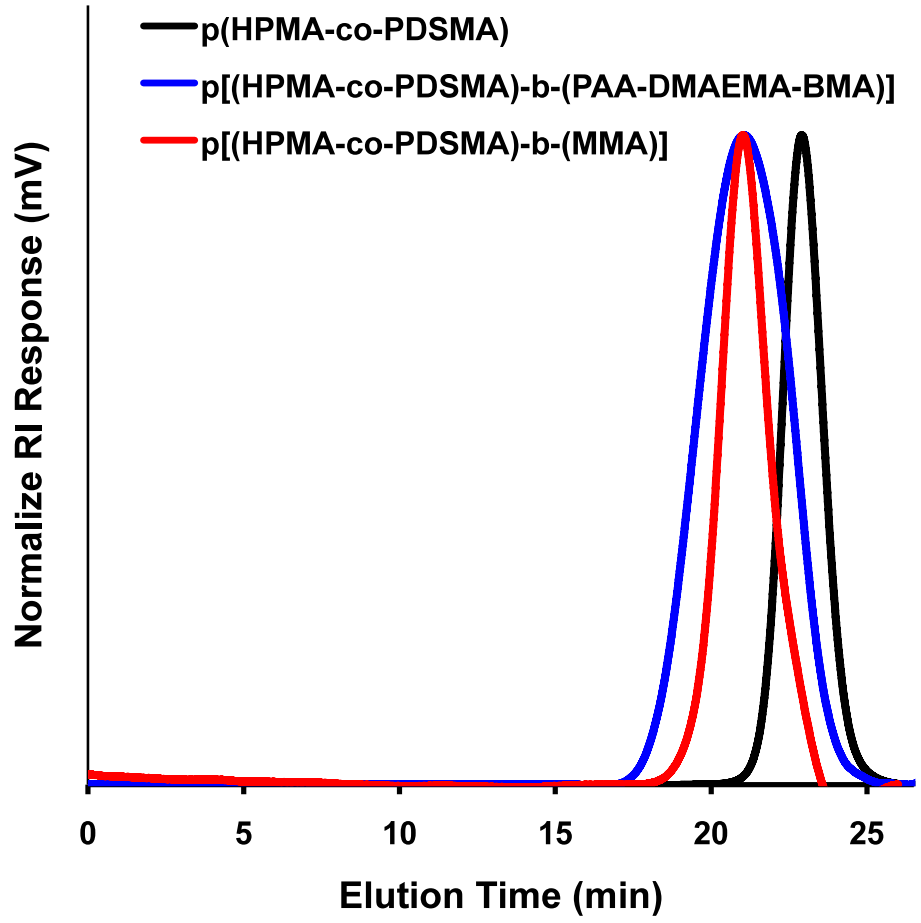

Supporting Figure S 2.1 SEC polymer characterization.

Size exclusion chromatogram for biotin-HPMA-co-PDSMA (Mn = 9,300 g/mol; PDI = 1.07), the corresponding diblock copolymer (Mn = 22,000 g/mol; PDI = 1.88), and control polymer (Mn = 17,300 g/mol; PDI = 1.04).

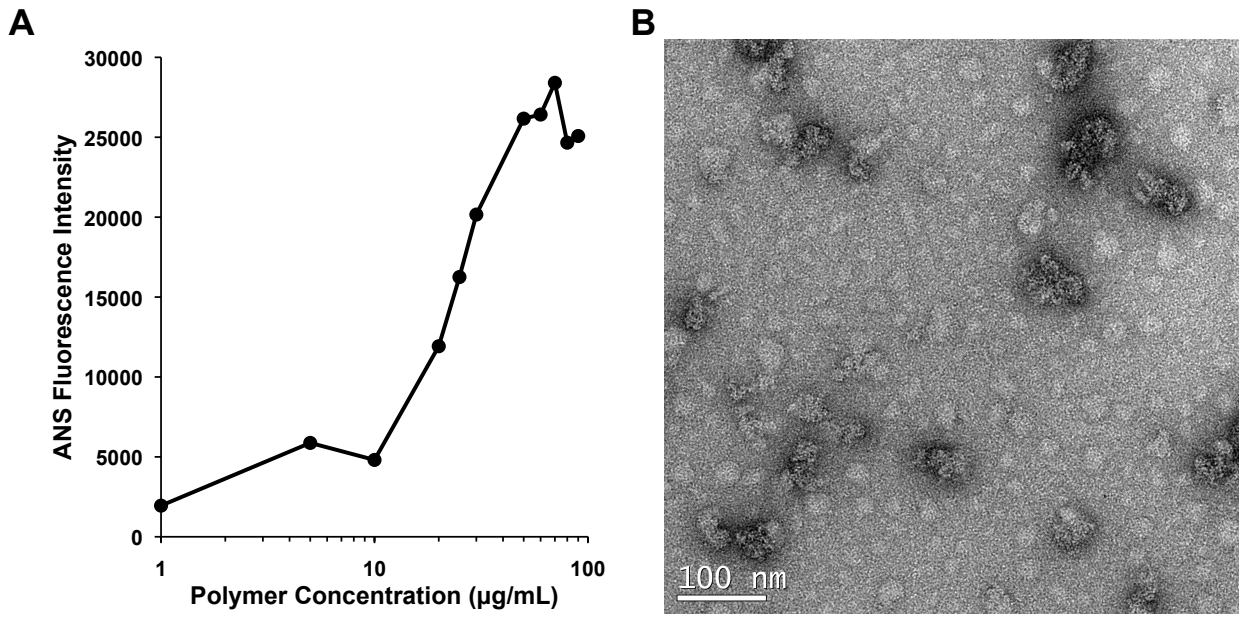

Supporting Figure S 2.2 CMC and TEM characterization.

(A) ANS fluorescence intensity vs. polymer concentration for poly[(HPMA-co-PDSMA)-b-(PAA-co-DMAEMA-co-BMA)] in 1 x PBS at pH 7.4. (B) Transmission Electron Microscope (TEM) image of micelles formed from an aqueous solution of 1 mg/mL poly[(HPMA-co-PDSMA)-b-(PAA-co-DMAEMA-co-BMA)] in 1 x PBS at pH 7.4.

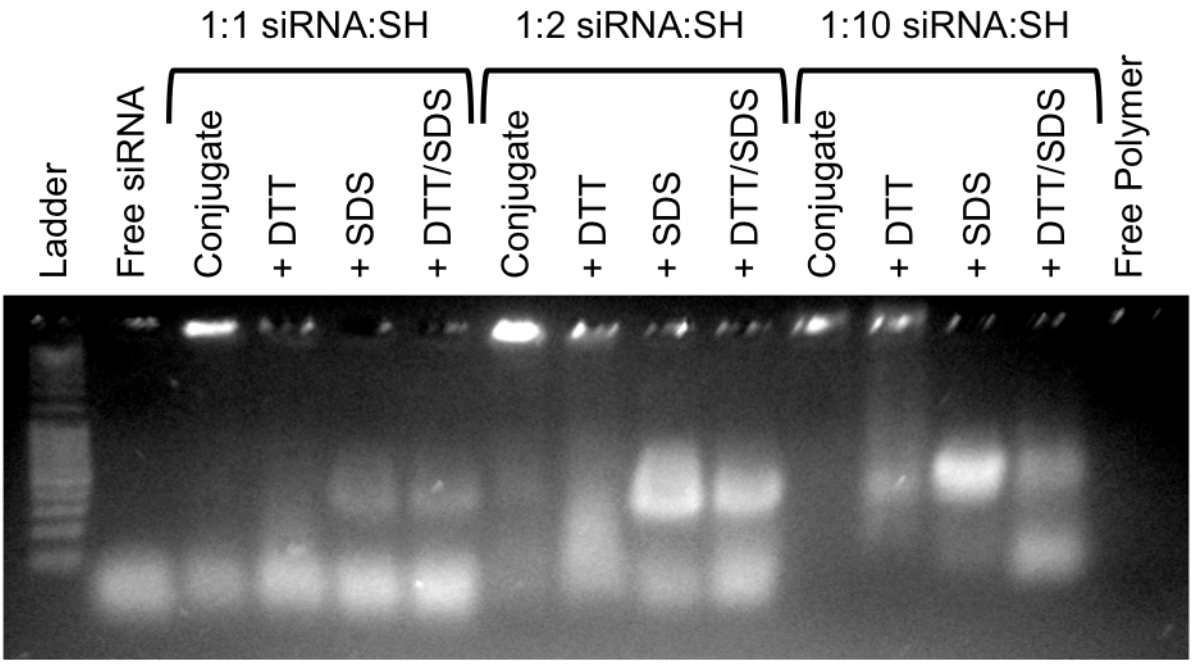

Supporting Figure S 2.3 siRNA-polymer conjugation ratios.

Gel Retardation Assay validating polymer-siRNA conjugation via a reducible disulfide linkage.

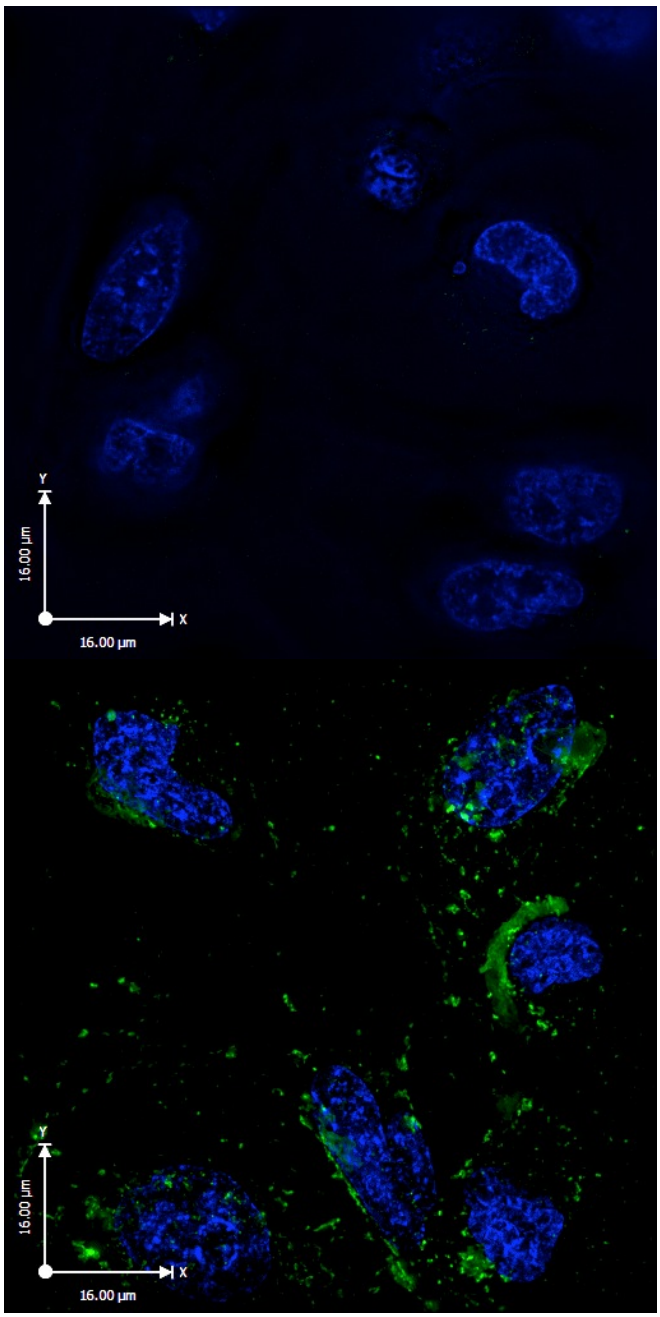

Supporting Figure S 2.4 Polymer internalization in HeLa cells.

Three-dimensional rendering of live HeLa cells using fluorescent microscopy after 30 minute incubation with 25 nM steptavidin dose with Alexa-488 labeled bounded to polymer-siRNA conjugates at a 4:1 polymer to steptavidin molar ratio (green) and Hoest nuclear stain (blue). Cells were washed with 1X PBS and imaged 1 hour later. Control Alexa-488 labeled SA (left). 25 nM streptavidin-Alexa 488 bound to Biotinylated polymer-siRNA conjugate (right).

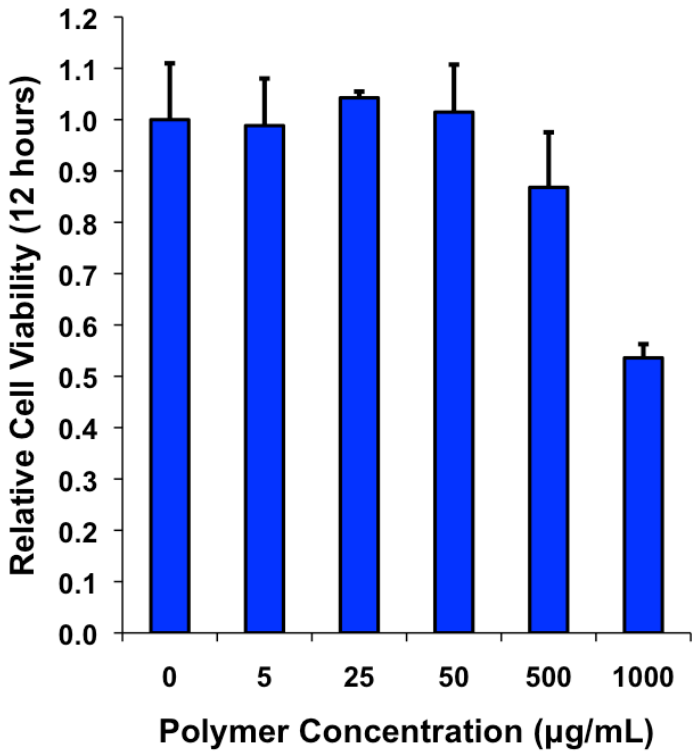

Supporting Figure S 2.5 Polymer toxicity.

MTS assay to determine polymer toxicity via HeLa cell survival after 24 hour incubation at various polymer concentrations..

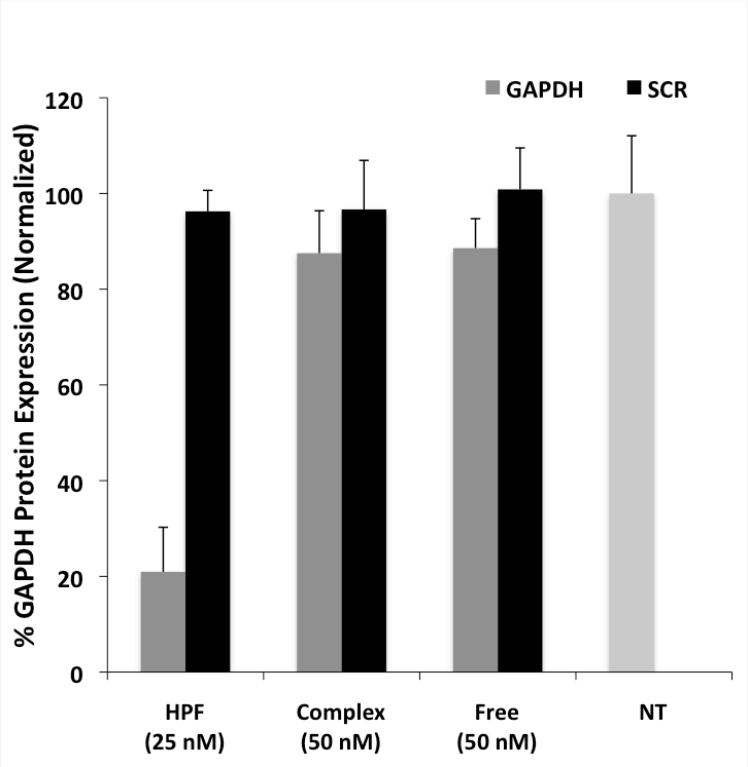

Supporting Figure S 2.6 RNA knockdown of controls.

GAPDH knockdown in HeLa cells was measured using KDalert GAPDH Assay following 48 hr incubation period with diblock copolymer to physical mixture siRNA and free siRNA (50 nM siRNA dose). Data was normalized with an LDH toxicity assay. Scrambled siRNA physical mixture and a commercially available transfection reagent, Hiperfect, were used as negative and positive controls, respectively. The data is represented with a N= 6 ± standard deviation.

Chapter 3. TRASTUZUMAB TARGETED NEUTRAL POLYMERIC MICELLES CONJUGATED TO BCL-xL siRNA SENSITIZES OVARIAN CANCER CELLS TO CARBOPLATIN

The effective treatment of ovarian cancer has been complicated by development of drug resistance associated with the Bcl-2 family of apoptosis regulators. RNA interference (RNAi) against Bcl-2 family members, including Bcl-xL, sensitizes ovarian cancer cells to chemotherapeutics, but effective delivery of short interfering RNA (siRNA) to the cytoplasm of cells remains a challenge. The human epithelial growth factor-2 (HER-2/neu) oncogene is overexpressed on the surface of 25-35% of breast and 10% of ovarian adenocarcinomas and has been correlated with a poor response to primary therapy and decreased survival. Trastuzumab is an internalizing monoclonal antibody that binds the HER-2/neu receptor and prevents uncontrolled proliferation. Here, we report the development of a trastuzumab-targeted Bcl-xL siRNA delivery carrier that successfully sensitizes ovarian cancer cells to carboplatin. The neutral polymeric delivery system is based on diblock copolymer micelles with conjugatable functionalities synthesized using Reversible Addition-Fragmentation chain Transfer (RAFT) polymerization. The first block contains poly[N-(2-hydroxypropyl) methacrylamide-co-N-(2-(pyridin-2-yldisulfanyl)ethyl)methacrylamide) (poly[HPMA-co-PDSMA]) synthesized with a biotin functionalized RAFT agent. This segment allows for conjugation via both thiol-disulfide exchange reactions and streptavidin-biotin associations. The second block composed of propyl acrylic acid (PAA), dimethylaminoethyl methacrylate (DMAEMA), and butyl methacrylate (BMA) exhibits pH-responsive behavior and facilities cytosolic delivery of siRNA. Polymers

composed of these two blocks self assemble into micelles and were successfully conjugated to thiolated siRNA and monoclonal antibody-streptavidin conjugates (mAb-SA). Trastuzumab targeted siRNA polymer conjugates increased cell uptake by 50 % in both ovarian and breast cancer cells expressing HER2/neu. Treatment with trastuzumab-targeted GAPDH-siRNA-polymer conjugates resulted a significant decrease in GAPDH mRNA levels as compared to the conjugates with no targeting antibody in both cell lines. In addition, trastuzumab targeted delivery of a therapeutic siRNA against Bcl-xL was able to silence target gene expression to 40 % and significantly reduce the IC(50) of carboplatin in ovarian cancer cells. This well-defined system overcomes many barriers to siRNA delivery to HER2+ cells and may be a valuable tool to combat chemotherapy drug resistance.

3.1 INTRODUCTION

The American Cancer Society estimates that 12,340 women will receive a new diagnosis and 4,030 women will die from ovarian cancer in 2013.[109] Chemotherapy agents such as carboplatin and paclitaxel, are the most common treatment for ovarian cancer,[110] but these treatments are limited by systemic toxicity and the emergence of drug resistance. These limitations likely contribute to the poor overall 43.5% 5-year survival of ovarian cancer patients.[109]

Bcl-xL, a structural and functional homologue of the Bcl-2 protein, provides protection against apoptosis and is associated with tumor progression, resistance to modern drug therapies, and recurrent cancer.[111-114] Inhibition of Bcl-xL, either from small molecule drugs such as ABT-737 or through RNA interference (RNAi), has been shown to sensitize ovarian cancer cells to carboplatin.[110,114-116] Furthermore, small interfering RNA (siRNA) against Bcl-xL inhibits proliferation, reduces invasion, and enhances radiosensitivity of human colorectal cancer cells in murine xenograft models.[117] Targeting Bcl-xL therefore is likely a promising strategy to inhibit carcinogenesis and prevent resistance to current ovarian cancer therapies.

The demonstrated potential of siRNA as a therapeutic cancer agent has been tempered by the need for an effective and robust delivery system. Vector- and adenovirus-mediated delivery of siRNA against Bcl-xL or other Bcl-2 family members has been reported to induce apoptosis in breast cancer and colorectal cancer *in vivo*;[117,118] however, a clinical limitation to both vector and adenoviral-based is that repeated administrations can trigger strong immune responses, thereby decreasing their therapeutic potential.[9] Non-viral delivery of Bcl-2 siRNA, was achieved via

poly(d, l-lactide-co-glycolide) (PLGA)-chitosan coated nanoparticles and showed significant tumor regression in animals,[119] however, this non-targeted approach required repeat injections directly into the tumor due to the lack of cancer-specific targeting.

Targeted siRNA conjugates are an attractive alternative approach for future clinical translation because targeting not only minimizes off-target effects, but it also reduces the effective dose necessary for therapeutic effects.[120] For example, Yu *et al*. engineered a clinically relevant CD20 antibody conjugated to lipopolyplex nanoparticles and Bcl-2 targeted antisense oligonucleotides, which demonstrated improved therapeutic efficacy *in vivo* for B-cell malignancies.[121] Trastuzumab is a clinically available HER2/neu targeting antibody that binds to the internalizing HER2 cell surface receptors. Despite HER2+ expression in ovarian cancer cells, clinical studies with trastuzumab have not met the same level of success as seen in breast and gastric cancers.[55] Recent studies, however, suggest the re-evaluation of trastuzumab as a therapeutic "primer" for other therapeutic drugs as a viable treatment for ovarian cancer.[122] Using Trastuzumab as a targeting strategy may provide an efficient method to deliver of Bcl-xL siRNA to ovarian cancer cells through target-specific uptake.

In comparison to each modality alone, combination strategies involving both therapeutic siRNA and chemotherapy drugs may represent a promising approach to combat drug resistant cancers. For example, PLGA nanoformulations of Bcl-2 siRNA have been used as an adjuvant in chemotherapy of cisplatin. Koganti, *et al*. reported the reduction in IC(50) values for cisplatin *in vitro* and improved survival of Ehrlich ascites carcinoma-bearing mice receiving combined treatments.[123] siRNA directed against other anti-apoptotic members, such as Survivin, has also

been reported to enhance chemosensitivity to cisplatin *in vivo*.[124] Based upon these studies, we hypothesized that a combination of carboplatin and a cancer antigen targeted polymer-based Bcl-xL siRNA delivery platform may be an effective therapeutic strategy.

Previously, we described the synthesis of pH-responsive, diblock copolymer siRNA carriers.[23,45,46,101,125] First generation carriers were composed of a positively charged block of dimethylaminoethyl methacrylate (DMAEMA) to mediate siRNA binding and a second pH-responsive endosomal-releasing block composed of DMAEMA, propylacrylic acid (PAA), and butyl methacylate (BMA) monomers. Although this carrier system displayed excellent delivery activity to ovarian cancer cells *in vitro*, it was limited by adverse toxicity profiles *in vivo*.[45] Second generation carriers contained a neutral, ampholytic diblock copolymer that replaces the cationic DMAEMA segment with a hydrophilic block of N-(2-hydroxypropyl) methacrylamide (HPMA) and a disulfide-conjugatable monomer *N*-(2-(pyridin-2-yldisulfanyl)ethyl)methacrylamide to directly conjugate siRNA.[125] Here, we have evaluated our multifunctional HER2-targeted siRNA-polymer conjugates in ovarian and breast cancer cells for biocompatibility and efficacy as well as tested synergistic effects with siRNA against Bcl-xL and carboplatin in ovarian cancer cells. We showed that the pretreatment of ovarian cancer cells with trastuzumab targeted Bcl-xL micelles significantly reduces the IC(50) of carboplatin, and that this method of combined therapy is a promising strategy for the treatment of ovarian cancer.

3.2 METHODS

3.2.1 Materials

All reagents were purchased from Sigma-Aldrich and Wako Chemicals and used without further purification unless specified otherwise. The trithiocarbonate CTAs ethyl cyanovaleric trithiocarbonate (ECT) and PEG3 Biotin ECT were synthesized as previously described.[101,102] Pyridyl disulfide methacrylate (PDSMA) was synthesized as described previously.[103] N,N-dimethylacrylamide was distilled under reduced pressure. Propylacrylic acid (PAA) was synthesized as previously reported. Radical initators (V70) and (V501) were purchased from Wako chemicals. BHV1 (a non-targeting isotype-matched IgG1 human anti-bovine herpes virus-1 antibody) was produced from a hybridoma obtained from American Type Culture Collection and purified from ascites fluid over a HiTrap Protein G HP column (GE Healthcare). Trastuzumab (Genentech) was obtained from pharmacy. Streptavidin conjugation to trastuzumab and BHV1 antibodies was performed as previously described.[126,127] Zeba Spin Desalting Columns and Slide-A-Lyzer Dialysis Cassettes were purchased from Pierce. Oregon Green 488 Iodoacetamide, High Capacity cDNA Reverse Transcription kit with inhibitor, and gene expression assay reagents were purchased from Life Technologies. The Cell Titer Glo Luminescence Assay was purchased from Promega. GAPDH and scrambled (SCR) thiolated siRNAs were gifted by PhaseRX, and the thiolated Bcl-xL siRNA was purchased from Thermo Scientific.

3.2.2 Thiolated siRNA

Thiolated siRNA were modified with a S-S on 5' end of sense strand. The Bcl-xL sense strand: GCUGGAGUCAGUUUAGUGAtt, and the anti-sense strand:

UCACUAAACUGACUCCAGCtg; GAPDH sense strand: GGUCAUCCAUGACAACUUUtt, and anti-sense strand: ttCCAGUAGGUACUGUUGAAA.

3.2.3 Synthesis of poly(N-(2-hydroxypropyl)methacrylamide (HPMA)-co-PDSMA) macro chain transfer agent (macroCTA)

Poly(HPMA-co-PDSMA) was synthesized as previously described.[125] HPMA (1.138 g, 7.9 mmol) was dissolved in ultra pure water (5.91 g) and the PDSMA (0.226 g, 0.89 mmol) was dissolved in ethanol (1 g) resulting in an initial molar ratio of 9:1. The biotinylated-4-Cyano-4-(ethylsulfanylthiocarbonyl) sulfanylvpentanoic acid (Biotin-ECT) (31.5 mg, 0.045 mmol), and the V501 initiator solution (1.24 mg/mL ethanol solution, 4.4 μmol) were individually dissolved in 1 g of ethanol each. The combined ethanol solutions were added to the aqueous HPMA solution in a 25 mL round bottom flask, resulting in a 2:1 (water to ethanol) final solvent ratio. The solution was purged with nitrogen for 30 min on ice and then allowed to react at 70 °C for 4 h. The reaction mixture was diluted with ultra pure water (35 g), frozen under liquid nitrogen, and lyphilized for 48 h. Isolation of the resultant polymer was conducted by repeated precipitation from ethanol into an excess of ether. Removal of excess ether was achieved by one polymer precipitation with pentane and dried overnight in vacuum oven. The macroCTA was characterized by SEC to be 10,500 g/mol with a PDI of 1.1 from the measured dn/dc of 0.091. ^{1}H NMR was used to determine the composition of 93 % HPMA and 7 % PDSMA, by evaluating the peak at 3.9 ppm and aromatic peaks at resonances between 7-8.5 ppm for HPMA and PDSMA, respectively.

3.2.4 Synthesis of poly[(HPMA-co-PDSMA)-b-(BMA-co-DMAEMA-co-PAA)]

Poly[(HPMA-co-PDSMA)-b-(BMA-co-DMAEMA-co-PAA)] was prepared as previously described.[125] The poly(HPMA-co-PDSMA) macroCTA (0.299 g, 28.5 μmol) was dissolved in dimethyl acidimid (DMAc) (2.9 g) with BMA (0.486 g, 3.42 mmol), DMAEMA (0.403 g, 2.56 mmol) and PAA (0.293 g, 2.56 mmol) (40:30:30 mol %) such that the final solvent concentration was 66 % by weight. The polymerization had an initial macroCTA to V70 initiator (3.5 mg, 11.4 μmol) ratio of 2.5:1 and degree of polymerization of 300. The polymerization solution was purged with nitrogen for 30 min before being allowed to react at 30 °C for 24 h. The final polymers were isolated by precipitation from ethanol into a 50x excess of pentane:ether (3:1 v/v). The polymer precipitant was rinsed with neat pentane, dried under vacuum overnight, and purified through PD10 desalting columns. The final dry polymers were obtained via lyophilization. The diblock copolymer was characterized by SEC to be 25,000 g/mol with a PDI of 1.8 from the measured dn/dc of 0.081. ^{1}H NMR was used to determine the composition of the second block to be 22 % PAA, 25 % DMAEMA, and 53 % BMA, as previously described.[125]

3.2.5 Polymer Characterization

Absolute molecular weights and polydispersities (PDI) were evaluated with SEC laser light scattering (LLS) using a Optimlab T-rEX (Wyatt) equipped with miniDAWN TREOS (Wyatt) for light scattering, refractive index, and UV. HPLC-grade DMF containing 0.1 wt. % LiBr at 60 °C was used as the mobile phase at a flow rate of 1 mL/min. Copolymer composition was determined via ^{1}H NMR spectra were recorded on a Bruker AV301 in deuterated methanol (CD_3OD) at 25 ºC. A deuterium lock (CD_3OD) was used and chemical shifts were determined in ppm at 3.35 and 4.78 (CD_3OD). Polymer concentration was 10 mg/mL.

3.2.6 siRNA Conjugation via thiol-exchange

The number of thiol reactive pyridyl disulfide groups on the diblock copolymer was determined as previously described,[125] by following the release of pyridine-2-thione at 343 nm following a 60 min incubation period in pH 7.4 phosphate buffered saline (PBS) (137 mM NaCl, 2.7 mM KCl, 8 mM Na_2HPO_4, and 2 mM KH_2PO_4). The thiolated siRNA was reduced (GAPDH, BCL-xL and SCR sequences) with 200 molar excess of DTT (0.1 M) and 2 μL of triethylamine (TEA) in RNAase-free water so that the final volume is 100 μL. Reactions incubated for 30 min and the solution was run through Zeba Spin Desalting Columns (7K MWCO) twice. Final RNA concentration was determined with UV spectroscopy. The lyophilized diblock polymer was predissolved in 100 % ethanol at 50 mg/mL, then diluted into phosphate buffer (RNAse-DNAse free), pH 7.4 at a final concentration of 5 mg/mL. The polymer was then added to the reduced siRNA at a 1:10 or 1:15 siRNA to polymer ratio. Sterile 10X PBS (RNAse-DNAse free), pH 7.4, was added to the final reaction in order to have a 1X PBS solution that was reacted overnight at 37 °C.

3.2.7 Gel Shift Assay

Polymer siRNA conjugation was determined by gel electrophoresis. A 2 % agarose gel was loaded with each lane containing 1 μg of free siRNA or siRNA conjugated with the diblock copolymer. 3 μL of a 500 mM Bond-Breaker TCEP solution, at a neutral pH, was reacted with the conjugates for 1 h prior to loading on gel to evaluate the reversibility of the siRNA conjugation. 5 μL of 2.5 % SDS solution were combined to siRNA-conjugates to determine if electrostatic interactions were driving complexation rather than conjugation. The gels were run

at 100 volts for 1 h and then stained with SYBR Safe dye diluted 1:5000 for 30 min for UV visualization.

3.2.8 Red blood cell hemolysis assay

Characterization of pH responsive membrane destabilizing activity was assayed by incubating polymer alone or polymer-siRNA conjugates into preparations of human red blood cells (RBCs) and determining membrane-lytic activity by hemoglobin release under 5 different pH conditions as previously described.[125] Whole blood collected in vaccutainers containing EDTA and RBCs were isolated, washed 3 times in normal saline and brought to a final concentration of 2 % RBCs in PBS at a specific pH (5.8, 6.2, 6.6, 7.0, or 7.4). Polymer alone or polymer-siRNA conjugates were evaluated at 40 μg in triplicate at each pH. RBCs with polymer alone or polymer-siRNA conjugates were incubated at 37 °C for 60 min and centrifuged to remove intact RBCs. Supernatants were transferred to a transparent 96-well plate and absorbance determined at 540 nm. Percent hemolysis is expressed as A540 sample/A540 of 1 % Triton X-100 treated RBCs (control for 100 % lysis).

3.2.9 HABA (2-Hydroxyazobenzen-4'-Carboxylic Acid) assay

A HABA assay was performed to determine the appropriate molar excess of biotinylated p[(HPMA-co-PSDMA)-b-(PAA-co-DMAEMA-co-BMA)] required to fill one biotin binding site on streptravidin (SA). SA was loaded with an excess HABA dye and incubated with 0, 0.5, 1, 2, 4, 6, 8, 10, 12, 16 M excess of biotinylated polymer to SA for 1 h. Displacement of HABA by biotinylated polymer was then monitored spectrophotometrically at 500 nm and quantified to

determine the optimum molar excess to conjugate SA targeting moieties to the biotinylated micelle.

3.2.10 PAGE Gel

To confirm the complete binding of biotinylated polymer to monoclonal antibody-streptavidin conjugates (mAb-SA) through the biotin RAFT agent, the conjugates were evaluated with gel electrophoresis at various ratios of polymer to mAb-SA. The mAb-SA was labeled with Alexa Fluor 647 Carboxylic Acid, Succinimidyl Ester at a 10 to 1 dye to protein ratio overnight at 4 °C. Protein was purified with Zeba Spin Desalting Columns (7K MWCO) twice and quantified spectrophotometrically. mAb-SA had approximately 1.8 dyes per protein conjugate. The biotinylated polymer was labeled with Oregon Green 488 Iodoacetamide at an equal molar ratio in a 50 mg/mL polymer solution in ethanol overnight at 4 °C. The reaction underwent 4 rounds of dialysis against methanol in a Slide-A-Lyzer Dialysis Cassette (7K MWCO), and a final round of dialysis against water. Purified labeled polymer was frozen, lyophilized, and labeling efficiency quantified by UV spectroscopy (85 % efficiency). All conjugates ratios were incubated for 1 hr and run on a native 4-20% Tris-HCl PAGE (Biorad) gel. Samples were loading with a bromophenol blue and glycerol loading buffer and run for 1 h at a constant voltage of 100 V. The gel was then imaged via Storm 860 Molecular Imager (GMI) to determine the fluorescent shift of the mAb-SA.

3.2.11 Cell lines

SKOV3 cells, derived from a papillary serous cystadenocarcinoma of the human ovary (ATCC) and SKOV3 EA8, were maintained in RPMI-1640 medium supplemented with 10% fetal bovine

serum and 1 % penicillin/streptomycin at 37 °C and 5 % CO_2. SKBR3 cells, derived from metastatic human breast tissue (ATCC), were maintained in McCoy's 5A medium supplemented with 10% fetal bovine serum and 1 % penicillin/streptomycin at 37 °C and 5 % CO_2.

3.2.12 Polymer siRNA Conjugate Internalization by Flow Cytometry

Internalization of the mAb-SA targeted diblock siRNA conjugates was evaluated using flow cytometry. siRNA-polymer conjugates were generated at a 1:15 siRNA to polymer ratio, with 33 % of the polymer labeled with Oregon Green. SKOV3 and SKBR3 were seeded in 12-well plates at a density of 200,000 cells/cm2 and allowed to adhere overnight. Trastuzumab targeted or a non-targeted (BHV1) polymer-siRNA conjugates were generated (4:1 M polymer to streptavidin) after 1 h incubation. Cells were treated with for 30 min at 37 °C with either Trast-SA or BHV1-SA targeted polymer-siRNA conjugates at a 50 nM siRNA dose. Cells were washed, trypsinized, and resuspended in PBS buffer containing 2% bovine serum albumin and 0.01 % bromophenol blue to quench extracellular fluorescence associated with surface bound polymer and allow discrimination of endocytosed polymers.[128] Flow cytometry was performed on a FACSCantoII (BD) using a 488 nm excitation source and a 530/30 nm band pass filter. Cells were gated by forward scattering area (FSC-A) and side scattering as well as FSC height (FSC-H) and FSC width (FSC-W) with 10,000 gated events per sample. Postacquisition analysis was performed using FlowJo flow cytometry analysis software (Tree Star, Ashland, Oregon).

3.2.13 Measurement of siRNA knockdown activity using quantitative PCR

Knockdown activity of antibody targeted siRNA-poly[(HPMA-co-PDSMA)-b-(BMA-co-DMAEMA-co-PAA)] conjugates was assayed in 96-well format by measuring specific gene

expression after 24 h and 48 h of treatment. Trastuzumab or BHV1 targeted siRNA-polymer conjugates were generated as described above. SKOV3, SKBR3, and EA8s cells were seeded 24 h prior to transfection in RPMI with 10 % FBS in a 12-well plate format at density of 13,000 cells/cm^2. The transfection growth media was RPMI with 5 % FBS and a final siRNA concentration of 50 nM. For the pulse-chase experiments, the transfection media was removed after 2 h, the cells were washed, and the media was replaced with RPMI containing 5 % FBS. Total RNA was isolated 24 and 48 h post treatment and GAPDH or Bcl-xL expression was measured relative to the internal normalizer gene, PPIA (Cyclophilin A), by quantitative PCR.

3.2.14 5'-RLM-RACE and sequencing

5'-RLM-RACE was performed using the GeneRacer Kit (Invitrogen) with some modification as previously described.[23,129] Briefly, 100 ng total RNA was directly ligated to 250 ng GeneRacer RNAOligo with T4 ligase. After phenol/chloroform extraction and ethanol precipitation, cDNA was synthesized using random primers. From this reaction, 2 μl was used for first round 5' RACE reaction using the GeneRacer 5' primer and Bcl-xl-specific reverse primer (5'-TCTACGCTTTCCACGCACAGTGCCC-3') with the following cycling conditions: 1 cycle of 94 °C for 2 minutes, then 5 cycles of 94 °C for 30 seconds and 72 °C for 1 minute, then 5 cycles of 94 °C for 30 seconds and 70 °C for 1 minute, then 20 cycles of 94 °C for 30 seconds, and 68 °C for 1 minute. Second-round 5' RACE reaction was then performed using 1 μl of the first-round reaction and internal GeneRacer 5' nested and Bcl-xL-specific nested (5'-GCTGTCCCTGGGGTGATGTGGAGCT-3') primers using the above cycling conditions except for an extension time of 15 seconds and 25 cycles. PCR were performed using an Eppendorf Mastercycler thermocycler. PCR products were run on a 3 % agarose gel containing ethidium

bromide then excised and extracted using a QIAquick Gel Extraction kit (Qiagen). Sequencing was performed using the ABI BigDye Terminator v3.1 Cycle Sequencing kit and subsequently analyzed on an ABI-3730xl DNA Analyzer (Applied Biosystems) per manufacturer's protocol.

3.2.15 Cell Titer Glo Assay

Synergistic effects of trastuzumab targeted Bcl-xL knockdown with carboplatin on the IC50 of EA8 cells were evaluated with a Cell Titer Glo assay. EA8 cells were plated in RPMI with 10% FBS on a white 96 well plate at a density of 5,000 cells/cm^2. Cell were transfected 24 h later, for 2 h with trastuzumab or BHV1 siRNA conjugates (1:15 siRNA to polymer) as described above. Final siRNA concentrations were 50 nM. Trastuzumab or polymer alone groups evaluated as controls. After 2 h, the cells were washed and the media replaced with RPMI containing 5 % FBS. 24 h after transfection, the media was removed and replaced with RPMI containing 10 % FBS and various concentrations of carboplatin (0 to 160 μM). We used the Cell Titer Glo assay, as described by manufacture's instructions after 96 h (72 h after carboplatin treatment). Cells were removed from incubator 45 min prior to the substrate addition. The manufacture's substrate reagent was added directly to the cells and incubated while shaking for 2 mins. Relative cell viability as function of luciferase activity was obtained via luminometer 10 mins later. IC50 was determined via 3 independent experiments with ED50 Plus software.

3.2.16 Statistical analysis

One-way ANOVA was used to test for treatment effects at a significance of $p<0.05$ with Tukey's test for post hoc pairwise comparisons between individual treatment groups.

3.3 RESULTS

3.3.1 Synthesis and characterization of the biotinylated diblock copolymer and polymer-siRNA conjugate

The neutral, hydrophilic region containing pyridyl disulfide functional groups was synthesized via RAFT polymerization with a biotinylated chain transfer agent (CTA)[23,46,101] in a mixed aqueous and organic solvent[125] (**Figure 3.1**). The thiol-reactive PDSMA monomer (10 mol % feed) was dissolved into ethanol with the biotin-CTA and V501 initiator, and the ethanol solution was then added to the aqueous solution containing the hydrophilic HPMA monomer (90 mol % feed). The resultant solution (1:2 ethanol to water) was previously reported to provide excellent control over the copolymerization.[125] This was confirmed by the narrow and symmetric molecular weight distribution of the resulting polymer (**Supporting Figure 3.S1**), which demonstrated a molecular weight and polydispersity of 10,500 g/mol and 1.1, respectively. The composition of the macroCTA was confirmed by ^{1}H NMR spectroscopy in CD_3OD (**Supporting Figure 3.S2**). The ratio of HPMA methyne resonance at 3.78 ppm to the PDSMA aromatic resonances at 8.45 ppm suggests that approximately 7 % PDSMA was incorporated into the polymer as compared to 10 % in the feed (**Table 3.1**). The pH-responsive block, consisting of PAA, DMAEMA, and BMA, was then RAFT synthesized in DMAc at 30 °C for 24 hours using the previous copolymer as a macroCTA and V70 as a source for free radicals. The final diblock copolymer was determined to have a molecular weight and polydispersity of 25,000 g/mol and 1.8, respectively (**Table 3.1**). Evaluation of the copolymer composition with ^{1}H NMR spectroscopy in CD_3OD indicated approximately 53 mol % BMA content in the second block with approximately equimolar quantities of PAA (22 mol %) and DMAEMA (25 mol %), which

facilitated near-neutral charge of this block at physiological pH values (**Supporting Figure 3.S2**).

This diblock copolymer has been previously reported to self-assemble into micelles at physiological pH, with a poly(HPMA-co-PDSMA) segment forming the corona and the poly(PAA-co-DMAEMA-co-BMA) segment comprising the core.[125] A hydrodynamic diameter of approximately 25-30 nm was observed by dynamic light scattering measurements in physiological solutions for both polymer and polymer-siRNA conjugates. Because the micellar morphology may impact the number of accessible functional groups available on the polymer chain, a TCEP reduction assay was used to evaluate the number of accessible PDSMA residues per polymer chain and corroborate the values determine by ^{1}H NMR. These values were in good agreement and the diblock copolymer was approximated to have 3 PDS groups per polymer chain (**Table 3.1**). We evaluated the amount of free biotins on the polymer-chains available to bind streptavidin and streptavidin conjugates via 4-hydroxyazobenzene-2'carboxylic acid (HABA) assay. Although the polymer was designed to have one biotin per polymer chain, the micellar morphology reduced the number of accessible biotins; in result, a four molar excess of polymer was required to displace one biotin-binding site (**Supporting Figure 3.S3**).

The polymer-siRNA conjugates were generated via a disulfide exchange reaction with the PDS functionalized polymer to the thiolated siRNA as previously reported[125] at a siRNA to polymer ratio of 1:10 (**Figure 3.1**), and complete siRNA conjugation was validated via agarose gel electrophoresis (**Supporting Figure 3.S4**). pH-responsive behavior of both the polymer and the polymer-siRNA conjugates was evaluated with a red blood cell lysis assay, which involved incubating the polymer and the polymer-siRNA conjugates (polymer concentration of 40 μg/mL)

with red blood cells for 1 hour at various pHs representative of the endosomal-lysosomal pathway. As expected, both the polymer and polymer-siRNA conjugate exhibited membrane disruptive behavior at pH values of 5.8 and 6.2 (**Supporting Figure 3.S5**).

3.3.2 Antibody-mediated polymeric micelle internalization in HER2+ cancer cells

Evaluation of monoclonal antibody-streptavidin conjugate (mAb-SA) binding to biotinylated micelles was conducted with native page gel electrophoresis. mAb-SA labeled with Alexa fluor 647 was incubated with Oregon Green 488-labeled polymers at various mAb-SA to polymer ratios. Successful conjugation via a biotin-streptavidin linkage formed between the free biotins on the RAFT chain transfer agent and the streptavidin of the mAb-SA was detected by the disappearance of the mAb-SA band on the gel. Complete binding of the polymer to the antibody conjugate occurred at a 4:1 polymer to mAb-SA ratio (**Figure 3.2**). All subsequent polymer conjugates to the mAb-SA were conducted at a 4:1 polymer to mAb-SA ratio to ensure maximum targeting potential of the micelle. The SKOV3 ovarian cancer cell line and the SKBR3 breast cancer cell line both overexpress HER2; however, SKOV3 cells have approximately half the number of HER2 receptors as SKBR3 cells.[130] In order to evaluate the effects of antibody-targeted uptake of the siRNA neutral micelles in both cell types, the HER2+ targeting antibody conjugate (Trast-SA) and a non-targeting mAb-SA (BHV1-SA) were conjugated to the fluorescently labeled siRNA-polymer conjugates. Both cell lines were incubated with the Trast-SA-siRNA conjugate and BHV1-SA-siRNA conjugate at a 50 nmol/L siRNA dose for 30 minutes at 37 °C. Internalization, evaluated with flow cytometry, showed a significant increase with Trast-SA targeting as compared to BHV1-SA in both SKOV3 (**Figure**

3.3 a, **b**) and SKBR3 (**Figure 3.3 c**, **d**) cell lines. Pre-incubation of the conjugates at 4 °C for 30 minutes to theoretically facilitate receptor-mediated binding did not affect the amount of uptake (data not shown). This data suggests that at early time points (30 minutes) trastuzumab-targeting robustly mediates internalization of the nanoparticles in both SKOV3 and SKBR3 cancer cells.

3.3.3 Functional activity of siRNA delivered by antibody-targeted polymeric micelle

We previously demonstrated that non-targeted, pH-responsive siRNA-polymer conjugates can efficiently deliver siRNA in the immortalized HeLa cervical cancer cell line.[125] The ability of trastuzumab targeting to enhance delivery of siRNA to HER2 expressing cells was evaluated with real-time quantitative PCR of RNA isolated from both SKOV3 and SKBR3 cells. Conjugates were prepared with either Trast-SA or BHV1-SA bound to polymers directly conjugated to either the Glyceraldehyde-3-phosphate dehydrogenase (GAPDH) siRNA or a negative control (SCR) siRNA sequence (with no known homology to human genes) at a 1:10 siRNA to polymer ratio (**Figure 3.4**). The cells were then incubated continuously for 48 hours with a final siRNA concentration of 50 nmol/L. Trast-SA GAPDH conjugates successfully reduced GAPDH to 51 % and 47 % after 48 hours in SKOV3 and SKBR3, respectively. The non-targeting BHV1-SA GAPDH conjugate did not exhibit GAPDH knockdown in SKOV3 cells; however, in SKBR3 the GAPDH mRNA level was reduced to 67 %. As expected, the negative control siRNA conjugates did not exhibit GAPDH mRNA knockdown.

To further enhance the delivery efficiency in the targeted carrier, we increased the amount of polymer in the siRNA conjugates to 1:15 siRNA to polymer. Although the overall siRNA dose remained the same (50 nmol/L) the overall polymer dose and mAb-SA dose were increased by 150 % to maintain a constant mAb-SA to polymer ratio. After 48 hours of continuous treatment

in SKOV3 cells, the GAPDH mRNA was significantly reduced in Trast GAPDH conjugate; however, the differential effect of targeting with Trast-SA compared to BHV1-SA was diminished (data not shown). Because long continuous incubation may not permit the ascertainment of differences in uptake between targeted and non targeted mAb-SA, functional siRNA delivery in SKOV3 cells was evaluated after a 2 hour pulse-chase with a 50 nmol/L siRNA dose and siRNA-polymer conjugates at a 1:15 siRNA to polymer ratio (**Figure 3.5**). The Trast-SA GAPDH conjugates exhibited successful GAPDH mRNA knockdown to 44 % and 27 % gene expression after 24 and 48 hours, respectively. GAPDH expression was reduced in the BHV1-SA GAPDH conjugates to 62 % and 74 % after 24 and 48 hours, respectively. Conversely, negative control siRNA conjugates showed negligible knockdown in SKOV3 cells at both time points. The addition of trastuzumab targeting doubled the efficacy of the siRNA carrier at the short 2 hour incubation time. Furthermore, changing the siRNA to polymer ratio from 1:10 to 1:15 improved GAPDH mRNA knockdown from 51% to 27% respectively.

3.3.4 Synergistic effect of Bcl-xL siRNA with carboplatin in ovarian cancer cells

The trastuzumab targeting system was evaluated to deliver a therapeutic siRNA directed against the gene target Bcl-xL in SKOV3 EA8 human ovarian carcinoma cells stably expressing the firefly luciferase gene (**Figure 3.6a**). These cells, derived from the parental line SKOV3, exhibited a reduction of B-cell lymphoma-extra large (Bcl-xL) mRNA with trastuzumab-targeting Bcl-xL conjugate at 24 hours (35% of untreated cells). Trastuzumab targeted GAPDH knockdown was similar after 24 hours in both SKOV3 and SKOV3 EA8, indicating that the constitutive expression of luciferase does not impact RNAi activity (**Supporting Figure 3.S6**). The SKOV3 EA8 cells exhibited negligible knockdown after treatment with the non-targeting

BHV1-SA conjugates. Reduction of Bcl-xL gene expression through the RNAi pathway was confirmed through the 5'-RLM-RACE assay (**Figure 3.6b**). The detection of the expected mRNA cleavage product was observed only in samples receiving the trastuzumab targeted Bcl-xL siRNA polymer conjugates.

Bcl-xL is a transmembrane molecule in the mitochondria that promotes cell survival. By reducing Bcl-xL expression, traditional chemotherapies including carboplatin, may be more effective. SKOV3 EA8 cells were pulse-treated for 2 hours with trastuzumab targeted Bcl-xL conjugates. After 24 hours, cells were treated with carboplatin (0-60 μg/mL) then assayed 72 hours later for viability (**Figure 3.7a**). The trastuzumab targeted Bcl-xL conjugates significantly decreased the relative cell viability at a carboplatin dose of 40 μg/mL. The IC(50) value of carboplatin was reduced from 39.9 to 32.0 μg/mL by pretreatment with trastuzumab targeted Bcl-xL siRNA conjugates (**Figure 3.7b**). The trastuzumab containing polymer-control siRNA conjugates slightly reduced the IC(50) value of carboplatin to 36.5 μg/mL; however, it was not statistically significant from any of the other treatments. BHV1-SA siRNA conjugates, polymer alone, and trastuzumab alone did not affect the relative cell viability. This data indicates that the trastuzumab-targeted Bcl-xL conjugates had a synergistic cytotoxic effect with carboplatin.

3.4 DISCUSSION

While siRNA technology holds immense therapeutic potential, a major challenge in utilizing siRNA for clinical application is a robust delivery system. We have previously described a RAFT polymerized, pH-responsive cationic polymer based siRNA delivery system capable of

facilitating cytoplasmic siRNA delivery.[45,46,101] More recent iterations of this polymer have incorporated a biotinylated RAFT agent to bind an anti-CD22 streptavidin-conjugated antibody for the treatment of non-Hodgkin's lymphoma.[23] The incorporation of antibody targeting reduced the required siRNA dose from 25 nmol/L to 15 nmol/L, achieving greater than 60 % gene silencing[23] and represented a particularly exciting result because lymphomas are traditionally difficult to transfect using traditional delivery systems *in vitro*. While promising, cationic delivery carriers are often associated with significant *in vivo* toxicity. To overcome this barrier, we have recently developed a neutral, hydrophilic siRNA delivery system for the direct conjugation of siRNA.[125] This system replaced the cationic DMAEMA siRNA-condensing block with a neutral block composed of the hydrophilic monomer HPMA. Non-targeted siRNA-polymer conjugates were first evaluated in the HeLa cervical cancer cell model as a proof-of-principle for a neutral polymeric siRNA delivery system.

Herein, we evaluated a strategy involving the direct conjugation of siRNA to this neutral, non-toxic diblock biotinylated micelle and the subsequent addition of trastuzumab as a targeting moiety. We tethered the siRNA to the polymer via reducible disulfide linkages that allow native cytoplasmic reducing agents such as glutathione to release the functional siRNA from the polymer backbone and activate the intracellular RNAi machinery. Trastuzumab-streptavidin conjugates bind exposed biotins on the micelle corona and enable receptor-mediated endocytosis via HER2/neu receptors on ovarian cancer cells. Together this conjugate-based trastuzumab-targeted strategy may overcome major barriers for the systemic delivery of siRNA that include cell-specific targeting, endosomal escape, normal tissue toxicity, and finally retention of efficacy. To our knowledge, this is the first demonstration of targeting with neutral, pH-responsive

polymer-siRNA conjugates and the first demonstration of efficacy with therapeutic siRNA in target specific cells.

As expected, trastuzumab targeted micelles selectively enhanced siRNA uptake and improved efficacy in HER2+ cells in our studies. Past generations of siRNA delivery systems have relied on electrostatic interactions to condense and release siRNA. These carriers have a net positive surface charge that increases electrostatically-driven association with the negatively charged cell membranes. The direct conjugation of siRNA to a neutral polymer negates electrostatic interactions and reduces indiscriminate cell uptake. Trastuzumab conjugation to the siRNA-polymer system compensates for this loss in non-specific uptake and promotes cellular internalization via receptor mediated endocytosis in HER2+ cells. The increased uptake provided by trastuzumab targeting contributed to the robust efficacy of the siRNA conjugates in both SKOV3 and SKBR3 HER2+ cancer cell lines.

We have recently reported the polymer-dependent efficacy of this system in HeLa cells, in which we can tune gene-silencing activity by increasing the polymer to siRNA ratio.[125] This phenomenon was also observed in SKOV3 ovarian cancer cells. When the polymer to siRNA ratio was increased from 10:1 to 15:1, GAPDH mRNA expression was reduced from 50 % to 27 % after 48 hours despite shortening the exposure time from a 48-hour continuous incubation to a 2-hour pulse treatment. However, HER2+ expressing cell lines required a higher polymer to siRNA ratio than HeLa cells to achieve similar level of RNAi activity. We hypothesize there is a critical polymer concentration necessary inside the endosomal compartment to achieve membrane destabilization activity when siRNA is present that may differ depending on the target cell type.

Effective gene silencing of Bcl-xL has been reported to sensitize ovarian cancer cells to carboplatin. In particular, 100 nmol/L Bcl-xL siRNA (resulting in greater than 60 % Bcl-xL mRNA knockdown) was previously required to reduce the IC(50) of carboplatin 2-fold.[116] In the present study, we observed greater than 60 % gene knockdown and a significant reduction in the IC(50) of carboplatin after a 2 hour treatment with 50 nmol/L Bcl-xL siRNA delivered by the trastuzumab polymer conjugate. Interestingly, trastuzumab and our polymer conjugates – regardless of the siRNA sequence – slightly reduced the IC(50) of carboplatin. Treatment with trastuzumab alone, the diblock copolymer alone, or the non-targeting BHV1-SA polymer-siRNA conjugates showed no difference in toxicity compared to the no treatment control. Perhaps, the increased uptake of the endosomal-lytic polymer via trastuzumab contributed to a higher cellular dose and was responsible for this effect in ovarian cancer. Inoue and colleagues engineered an antisense oligonucleotides delivery system composed of poly(β-l-malic acid) with 40% leucine ethyl ester to provide endosomal escape and trastuzumab targeting. SKBR3 cell viability and tumor growth *in vivo* were both reduced with the treatment of this nanobiopolymer; however, there was no difference between this treatment and trastuzumab control.[131] Since trastuzumab has an extracellular target, it is unlikely that its endosomal-escape via a pH-responsive polymer would have a synergistic effect with carboplatin.

Other gene targets have also been investigated *in vitro* to sensitize cancer cells to chemotherapies agents via polymeric delivery. We previously reported the cationic version of this endosomal polymer reduced the IC(50) of doxorubicin 5-fold through plk1 knockdown in ovarian cancer cells after a 25 nmol/L siRNA dose for 4 hours.[45] Koganti, *et al*. reported a 1.3 fold reduction in the IC(50) value of cisplatin in HeLa cells after 24 hour incubation with 50 ng of Bcl-2 siRNA.[123] Although higher siRNA doses were required for our studies, shorter incubation times were used,

which is more representative of the short exposure times that the target cells of interest may encounter in an *in vivo* setting

3.5 CONCLUSIONS

We report the development of a HER2-targeted neutral, ampholytic polymer micelle carrier for siRNA delivery that exploits direct disulfide drug conjugation. Using RAFT polymerization, a p[(HPMA-co-PDSMA)-b-(DMAEMA-co-PAA-co-BMA)] diblock copolymer was synthesized with a biotinylated RAFT agent to allow for targeting via biotin-streptavidin linkages with monoclonal antibody streptavidin conjugates. Therapeutic Bcl-xL thiolated siRNA was reacted with the pyridyl disulfide moieties within the corona of the micelle. This siRNA delivery system was designed specifically to overcome the major hurdles of *in vivo* siRNA delivery by possessing antibody mediated cell-specific uptake, low toxicity, reducible siRNA-polymer linkages via glutathione, and pH-responsive membrane-destabilizing activity to provide cytosol delivery of the siRNA molecules. Trastuzumab targeting increased siRNA-polymer conjugate uptake in two different HER2+ cancer cells lines, SKOV3 and SKBR3. Trastuzumab-targeted micelles conjugated with Bcl-xL siRNA reduced Bcl-xL mRNA expression to less than 40 % and exhibited synergy with carboplatin by significantly reducing the IC(50) of carboplatin 1.25-fold in ovarian cancer cells. The robust knockdown activity and the ability to sensitize ovarian cancer cells to carboplatin makes this targeted siRNA delivery system a promising candidate for future *in vivo* combination therapy studies for cancer applications.

Table 3.1 Polymer characterization.

Molecular weight and chemical composition of the diblock copolymer for siRNA conjugations employed in these studies.

Polymer	Composition (Feed)	Composition[a] (Exp.)	M_n [b] (g/mol)	PDI[b] (M_w/M_n)
($HPMA_{68}PDSMA_3$)	90:10	93:7	10,500	1.1
($HPMA_{68}PDSMA_3$)-b-($PAA_{28}DMAEMA_{23}BMA_{54}$)	30:30:40	22:25:53	25,000	1.8

[a] As determined by ^1H NMR (CD_3OD) spectroscopy (Bruker AV 500) (Supplemental Figure 2)
[b] As determined and size exclusion chromatography.

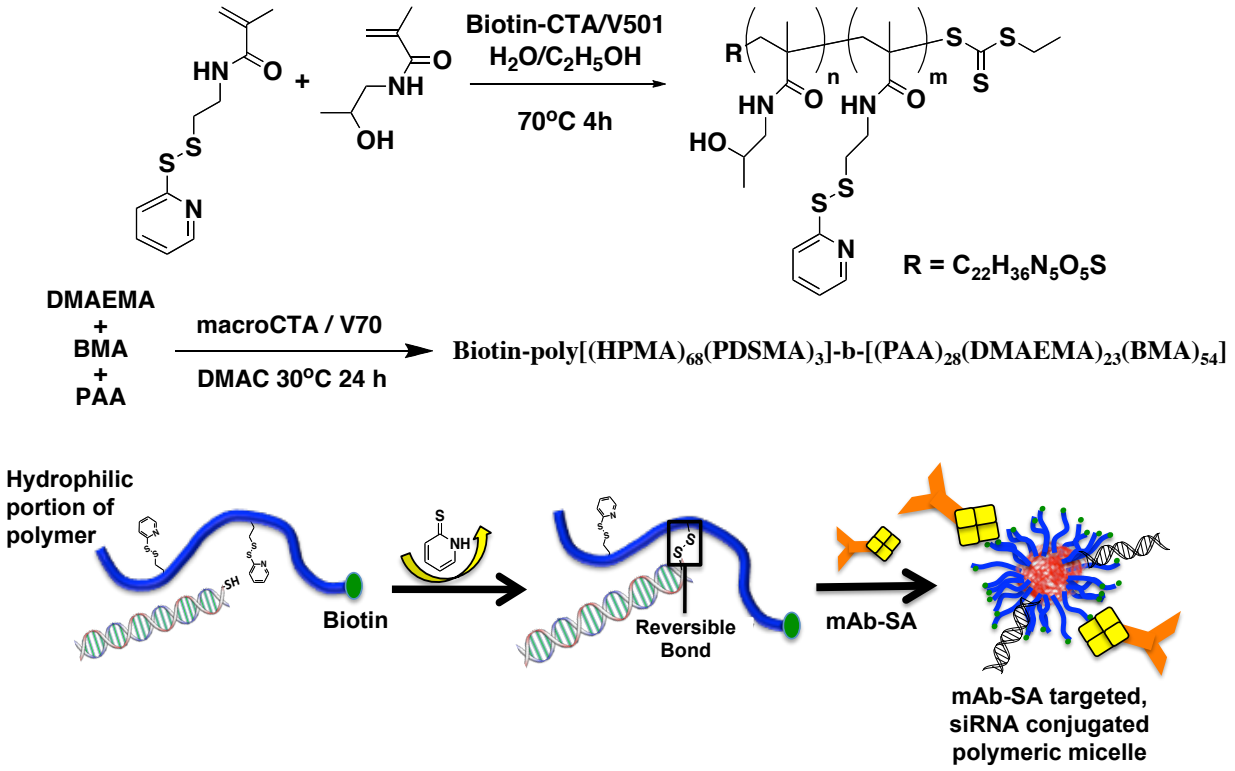

Figure 3.1 Antibody-targeted polymer-siRNA conjugate development.

Illustration of polymer synthesis and antibody-targeted, siRNA conjugated polymeric micelle formation. A biotin functionalized polymer is synthesized via a biotinylated reversible addition fragmentation chain transfer (RAFT) agent to produce a biotinylated poly(HPMA-co-PDSMA) block that reversibly conjugates small interfering RNA (siRNA). A subsequent pH-responsive block of DMAEMA, PAA, and BMA subunits is chain extended via RAFT polymerization. Polymers self assemble into micelles and are directly conjugated to thiolated siRNA via a disulfide exchange reaction. Subsequent addition of mAb-SA results in streptavidin binding to available surface biotin and generation of an antibody-targeted polymeric micelle. BMA, butylmethacrylate; DMAEMA, dimethylaminoethyl methacrylate; HPMA, N-(2-hydroxypropyl) methacrylamide; mAb-SA, monoclonal antibody-streptavidin conjugate; PAA, polyacrylic acid; PDSMA, pyridyl disulfide methacrylate; siRNA, small interfering RNA.

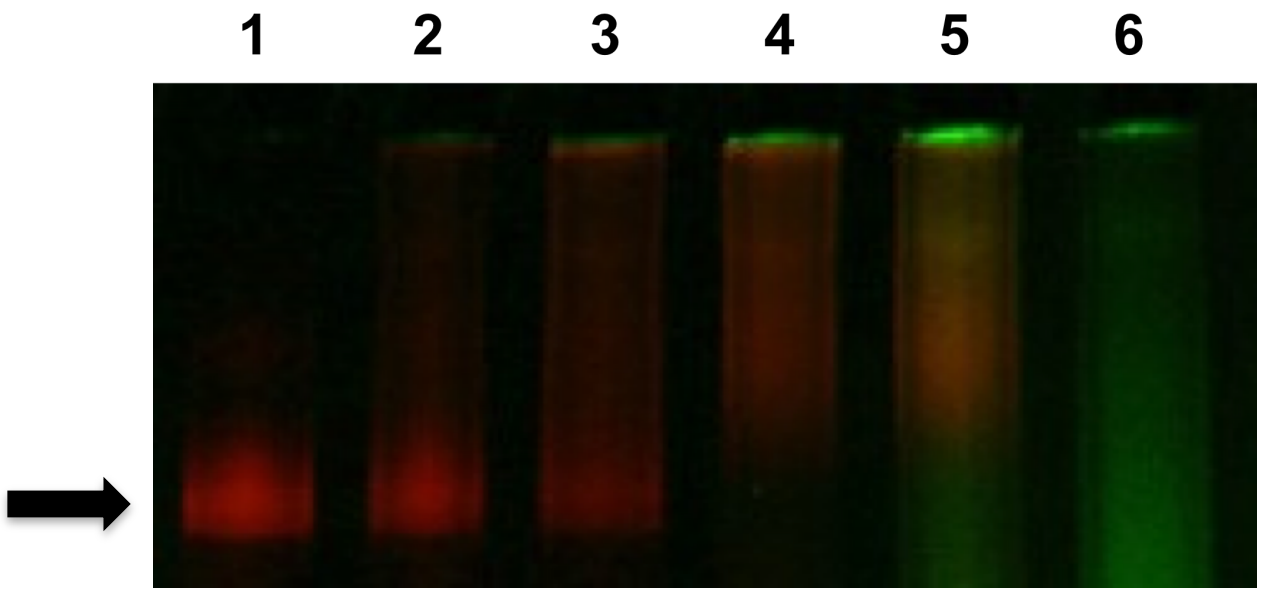

Figure 3.2 Antibody polymer conjugation validation.

Native page gel electrophoresis validating of mAb-SA conjugation with biotinylated poly[(HPMA-co-PDSMA)-b-(PAA-co-DMAEMA-co-BMA)] labeled with Oregon Green-488. 10 μg Alexa fluor-647 mAb-SA/lane. Lane: mAb-SA (1), 1:1 mAb-SA to polymer (2), 1:1 mAb-SA to polymer (3), 1:4 mAb-SA to polymer (4), 1:8 mAb-SA to polymer (5), polymer (6).

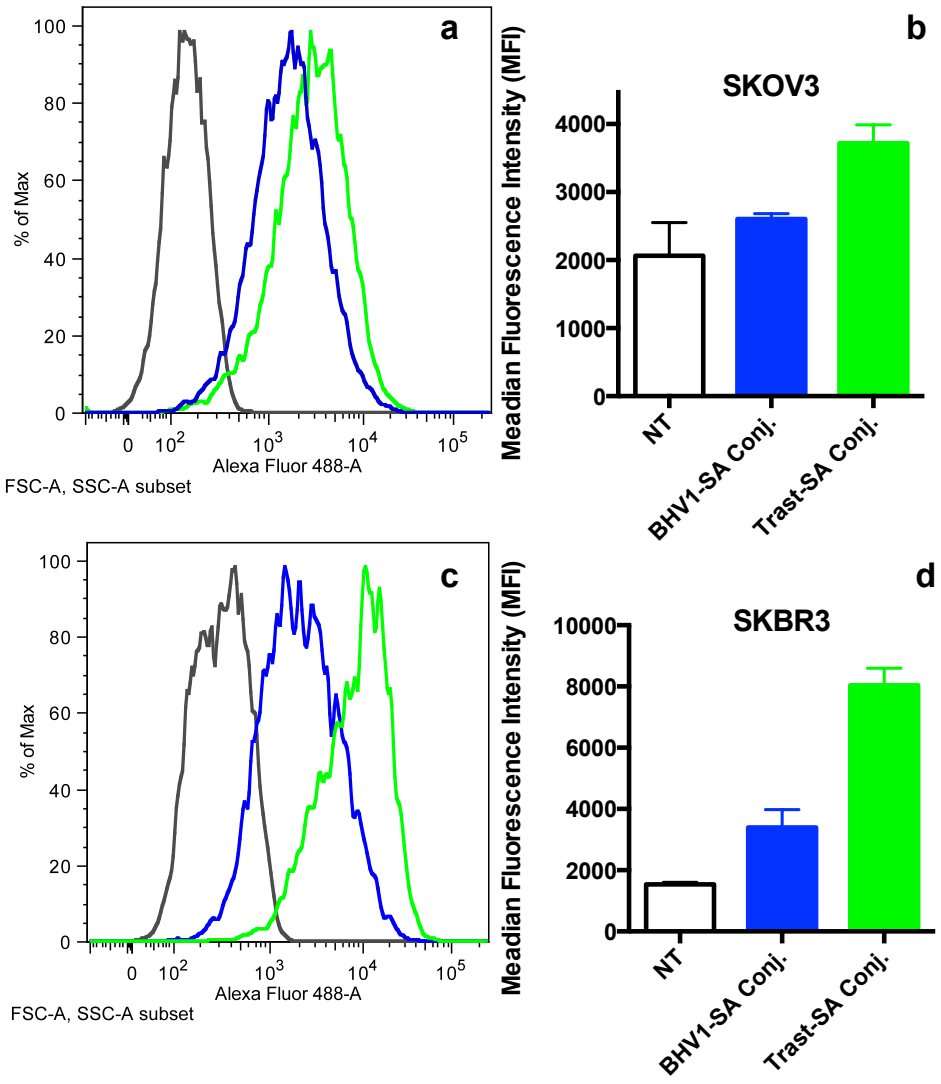

Figure 3.3 Trastuzumab mediated cell uptake.

Internalization of siRNA-polymer conjugates containing Oregon Green 488-labeled polymer with or without monoclonal antibody-streptavidin conjugate (mAb-sA) targeting. (a,b) SKOV3 or (c,d) SKBR3 cells were incubated at 37°C in the presence of polymeric micelles containing 50 nmol/L of siRNA conjugated to biotinylated polymer and bearing Trastuzumab-SA conjugate or nontargeting BHV1-SA conjugate. After 30 mins of treatment, cells were rinsed with phosphate-buffered saline (PBS), trypsinized, and resuspended in flow cytometry buffer containing 1% bromophenol blue to quench surface bound fluorescent polymeric micelles then analyzed for fluorescence by flow cytometry. (a) SKOV3 or (c) SKBR3 cells treated with polymeric micelles bearing Trastuzumab-SA (green line), BHV1-SA (blue line) or no treatment (black line). Vertical axis is percentage of maximum intensity (% of Max), Representative histograms depict fluorescence intensity (horizontal axis) of SKOV3 or SKBR3 cells. (b,d) Median relative fluorescence intensity (RFI) ± standard deviation of quadruplicate samples is shown.

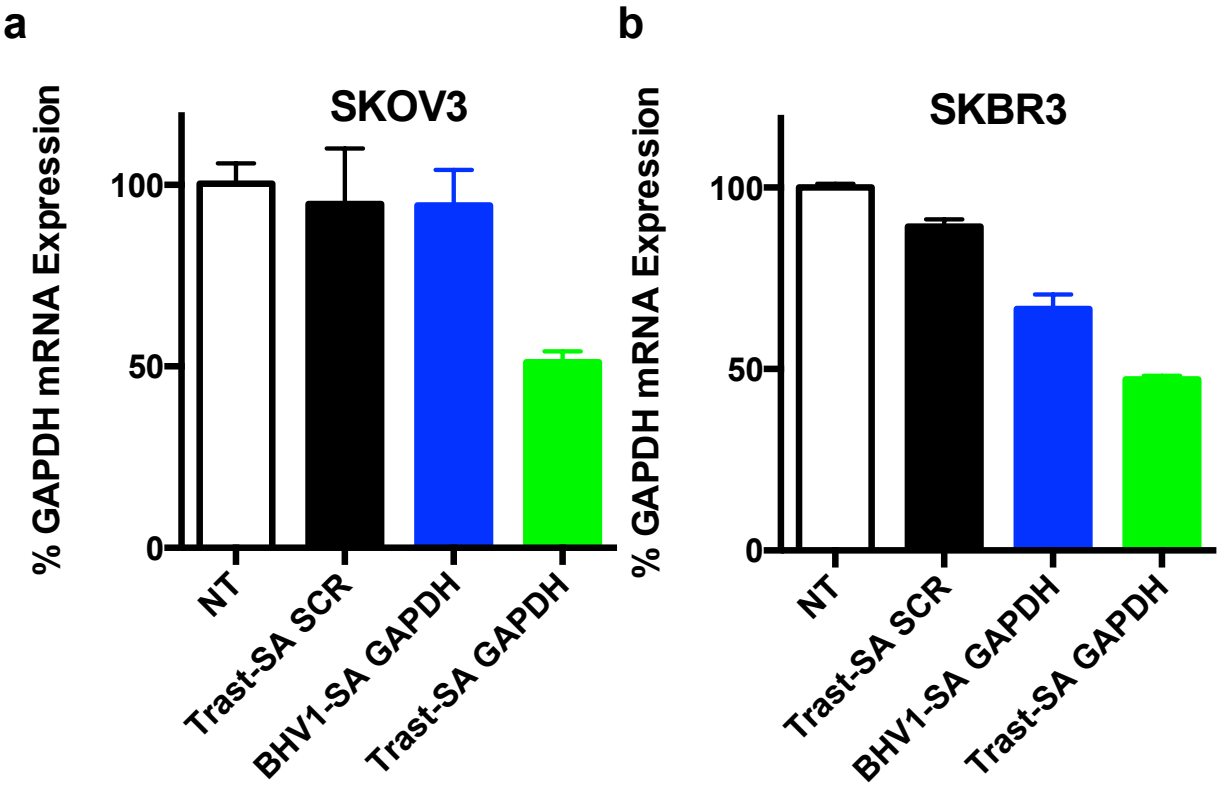

Figure 3.4 Trastuzumab mediate siRNA-polymer conjugate gene silencing.

Trastuzumab-mediated reduction of Glyceraldehyde-3-phosphate dehydrogenase (GAPDH) gene expression in HER2 expressing cancer cells lines, (a) SKOV3 and (b) SKBR3. GAPDH mRNA levels were assayed by quantitative reverse transcription (qRT)-PCR after a 48 hour incubation with siRNA-polymer conjugates bearing Trast-SA (Trastuzumab-targeted conjugate) and BHV1-SA (nontargeted conjugate). The poly [(HPMA-co-PDSMA)-b-(PAA-co-DMAEMA-co-BMA)] diblock copolymer was conjugated with thiolated siRNA at 1:10 siRNA to polymer ratio and cells were dosed with 50 nmol/L siRNA directed against GAPDH or a negative control siRNA (SCR) with no sequence homology to known human genes. Values are normalized to the housekeeping gene PPIA (Cyclophilin A) and relative to GAPDH expression in untreated cells (NT). Error bars represent the mean GAPDH expression ± standard error of triplicate samples.

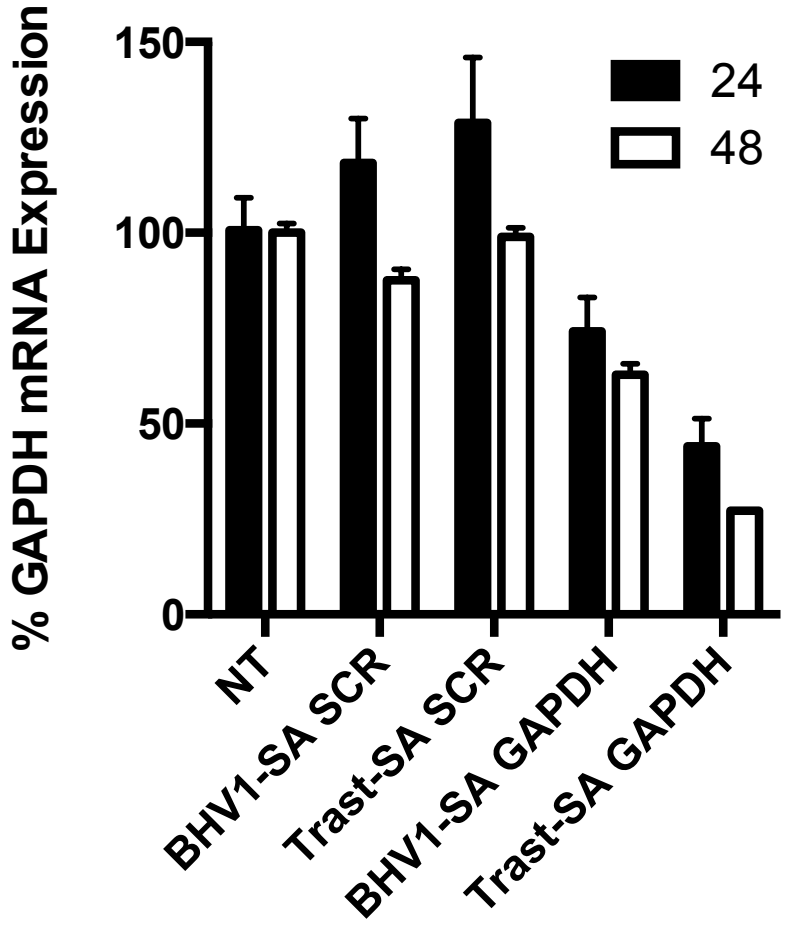

Figure 3.5 GAPDH gene silencing time course.

Trastuzumab-mediated reduction of Glyceraldehyde-3-phosphate dehydrogenase (GAPDH) gene expression in HER2 expressing cancer cells, SKOV3. GAPDH mRNA levels were assayed by quantitative reverse transcription (qRT)-PCR 24 and 48 hours after a 2 hour pulse-chase with siRNA-polymer conjugates bearing Trast-SA (Trastuzumab-targeted conjugate) and BHV1-SA (nontargeted conjugate). The poly [(HPMA-co-PDSMA)-b-(PAA-co-DMAEMA-co-BMA)] diblock copolymer was conjugated with thiolated siRNA at 1:15 siRNA to polymer ratio. Cells were dosed with 50 nmol/L siRNA directed against GAPDH or a negative control siRNA (SCR) with no sequence homology to known human genes for 2 hours. Values are normalized to the housekeeping gene PPIA (Cyclophilin A) and relative to GAPDH expression in untreated cells (NT). Error bars represent the mean BCL-xL or GAPDH expression ± standard error of triplicate samples.

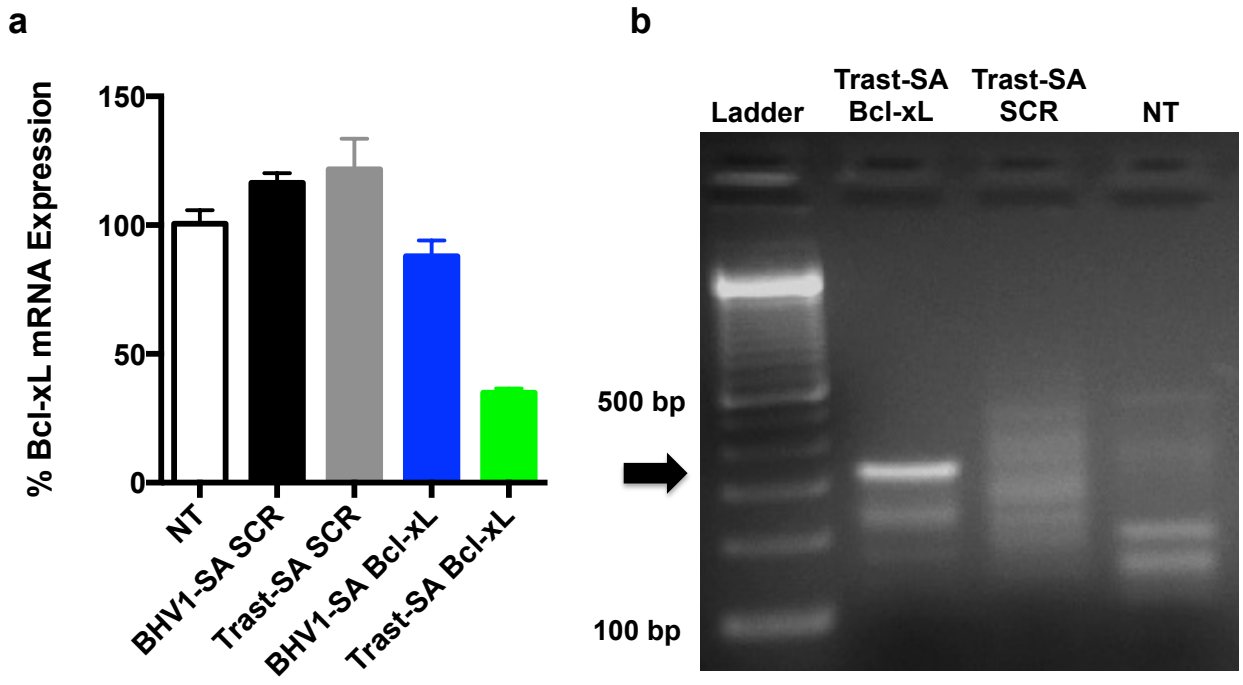

Figure 3.6 Bcl-xL gene silencing and validation.

Trastuzumab-mediated reduction of Bcl-xL gene expression of EA8 cells treated with Trastuzumab targeted siRNA-polymer conjugates containing siRNA directed against Glyceraldehyde-3-phosphate dehydrogenase (GAPDH), or BCL-xL, or a negative control siRNA (SCR) with no sequence homology to known human genes. (a) BCL-xL mRNA levels were assayed by quantitative reverse transcription (qRT)-PCR at 24 hours after a 2 hour pulse-chase with siRNA-polymer conjugates bearing Trast-SA (Trastuzumab-targeted conjugate) and BHV1-SA (nontargeted conjugate). The poly [(HPMA-co-PDSMA)-b-(PAA-co-DMAEMA-co-BMA)] diblock copolymer was conjugated with thiolated siRNA at 1:15 siRNA to polymer ratio and cells were dosed with 50 nmol/L siRNA for 2 hours. Values are normalized to the housekeeping gene PPIA (Cyclophilin A) and relative to BCL-xL expression in untreated cells. Data represents two independent experiments. Error bars represent the mean BCL-xL expression ± standard error of triplicate samples. (b) 5′-RLM-RACE analysis for the specific detection of Bcl-xL mRNA cleavage products performed using RNA from each treatment group: Trast Bcl-xL siRNA conjugate, Trast SCR conjugate (negative control siRNA), and untreated cells (NT). PCR products were analyzed by agarose gel electrophoresis and run alongside a 100 base pair DNA ladder. The arrow indicates the correct cleavage product at 309 bp.

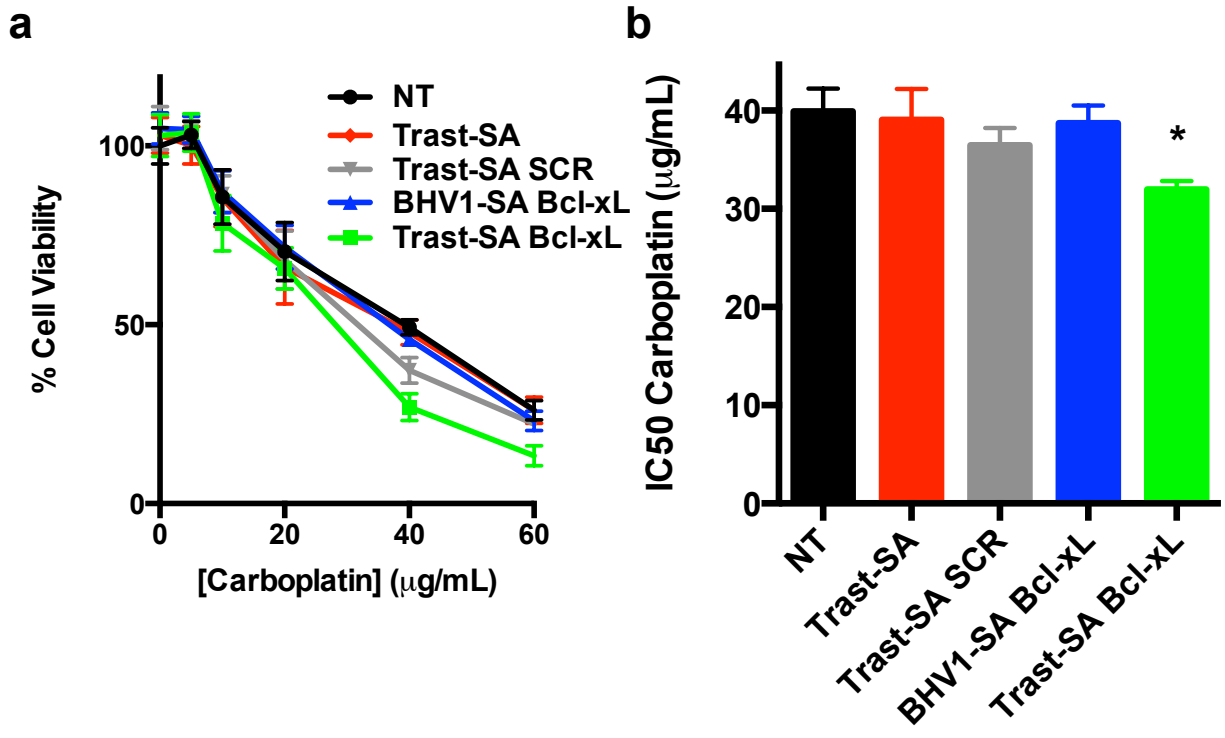

Figure 3.7 Bcl-xL-polymer conjugates sensitize ovarian cancer cells to carboplatin.

Effect of trastuzumab targeted Bcl-xL siRNA conjugates on viability of EA8 cells treated with Carboplatin. (a) EA8 cells were transfected for 2 hours with a sensitizing Bcl-xL siRNA or a negative control siRNA (SCR) with no sequence homology to known human genes (50 nmol/L siRNA and 1:15 siRNA to polymer ratio) and treated with increasing concentrations of Carboplatin (0-60 μg/mL) for 72 hours. Cell viability was measured by cell luminescence via CellTiterGlo Assay and normalized to untreated cells. Data are from three independent experiments conducted in quadruplicate, with error bars representing standard deviation of the mean. (b) IC(50) of carboplatin with the 2 hour treatment of antibody targeted siRNA conjugates at 50 nmol/L siRNA dose 24 hours prior to carboplatin. Statistical significance was evaluated at a level of $p<0.05$ with the following symbol * indicates significance versus NT, Trast-SA, and BHV1-SA Bcl-xL.

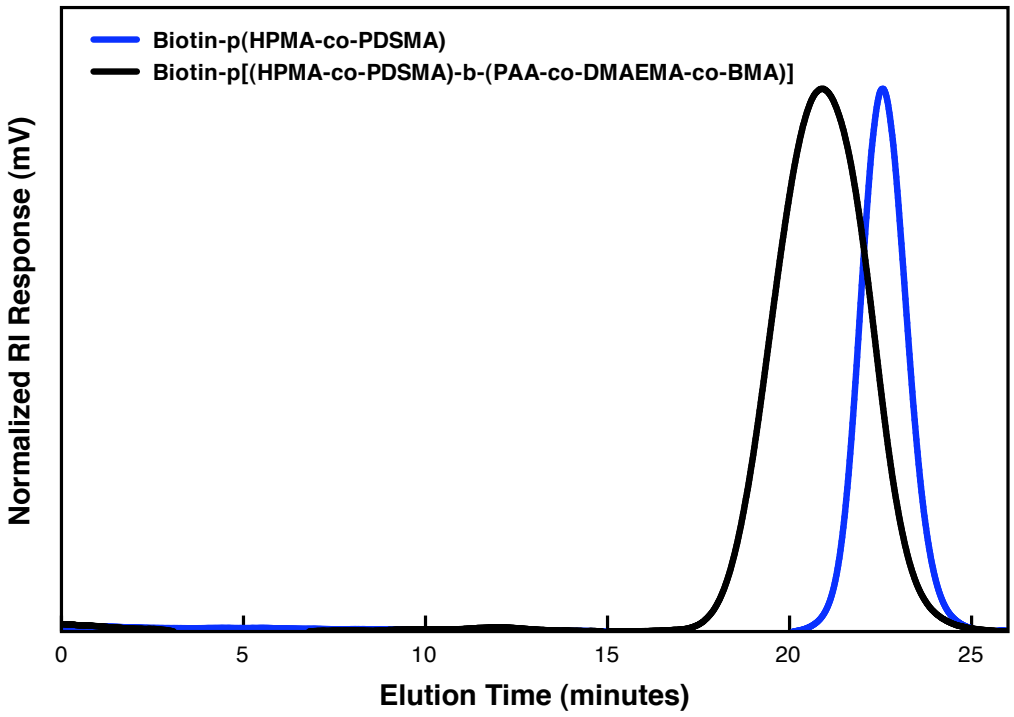

Supporting Figure S 3.1 Polymer characterization by SEC.

Size exclusion chromatogram for biotin-HPMA-co-PDSMA (Mn = 10,500 g/mol; PDI = 1.1), the corresponding diblock copolymer (Mn = 25,000 g/mol; PDI = 1.8).

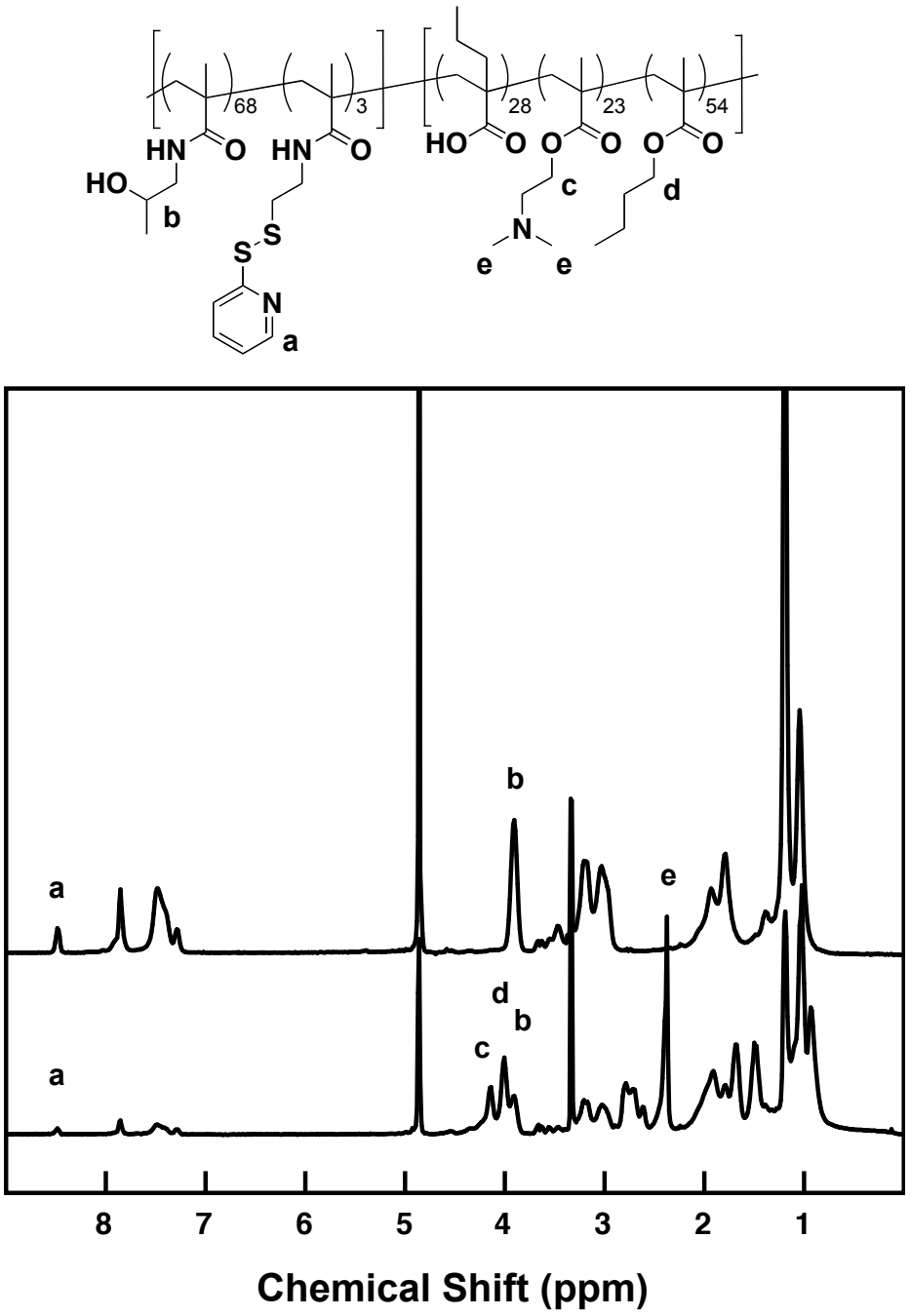

Supporting Figure S 3.2 Polymer characterization via ^{1}H NMR.

^{1}H NMR spectra of the macroCTA (top) and diblock copolymer (bottom) in deuterated methanol (CD_3OD) at 25 ºC. (a) is one proton from PDSMA, (b) is one proton from HPMA, (c) is two protons from DMAEMA, (d) is two protons from BMA, (e) is 6 protons from DMAEMA and the sum of protons from 0.5-3.1 ppm are from HPMA (10), DMAEMA (13), PDSMA (9), PAA (9), and BMA (12).

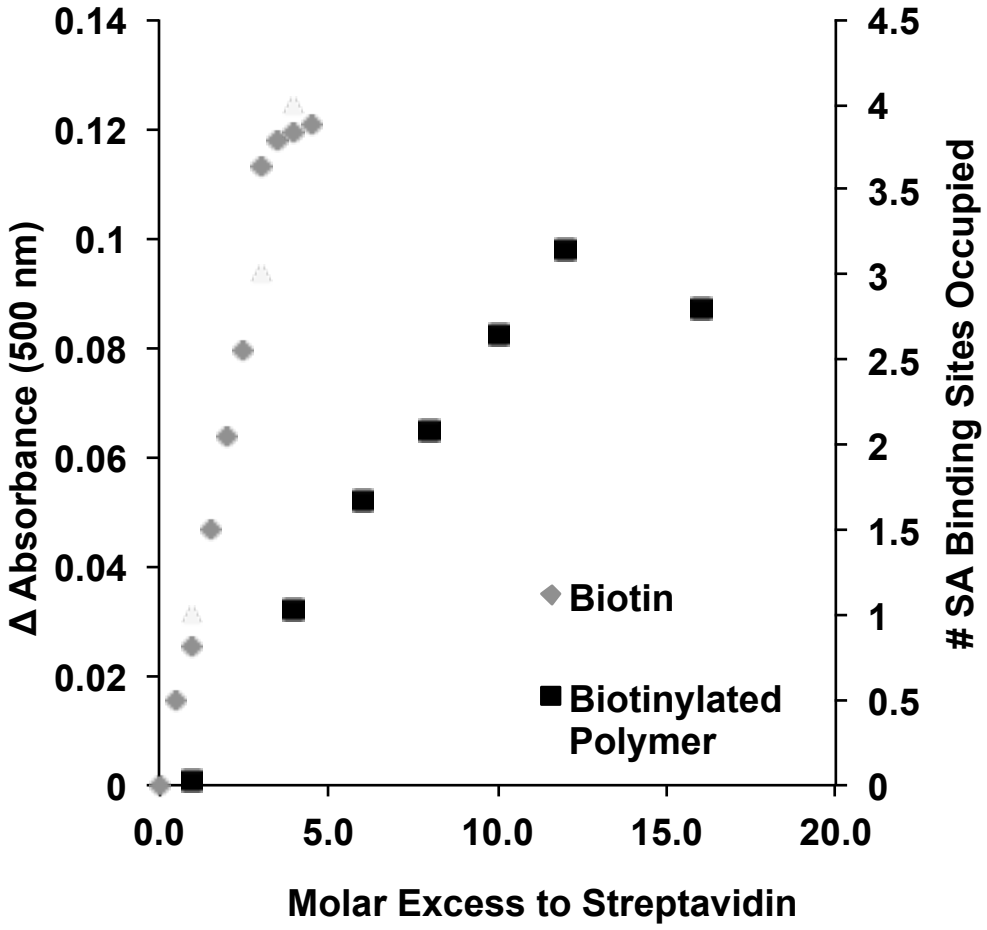

Supporting Figure S 3.3 Quantitative analysis of biotin on polymer.

HABA (4-hydroxyazobenzene-2'carboxylic acid) assay to determine the molar excess of polymer required to occupy one-biotin binding site on streptavidin.

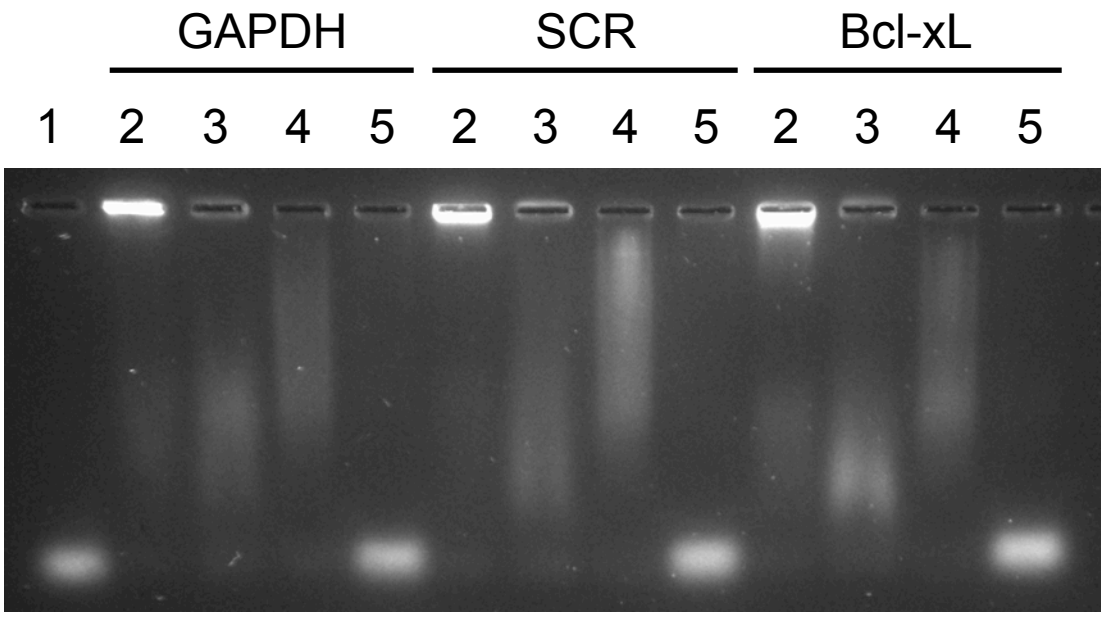

Supporting Figure S 3.4 siRNA-polymer conjugation validation.

Gel Retardation Assay validating polymer-siRNA conjugation via a reducible disulfide bond for thiolated GAPDH, SCR, and Bcl-xL siRNA. 1 μg siRNA/lane. Lane: Free thiolated siRNA (1), 1:10 (siRNA:Polymer) polymer-siRNA conjugate (2), polymer-siRNA conjugate and 0.1 M DTT to reduce disulfide linkages (3), polymer-siRNA conjugate and 1 % SDS to disrupt electrostatic interactions and micelle morphology (4), polymer-siRNA conjugate, 0.1 M DTT and 1 % SDS (5).

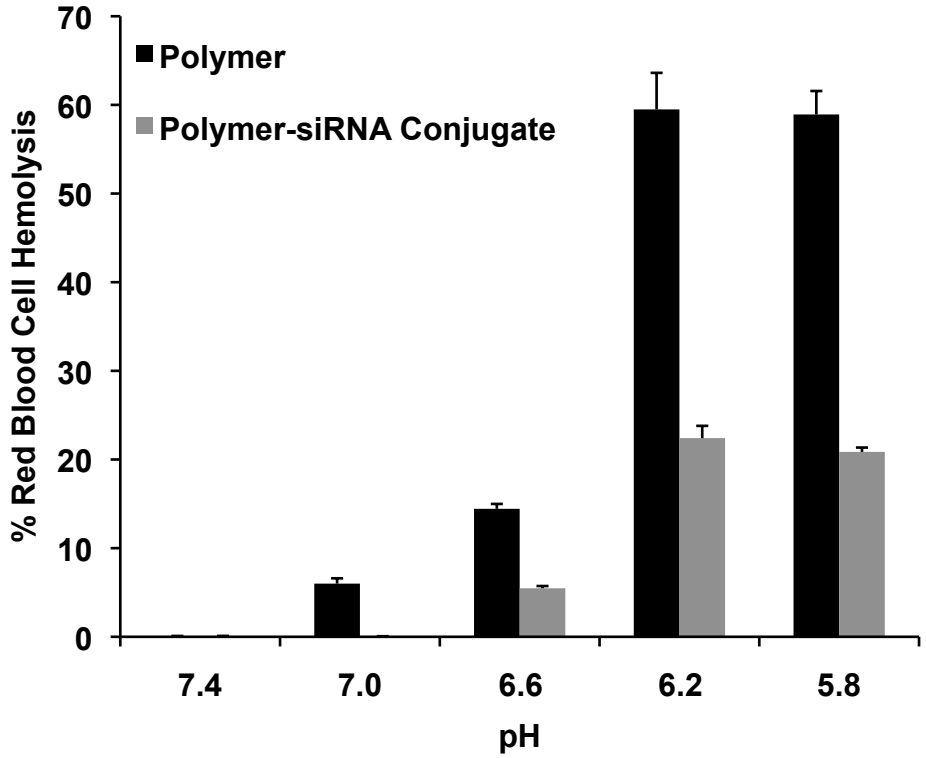

Supporting Figure S 3.5 siRNA-polymer pH-responsive membrane destabilization.

Hemolysis of the poly [(HPMA-co-PDSMA)-b-(PAA-co-DMAEMA-co-BMA)] diblock copolymer, poly [(HPMA-co-PDSMA)-b-(PAA-co-DMAEMA-co-BMA)] diblock copolymer-siRNA conjugates at a 1:10 siRNA to polymer ratio at pH concentrations of 5.8, 6.2, 6.6 and 7.4 of 40 μg polymer/mL. Hemolytic activity is normalized relative to a positive control, 1 % v/v Triton X-100, and the data represent a single experiment conducted in triplicate ± standard deviation.

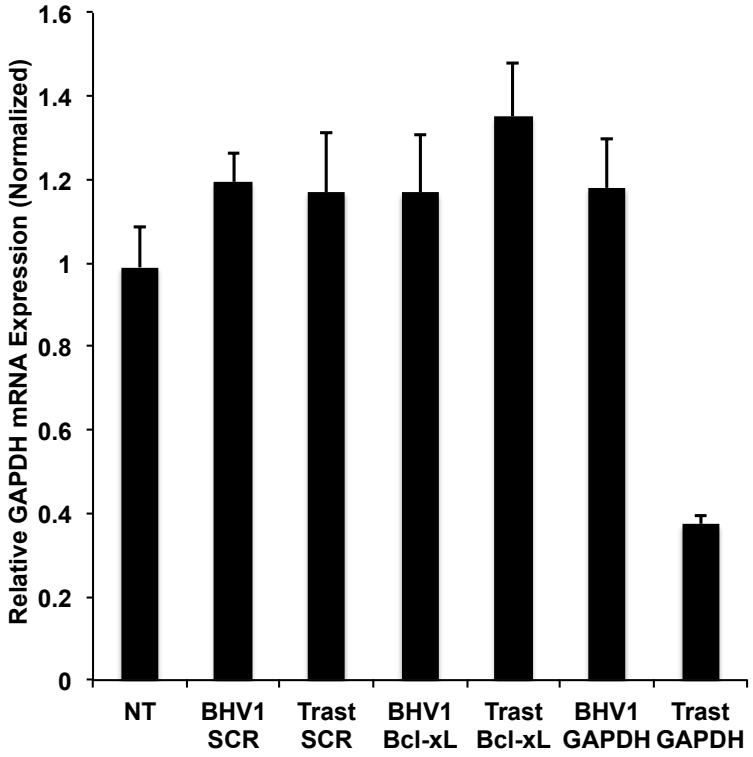

Supporting Figure S 3.6 Validation of RNA silencing in SKOV3 EA8 cells.

Trastuzumab-mediated reduction of Glyceraldehyde-3-phosphate dehydrogenase (GAPDH) gene expression of EA8 cells treated with Trastuzumab targeted siRNA-polymer conjugates containing siRNA directed against GAPDH, or BCL-xL, or a negative control siRNA (SCR) with no sequence homology to known human genes. GAPDH mRNA levels were assayed by quantitative reverse transcription (qRT)-PCR at 24 hrs after a 2 hr pulse-chase with siRNA-polymer conjugates bearing Trast-SA (Trastuzumab-targeted conjugate) and BHV1-SA (nontargeted conjugate). The poly [(HPMA-co-PDSMA)-b-(PAA-co-DMAEMA-co-BMA)] diblock copolymer was conjugated with thiolated siRNA at 1:15 siRNA to polymer ratio and cells were dosed with 50 nmol/L siRNA for 2 hours. Values are normalized to the housekeeping gene PPIA (Cyclophilin A) and relative to GAPDH expression in untreated cells. Data represents two independent experiments. Error bars represent the mean GAPDH expression ± standard error of triplicate samples.

Chapter 4. IN VIVO ASSESSMENT OF SIRNA-POLYMER CONJUGATE FOR THE TREATMENT OF ACUTE LUNG INJURY

Small interfering RNA (siRNA) has the potential to become a robust therapeutic strategy to control cellular processes at the post-transcriptional level. However, the systemic administration of siRNA *in vivo* has many additional challenges prior to cytosolic delivery to a target cell, including renal clearance, uptake by phagocytes, aggregation with serum proteins, and enzymatic degradation by endogenous nucleases. To overcome these challenge, siRNA has been previously formulated into nanoparticles composed of lipid and lipid-like materials, polymer-based nanocarriers, or siRNA conjugates. Here we describe the development and systemic administration of a neutral, pH-responsive polymer for the direct conjugation of a therapeutic siRNA against transforming growth factor beta 1 (TGF-β1). TGF-β1 is secreted by immune cells during inflammation and plays a substantial role in wound healing. TGF-β1 has been implicated in acute lung injury (ALI), a disease characterized by rapid increases in lung inflammation, inadequate perfusion, and high morbidity and mortality. Here, we evaluated pharmacokinectic behavior, cellular uptake, safety, and efficacy of our neutral siRNA-polymer conjugates *in vivo* for the treatment of inflammation after ALI. We found that systemic delivery of macrophage targeted siRNA-polymer conjugates at a 2 mg TGF- β1 siRNA/kg daily dose for 3 consecutive days was insufficient to reduce TGF-β1 mRNA levels in alveolar macrophages *in vivo*. We presumed this was due to poor carrier distribution to the resident lung macrophages, and future work will be conducted to evaluate gene-silencing capabilities of this system in peritoneal macrophages after intraperitoneal administration.

4.1 INTRODUCTION

ALI is a severe form of rapid-onset diffuse lung disease that causes insufficient gas exchange and poor end-organ perfusion. Approximately 190,000 patients are diagnosed each year in the Unites States, and nearly half of these patients die annually from the condition[132]. Due to the variability and complexity of the clinical course, the underlying pathophysiology is only marginally understood[133]. ALI is often secondary to other illnesses such as sepsis or pneumonia, but other insults such as physical trauma or chemotherapy agents like Bleomycin can also precipitate the disease[133,134], which only complicates the understanding its pathophysiology. In high doses, bleomycin, can lead to lethal ALI via recruitment of neutrophils, macrophages, and lymphocytes, and pulmonary fibrosis in both humans and mice[134], which has allowed researchers to study ALI and its treatment in mice models.

Animal models of ALI have suggested several critical processes in pathophysiology of ALI. These include processes involving the alveolar epithelium, endobronchial homeostasis, and the immune response of neutrophils and alveolar macrophages[135]. The pathophysiology of ALI has three primary stages (**Figure 4.1**); (1) initial onset of acute inflammation with neutrophil infiltration, (2) fibroproliferation with varying degrees of fibrosis, and (3) resolution. The resolution phase is not defined by the relief of injurious agents but rather by removal of apoptotic neutrophils, remodeling of the matrix, and reabsorption of the protein rich alveolar fluid[133].

The current standard of care for the treatment of ALI is to place patients on low-tidal volume ventilation and administer glucocorticoids to reduce inflammation[133]. Unfortunately this course

of action is not always effective. Therapeutic strategies are thus limited and do not specifically target the progress of the illness.

To date researchers have primarily focused on investigating the first stage of ALI in hopes of identifying potential therapeutic strategies. These candidate targets include preserving alveolar epithelial/endobronchial homeostasis and modulating the immune response in alveolar neutrophils. Literature reports have implicated that factors including transforming growth factor-β (TGF-β), tumor necrosis factor-α, IL-1B, macrophage-inflammatory protein-1α, monocyte chemoattactant protein-1, reactive oxygen species, and Fas/Fas ligand interactions all play a role in bleomycin-induced ALI[134]. The disruption of one or several of these candidate genes may provide a clinical benefit in patients with ALI.

Recent studies have investigated the use of siRNA to disrupt gene expression and minimize ALI morbidity and mortality. Perl, *et al*. recently demonstrated the efficacy of preventative therapeutic siRNA against caspase-3 in lung epithelial cells for the prevention of apoptosis and inflammation. A single intratrachael treatment (3 mg siRNA/kg mouse) before ALI initiation subsequently improved ALI symptoms and 10-day survival of hemorrhaged septic mice[136]. Thus far, successful studies to ameliorate ALI with specific gene suppression have been conducted *in vivo* in pre-treatment animal models.

Here, we report the evaluation of the neutral siRNA-polymer conjugates reduce gene expression in alveolar macrophages with mannosylated and non-targeting siRNA-polymer conjugates in a bleomycin-induced lung injury model. We have characterized the biodistribution,

pharmacokinetic properties, macrophage targeting, and toxicity of this system in both healthy and ALI mice.

4.2 Materials and Methods

4.2.1 Materials

Alexa Fluor 750 C5-maleimide probe and Quant-iTTM OliGreen® ssDNA Reagent were purchased from Invitrogen. PD10 columns were obtained from GE life sciences. Amicon Ultra-0.5 mL Centrifugal Filters for Protein Purification and Concentration buffer exchange columns were obtained for Millipore. Amplite Ethanol Quantification Assay kit was purchased from AAT Bioquest.

4.2.2 Mannosylated polymer synthesis and characterization

The poly[(HPMA-co-PDSMA-co-ManEMA)-(PAA-co-DMEAMA-co-BMA)] was synthesized and characterized with SEC and ^{1}H NMR by Salka Keller (Stayton Laboratory). siRNA conjugation protocol and validation with an agarose gel electrophoresis was describe in Chapter 2. An agglutination assay was conducted to evaluate the mannose-binding lectin A of the polymer and polymer siRNA conjugates. 1 μM polymer was incubated with 1mM Concanavalin A in 1X PBS (pH 7.4) and the change in absorbance at 350 nm was monitored spectrophotometrically for 30 mins. *In vitro* conditions for polymer-siRNA conjugate efficacy in HeLa cells was described in Chapter 2.

4.2.3 Polymer conjugate purification and characterization

siRNA-polymer conjugates (described in Chapter 2) were purified using Amicon Ultra-0.5 mL Centrifugal Filters (3k MWCO) to remove trace organic solvents remaining from the conjugation protocol. Briefly, conjugates and polymer controls underwent 5 buffer exchanges with RNAse/DNAse-free 1x PBS (pH 7.4) to yield a final ethanol concentration of < 0.001% as determined with the Amplite ethanol quantification kit. Final polymer concentration was estimated spectrophotometrically by measuring absorbance at 286 nm, which corresponded to the PDS groups retained on the polymer. The final siRNA conjugate concentration was determined by a fluorescent assay using Quant-iTTM OliGreen® ssDNA Reagent.

4.2.4 Labeling polymer with Alexa 750

4.0 mg of poly[(HPMA-co-PDSMA)-b-((BMA)-co-(DMAEMA)-co-(PAA))] in 1X PBS (pH 7.0) was reduced with 10 M excess TCEP for 30 minutes to introduce free thiols on the polymer. 5M excess of Alexa Fluor 750 C5-maleimide (Invitrogen) reconstituted in DMSO (50 mg/mL) was added to polymer solution and purged under nitrogen. The reaction was allowed to run at 4°C for 2 hours. Fluorescently labeled polymer was purified with PD10 desalting columns and subsequently dried by lyophilization. The degree of labeling was determined spectrophotometrically at the maximum absorbance wavelength (754 nm with an extinction coefficient of 270,000 $cm^{-1}M^{-1}$ in methanol).

4.2.5 Labeling polymer with Oregon Green 488

Polymers were labeled with Oregon Green 488 Iodoacetamide at an equal molar ratio in a 50 mg/mL polymer solution in ethanol overnight at 4 °C. The reaction underwent 4 rounds of dialysis against methanol in a Slide-A-Lyzer Dialysis Cassette (7K MWCO), and a final round of dialysis against water. Purified labeled polymer was frozen, lyophilized, and labeling efficiency quantified with UV-vis spectroscopy.

4.2.6 Radiolabeling of Polymeric Carrier

A solution of poly[(HPMA-co-PDSMA)-b-(BMA-co-DMAEMA-co-PAA)] was prepared at 50 mg/mL in ethanol and reacted with 100 μCi of ^{3}H-labeled iodoacetamide for 24 hours at room temperature to quaternize the tertiary amines of the pH-responsive core. Reaction was then purified via gel chromatography with PD-10 columns twice and then evaluated on a scintillation counter to determine labeling efficiency. Polymer concentration was then quantified spectrophotometrically.

4.2.7 Establishment of Bleomycin-Induced Lung Injury in a Mouse Model

C57BL/6J mice (8-16 weeks, Jackson Laboratories) were administered bleomycin via intratracheal instillation at a dose of 2.1 U/kg and monitored for behavior, survival and weight loss. 72 hours later, GAPDH or scrambled siRNA-polymer conjugates or polymer alone were administered via retro-orbital injection.

4.2.8 In vivo polymer delivery

siRNA-polymer conjugate or polymer alone was administered either intranasally or intratracheally. For experiments requiring intranasal delivery, animals were anesthetized using Isoflurane and 25 μL of siRNA-polymer conjugate or polymer alone was deposited at the surface of the nose. For experiments requiring intratracheal (IT) delivery, animals were anesthetized, intubated with a 24 gauge trochar, and administered 50 μL of siRNA-polymer conjugates or controls intratracheally. For experiments required intravenous (IV) delivery, animals were anesthetized, and 200 uL of the polymer-siRNA conjugates was injected retro-orbitally. Mice were sacrificed 72 hours later with Euthanasia solution, and the alveolar macrophages were isolated via bronchoalveolar lavage (BAL) with PBS with 5 mM EDTA. The total remaining lung tissue was also harvested for qPCR analysis.

4.2.9 In vivo Toxicity Evaluation

Toxicity of the siRNA-polymer conjugate was monitored via animal weight loss and the BAL fluid was subjected to a complete blood count with differential. To evaluate toxicity, C57BL/6J mice were administered polymer at escalating doses (7.5 mg/kg to 120 mg/kg polymer in healthy mice and 30 mg/kg to 90 mg/kg in bleomyocin-injured mice). Mice were then monitored for survival, behavior, and weight loss daily. After 24 hours (for injured mice) and 72 hours (for healthy mice), mice were weighed and sacrificed followed by bronchoalveolar lavage was performed to collect samples to determine the presence or absence of lung injury. Blood was also collected via cardiac puncture for evaluation of levels of liver enzymes. To evaluate lung injury, BAL fluid was evaluated for red blood cell and white blood cell count, as well as total protein concentration by a Bradford protein assay. Organs were collected for histology.

4.2.10 Biodistribution of ^{3}H-radiolabeled carrier in healthy mice

To evaluate biodistribution within healthy mice, C57BL/6J mice (Jackson Laboratories) were administered ^{3}H-labeled polymer at polymer doses of 90 mg/kg with each mouse receiving 2 μCi of tritium labeled polymer via retro-orbital injection. Blood samples were taken from mice retro-orbitally from the opposite eye at time points of 2, 5, 30, 120, 240, 480, and 1440 minutes ($n \geq 3$). Mice were sacrificed at time points of 2, 8, and 24 hours at which point a bronchoalveolar lavage was performed with 1 mL of PBS via a 20 gauge tubing adapter to collect alveolar macrophages followed by organ harvesting for evaluation including the brain, heart, intestines, kidneys, liver, lung, spleen, and stomach. Tissues were then washed in PBS and homogenized in ddH_2O at 0.1g/mL. 200 μL of homogenate was taken for each organ and treated with 500 μL of Solvable (Perkin Elmer) at 60°C overnight to solubize tissues. Samples were decolored by the addition of 250 μL of 40 mM EDTA / 24 % H_2O_2 and incubated overnight at room temperature. Samples were then treated with 25 μL of 1N HCL and 15 mL of Ultima Gold scintillation fluid. Samples were vortexed and incubated for 24 hours at room temperature, and then read on a scintillation counter. Blood samples were directly added to 500 μL of solvable and treated identically for the remainder of the preparation.

4.2.11 Biodistribution of Alexa fluor 750-labeled carrier in bleomycin-injured mice

To evaluate the biodistribution within an acute lung injury model, a bleomyocin-induced injury was conducted C57BL/6 mice. Mice were monitored for 72 hours, and then intravenously administered fluorescently labeled polymer at a dose of 60 mg/kg via retro-orbital injection. The control mice were uninjured, uninjured and administered polymer, or bleomycin-injured with

PBS administration. At 2 and 24 hours post-administration mice were lavaged to collect alveolar macrophages. Following lavage, blood was collected via cardiac puncture and relevant organs (lungs, liver, spleen, heart, and kidneys) were harvested for evaluation. Tissues were washed in PBS and then imaged as whole organs on the Xenogen Spectrum IVIS to visualize dosing. Organs were then homogenized at 0.2 g/mL in ddH_2O and evaluated on a fluorescence plate reader (Tecan Safire 2) to determine polymer concentrations within the tissues. Isolated alveolar macrophages were then fixed in paraformaldehyde and evaluated for mean and median fluorescence intensity using flow cytometry (FACSCalibur).

4.2.12 Macrophage Targeting with Oregon Green 488 Polymer

To evaluate the relative polymer uptake by macrophages in C57BL/6 mice, mice received an intravenous injection of fluorescently labeled mannosylated or non-targeting polymer at a dose of 60 mg/kg or 120 mg/kg via retro-orbital injection. Control mice received a retro-orbital injection of PBS. At 24 hours post-administration mice were lavaged to collect alveolar macrophages. Following lavage, blood was collected via cardiac puncture and the spleen was harvested for macrophage isolation. Red blood cells (RBCs) in the blood were lysis with two round 5 minute incubators in RBC lysis buffer. The spleen was crushed with a plunger to cells were isolated. Isolated alveolar macrophage, circulating macrophages, and splenic macrophages double stained with CD11 and F40/80 macrophage markers, fixed in paraformaldehyde, and evaluated for mean and median fluorescence intensity using flow cytometry (FACSCalibur).

4.2.13 Evaluation of mRNA Knockdown

Animals were sacrificed at 72 hours with an intraperitoneal injection of Euthanasia solution, and alveolar macrophages were isolated via bronchoalveolar lavage with PBS with 5 mM EDTA. Total mRNA was isolated from homogenized lung tissue and reverse transcribed. Total RNA from both the alveolar macrophages and whole organ homogenate was isolated 72 hours post treatment, and GAPDH or TGF-β1 expression was measured relative to the internal normalizer genes, B-actin or HPRT, by quantitative PCR.

4.2.14 Statistical analysis

ANOVA was used to test for treatment effects at a significance of $p<0.05$, and Tukey's test was used for post hoc pairwise comparisons between individual treatment groups.

4.3 Results And Discussion

4.3.1 Intranasal (IN) delivery

We have previously demonstrated successful mRNA and protein knockdown *in vitro* using this pH-responsive siRNA conjugate system, but in order to test this platform as a potential future therapeutic, evaluation of this neutral siRNA delivery system *in vivo* is also necessary. We first assessed siRNA conjugate safety by using intranasal delivery to target alveolar macrophages (AMs) due to their robust intrinsic endocytosis characteristics. Female BALB/c mice (n=3) received either 0.75 mg/kg siRNA (GAPDH-siRNA conjugate) or PBS. The mice were monitored daily for changes in weight or behavior, and after 72 hours the lung tissue was

harvested and homogenized. No weight loss or behavior changes were observed throughout the course of the study, which grossly suggests adequate biocompatibility of the siRNA-polymer conjugates. Furthermore, real time quantitative PCR on RNA isolated from the tissue revealed GAPDH knockdown in 2 out of the 3 mice administered with GAPDH-polymer conjugates (**Figure 4.2**). While these values trended towards successful knockdown, this study was underpowered, and in the future a larger study must be undertaken. Based on this result, we hypothesized that changing the delivery route to intratracheal (IT) administration would result in more consistent siRNA delivery to the lungs.

4.3.2 Intratracheal (IT) delivery

In collaboration with the Schnapp Laboratory, we delivered siRNA-conjugates using IT delivery and a more rigorous toxicity evaluation. To reduce ethanol concentration to less than 0.001%, we first revised the conjugate purification protocol to include 5 buffer exchanges, and we then determined the siRNA concentration via a fluorescent RNA assay. Next, we administered the conjugates to male C57Bl/6 mice (N=3) with GAPDH or scrambled siRNA-polymer conjugates (0.25 mg/kg siRNA dose). As expected, we did not see any significant weight loss in siRNA conjugate groups at this low siRNA concentration. A sham (PBS) animal was observed to have 8% weight loss in 72 hours, which was attributed to either a complication with anesthesia or a complication with the delivery of liquid to the lungs. Total red blood cell (RBC) counts of the BAL fluid had less than 20,000 RBCs in both the siRNA-conjugate groups and PBS control (data not shown). Since there was no difference in BAL RBC quantity between these groups, we concluded that the low siRNA-conjugate dose appears to be well tolerated by the mice. This conclusion is also supported by the low amount of white blood cells (75,000-150,000 cells) in

experimental animals, well within the range of the PBS control groups. Total BAL protein in all groups was less than 0.5 mg/mL, suggesting again that the polymer-siRNA conjugates have low toxicity at this dose. Although the local dose received in the lungs may be comparable to the dose received from the previous IN study, unfortunately no GAPDH mRNA suppression was observed in whole lung preparations (data not shown). RNA isolation from AMs was also unsuccessful.

The study was repeated to increase the siRNA dose (0.5 mg/kg) and to include a free polymer group (N=2) in addition to the GAPDH and scrambled siRNA-polymer conjugates (N=3). The animals that received polymer alone received the same amount of polymer as the siRNA conjugates groups (8.75 mg/kg). Weight loss was observed in 1 mouse from the polymer-only group and in 1 mouse from the GAPDH-conjugate group. All other animals did not show adverse signs with this higher dose. mRNA was successfully isolated from whole lung tissue, but again we observed no difference in GAPDH mRNA expression between sample groups. RNA knockdown was not observed in any organ isolated 72 h after IT administration. It is possible that the toxicity observed in the two animals may be a result of polymer toxicity or from other unknown factors during the delivery procedure. Ultimately, it was difficult to elucidate meaningful statistical conclusions with a sample size this small. Nevertheless, with at most only 1 out of 6 mice exhibiting any signs of toxicity after receiving siRNA conjugates, we felt we had satisfactory evidence that these conjugates are moderately tolerated. On the other hand, we administered polymer alone from 0 to 70 mg/kg (corresponding to siRNA doses of 0.5, 1, 2, and 4 mg/kg) and observed toxicity above 15 mg polymer/kg as evidenced by significant weight loss

and death. We concluded that the surfactant-like nature of the polymer prevented this method of delivery from being clinically viable for siRNA-based therapy delivery to the lungs.

Moving forward, we hypothesized that our repeated inability to isolate RNA from the BAL macrophages was a result of the insignificant quantity of AMs in the non-injured mouse model. By inducing a lung injury as described by Kass *et al*.[9,137], we expected to see pneumonitis and edema with an influx of inflammatory cells into the alveoli as assessed by alveolar lavage[138].

4.3.3 Intravenous (IV) delivery

Male C57BL/6 mice from 8-16 weeks of age were injected via retro-orbital injection to healthy and bleomycin-injured mice in order to test polymer toxicity in the bloodstream. The polymer batches synthesized as previous described in chapter 2 had a similar composition and block ratio of 1 to 2.25.

To evaluate carrier toxicity, mice were administered polymer via retro-orbital injection at range from 7.5 mg/kg to 120 mg polymer/kg mouse in PBS and subsequently evaluated for signs of general toxicity including weight loss, aspartate aminotransferase (AST) and alanine aminotransferase (ALT) liver enzyme levels, signs of lung injury (total protein, red blood cell, and white blood cell levels in bronchoalveolar lavage (BAL) fluid), and tissue histology. Criteria for acceptable levels in each of these categories was as follows: Mean values of less than 10 % weight loss at 3 days post administration, no greater than 2-fold increase in liver enzymes (ALT/AST), and less than 50 % change in BAL cell counts.

Our results demonstrated that the average weight loss 72 hours following administration was below 10 % for all polymer doses evaluated; however, there was a positive correlation between increased weight loss and polymer dose (**Figure 4.3a**). For all the polymer doses, AST and ALT liver enzyme levels were increased by 19 % and 45 % respectively, but these values are still considered to be in the normal range (**Figure 4.3b, 4.3c**). Common markers of lung injury were also evaluated to determine any polymer-related lung toxicity. Results from our studies demonstrated less than 50 % increases in total protein, red blood cells/mL and white blood cells/mL in the BAL samples isolated from each mouse 72 hours post-administration for polymer doses of 90 mg/kg or less (**Figure 4.3d, 4.3e, 4.3f**). The 120 mg/kg dose demonstrated minimal signs of lung injury as determined by total protein and white blood cell levels; however, this dose did have a near 2-fold increase in red blood cells in the BAL fluid. Lung histology demonstrated no apparent lung injury, as shown by representative images from the 90 mg/kg dose (**Figure 4.4**). From these results, we have determined that the maximum tolerated polymer dose for intravenous administration is 120 mg/kg body weight in non-injured mice.

To determine the upper limit of polymer for IV administration, polymer toxicity was evaluated in mice with a bleomycin-induced acute lung injury (ALI). ALI was established with an IT administration of bleomycin at 2 U/kg. Mice were then monitored for 72 hours to allow for disease progression. Body weight for these mice was taken daily to evaluate systemic toxicity. Three days post injury, mice were treated with either PBS or polymer at doses of 30, 60, or 90 mg/kg via retro-orbital IV injection. Due to their higher susceptibility to toxicity following ALI, signs of toxicity described above were evaluated at 24 hours rather than the 72 hours post-

administration studied for healthy mice; however, criteria to evaluate an acceptable polymer dose with low toxicity remained the same.

Baseline observations at 3 days post-injury showed weight loss for the injured mice varied from 0 to 12.4 %. Following polymer administration, only mice receiving a 90 mg/kg polymer dose demonstrated a overall mean weight loss above 10 % at 24 hr (data not shown). When evaluated as a percent weight loss from the time of carrier administration, however, all dosage groups demonstrated a mean weight loss at 24 h of less than 10 % as shown in **Figure 4.5a**. Furthermore, levels of the liver enzymes following polymer administration demonstrated less than 2-fold increases for both AST and ALT for polymer doses at 60 mg/kg and below (**Figure 4.5b, 4.5c**). No elevation greater than 50 % in value of common lung injury markers (BAL values of total protein, red blood cell, and white blood cell concentrations) was observed (**Figure 4.5d, 4.5e, 4.5f**). It should be noted that while the mean value of the BAL RBC concentration for the 60 mg/kg dose was greater than 50 % higher than the control bleomycin-injured mice, this result was due to a single mouse which demonstrated a significantly higher overall injury (based on weight loss) even prior to carrier administration. The weight loss and elevated liver enzyme results from this study prompted us to limit our maximum dose in RNA knockdown studies to 60 mg/kg polymer in bleomycin-injured mice.

4.3.4 Biodistribution

To evaluate polymer biodistribution after an IV administration, C57BL/6 mice (6-10 weeks in age) were given ^{3}H-radiolabeled polymer via retro-orbital injections and blood and organs were collected at various time points. Polymers were modified by quarternization of primary amines

with a tritium(^{3}H)-containing iodoacetamide reagent, and samples were purified via gel chromatography and evaluated for labeling efficiency. A mixture of radiolabeled and unlabeled polymer constituted a 2 μCi dose of tritium with a final polymer dose of 90 mg/kg. Blood was collected was conducted 2, 5, 30, 60, 120, 240, 480, and 1440 minutes after injection. Organs were harvested after 2, 8, and 24 h with 5 mice per time point. Organ and blood specific radiation content was assessed and utilized to determine the polymers pharmacokinetic parameters and quantify organ specific accumulation.

Detectable levels of the polymer were observed within the blood circulation for as long as 24 h following retro-orbital injection (**Figure 4.6a)**. Pharmacokinetic parameters of the polymer system were determined using a non-compartmental model with the Graph Pad Prism software and are presented in **Table 4.1**. The polymer had early and late half-lives of 0.511 h and 2.15 h, respectively. This data signifies a precipitous clearance followed by a more linear, gradual clearance as seen in **Figure 4.6a**. The area under the serum concentration-versus-time curve (AUC) was calculated using the logarithmic trapezoidal method. Here we have determined an $AUC_{o-\infty}$ value of 124.4 mg•h/mL.

Polymer accumulation in solid organs demonstrated high uptake within the liver and spleen at all time points (**Figure 4.6b**). Accumulation in the kidneys and lungs was also noted with decreased accumulation over time in both organs. Minimal uptake was seen in the BAL fluid. Without the presence of injury, the lung vasculature is well maintained; therefore this result is not unexpected. Minimal uptake was observed in the brain, heart, stomach and intestines. In

summary, we have determined that the bulk of uptake was largely focused within the liver and spleen; however uptake in the lungs could potentially be increased in mice with ALI.

While the polymeric carrier demonstrated minimal uptake in the BAL cells in healthy mice, we hypothesized that the vascular leakage in the lungs during acute lung injury will provide enhanced access to the macrophage populations, which are also found in greater numbers in the injured lung. To evaluate this hypothesis, bleomycin-injured mice were administered fluorescently labeled carriers via retro-orbital injection 72 h following lung injury. Mice were then sacrificed at time points of 2 and 24 h post administration for organ, blood, and BAL evaluation for carrier content. Based on our initial polymer toxicity studies in the injured mice, a dose of 60 mg/kg was utilized for these studies. Only the relevant tissues of interest (lungs, liver, spleen, heart, and kidneys) were evaluated. Detection of fluorescence was conducted by Xenogen, plate reader, and flow cytometry.

Polymer uptake profiles were similar to those observed to in healthy mice (**Figure 4.7**). While higher uptake within the kidneys was noted in this study as compared to our initial radiolabeled study in healthy mice, the non-injured control mouse also demonstrated this increase, which suggests the effect may be due to differences in polymer labeling methodology. Polymer uptake in the total lung was 40 % higher on average for injured mice as compared to the healthy mouse at 2 h (data not shown).

Polymer uptake by macrophages in the BAL fluid was evaluated by flow cytometry. After 24 hr, the polymer had a 2.5 fold increase in mean fluorescence over the PBS treated mice in ALI,

while the amount of polymer taken up by macrophages in healthy mice was barely above baseline (**Figure 4.8**). Although, this initial data appeared to be promising, the overall fluorescence was still relatively low, and only 25 % of the AMs from injured mice were considered positive for the presence of polymer. Based on these results, we next incorporated mannose targeting in the diblock copolymer to facilitate macrophage uptake. Yu, *et al*. reported that mannose targeting nanoparticles improved the delivery of siRNA into primary macrophages by 4-fold relative to a nontargeted control[119,139]. We hypothesized with a greater percentage of cells taking up the carrier via receptor mediate endocytosis that we would have a greater probability of observing RNA knockdown within this population of cells.

4.3.5 Development of a Mannose-targeted diblock copolymer for targeted siRNA delivery

A diblock glycopolymer containing functional mannose targeting, pyridyl disulfide groups for thiolated siRNA conjugation, and a pH-responsive, membrane-lytic segment was successfully synthesized via two sequential RAFT polymerizations (**Scheme 4.1**). Salka Keller (Stayton Lab) developed the synthetic conditions to incorporate a mannosylated monomer (ManEMA) into the corona of our existing diblock copolymer system. The mannose-targeted macroCTA was prepared via RAFT polymerization with similar reactions conditions to the non-targeted diblock. Briefly, the ethanol and water mixed solvent system was employed at the previously specified volume ratio in order to predissolve the hydrophobic and hydrophilic reaction components, respectively. The reaction occurred at a 16 weight % monomer and macroCTA was to solvent at 70 °C under a nitrogen atmosphere for 6 h. ManEMA was targeted at 10 % and the PDSMA content was reduced slightly to 7 %. The initial CTA to monomer molar ratio ($[CTA]_0$:$[M]_0$) and the initial CTA to initiator molar ratio ($[CTA]_0$:$[I]_0$) was 100:1 and10:1, respectively. ECT was

used as chain transfer agent (CTA) and V501 was the source of free radicals. Purified polymer was achieve via dialysis against water for 48 h at 4 °C using a 1000 MWCO dialysis membrane, followed by lyophilization for 48 h. The second block was polymerized and characterized with the same conditions previously described in Chapter 2.

The RAFT synthetic conditions for the glycopolymer were similar to the non-targeting polymer previously described in chapter 2 and 3, and more importantly yielded polymers with similar overall characteristics. Successful chain extension was confirmed by unimodal molecular weight distributions and a clear shift in elution times by SEC (**Figure 4.9**). The first block was reported at 9.9 kDa with PDI of 1.1 and the overall polymer was 32 kDa with a broaden PDI of 1.4. Polymer composition was determined by ^{1}H-NMR spectroscopy in DMSO (**Figure 4.10**). Analysis revealed 19 % ManEMA, 4 % PDSMA, and 77 % HPMA in the first block, and a 31 % PAA, 20 % DMEAMA, and 49 % BMA in the second block. Accessible PDS groups measured via a TCEP reduction assay were determine to be 2 – 3 PDS per polymer chain.

The methodology for siRNA conjugation to the mannosylated diblock copolymer was previously described in chapter 3. As expected, siRNA conjugations conducted at a 10:1 polymer to siRNA ratio showed greater than 95 % siRNA conjugation (**Figure 4.11**). Electrophoresis of the conjugates following incubation with DTT and SDS resulted in a reappearance of the free siRNA band. These reversible bonds can be cleaved in the cytoplasm of target cancer cells by glutathione reduction.

To confirm mannose binding capability of this mannosylated diblock copolymer, an agglutination assay was performed. Briefly, the mannose polymer and mannose polymer-siRNA conjugates were incubated with Concanavalin A. As the mannose binds the lectin Concanavalin A, the aggregation of sugar polymers tethered together via the binding protein increases and the solution becomes turbid. By monitoring the absorbance at 350 nM for 30 min, we concluded that the siRNA-polymer conjugates successfully agglutinates mannose-binding lectin Concanavalin A (**Figure 4.12**). The non-targeted control polymer poly[(HMPA-co-PDSMA)-b-(PAA-co-DMAEMA-co-BMA)] did not change in absorbance in the presence of Concanavalin A.

Membrane-lytic behavior of the mannosylated polymer and siRNA conjugates was evaluated with a red blood cell (RBCs) lysis assay. The mannose targeted polymer and siRNA conjugates (1:10 siRNA to polymer ratio) were incubated in solutions containing RBCs at pH-values representative of the endosomal-lysosomal pathway for 1 h. Total polymer concentration was normalized to 40 μg/mL. The supernant containing released hemoglobin was evaluated at 541 nm with UV-spectroscopy, and the percent RBC lysis was normalized to the surfactant, Triton-X. As expected, both the mannosylated polymer and mannosylated polymer-siRNA conjugate exhibited membrane disruptive behavior at pH values of 5.8 and 6.2 (**Figure 4.13**).

We previously demonstrated that non-targeted, pH-responsive siRNA-polymer conjugates can efficiently deliver siRNA in the immortalized HeLa cancer cell line[125]. The ability of mannosylated polymer-siRNA conjugates was evaluated with real-time quantitative PCR of RNA isolated from HeLa cells. Conjugates were prepared with either mannosylated polymer or

the non-targeting poly[(HPMA-co-PDSMA)-b-(PAA-co-DMEAMA-co-BMA)] control polymer conjugated to the Glyceraldehyde-3-phosphate dehydrogenase (GAPDH) siRNA at a 1:10 siRNA to polymer ratio (**Figure 4.14**). The cells were then incubated for 48 hours with the conjugates in media containing 10 % FBS. The final siRNA concentration for the conjugates was 50 nmol/L and 25 nmol/L for the commercial available HiPerFect positive control. Mannosylated GAPDH conjugates successfully reduced GAPDH to 30 % and their knockdown ability was similar to the non-targeted polymer-siRNA conjugates previously evaluated. Based on this result, we believe that mannosylated polymer-siRNA conjugates would be as effective as the previously described non-targeting polymer *in vivo*. Furthermore, any enhanced RNA interference activity may be attributed to the addition of mannose moieties to enhance macrophage specific uptake.

4.3.6 Macrophage Uptake with Mannose Targeting Polymer in vivo

Prior to evaluating the effect of mannose incorporation in the polymer system, we evaluated the biocompatibility of both our carrier systems (mannose-targeted and non-targeted) following intravenous injection. In the case of both polymers at up to 120 mg/kg doses, the weight loss was minimal while increases in liver enzyme production remained within a reasonable range (data not shown).

To determine the effects of incorporating mannose residues within our polymeric carriers, we studied both the biodistribution and specific uptake within alveolar macrophages following administration of the carriers by retro-orbital injections at a 60 mg/kg polymer dose in both healthy and bleomycin-injured mice. The organs evaluated during these studies included liver,

lungs, spleen, heart, and kidneys. Tissue homogenates and blood were then evaluated on a fluorescence plate reader. Initial studies showed non-difference in the mannosylated polymer accumulation compared to the non-targeted polymer in the bleomycin-injured mice (data not shown). We hypothesized that the nature of the injury caused significant vasculature disruption negating the effect of targeting. However, the mannose-targeted carrier did seem to have a slight increase in uptake in alveolar macrophages of healthy mice as determined via flow cytometry. We repeated the study and looked for specific uptake within alveolar macrophages, circulating macrophages in the blood, and macrophages in the spleen. Fluorescently-labeled polymers were administered to healthy male C57BL/6J mice by retro-orbital injection, and tissue collection was performed at 24 hours post-administration. Uptake was evaluated at two different polymer doses (120 mg/kg and 60 mg/kg) to determine if there was a dose-dependent macrophage uptake effect. Cells from the BAL, blood, and spleen were double stained for macrophage markers (CD11+ and F4/80+) and present of polymer in these populations was evaluated via flow cytometry (**Figure 4.15**).

Cells isolated from the BAL fluid approached 100 % CD11+ and F40/80+ for all groups, indicating that the recovered cells were alveolar macrophages and that the administration of polymer did not cause an influx of other immune cells into the lungs at 24 hours. Approximately, 5 % and 10 % of the cells isolated from the blood and spleen were determined to be macrophages, which is consistent with what is expected. However, we do see a 50 % increase of macrophages with the high dose polymer administration in the spleen, indicating there may be an immune response associate with this dose.

The mean fluorescent intensity was slight greater in the alveolar macrophages (AMs) with the mannose-targeting polymer than the non-targeting polymer at the 60 mg/kg dose. However, at the higher dose (120 mg/kg) we did not observe any targeting effect (**Figure 4.16**). Surprisingly, the mean fluorescent intensity was reduced compared to the low dose (60 mg/kg). Although, we do see a slight increase in the MFI with the mannose polymer in AMs, the overall fluorescent intensity is significantly less than the macrophages isolated from the blood or lungs (**Figure 4.17**). In particular, the non-targeting polymer appears to have a greater accumulation in the macrophages isolated from the blood and spleen, particularly at the higher dose. Therefore, from this data, it does not appear that mannose-targeting will facilitate macrophage targeting and efficacy of the siRNA conjugates. Although, Yu, *et al*. reported that mannosylated nanoparticles similar in composition to the ones we developed, they were only able to demonstrate targeted specific uptake *in vitro* with a 4 hour incubate of their conjugates in primary macrophages[120,139]. Perhaps, delivery of siRNA carriers via systemic administration allows for the internalization by phagocytosing cells to such an extent that the presence of mannose to target macrophages is mute.

4.3.7 Polymer-siRNA Conjugate Efficacy in vivo

While the siRNA-polymer conjugates have been evaluated for effective gene silencing in vitro, here we present our results evaluating *in vivo* gene silencing of the metabolic and model protein GAPDH as well as a therapeutic siRNA against TGF-β1. An initial pilot study was conducted with GAPDH siRNA non-targeted polymer conjugates at doses of 4 mg/kg and polymer doses of 90 mg/kg administered intravenously by retro-orbital injection into healthy, male C57BL/6J mice. After 72 h after administration, the animals were euthanized and a bronchioalveolar lavage was

performed to isolate alveolar macrophages. The lungs, liver, spleen, kidneys, and heart were also collected. We observed significant gene silencing in the liver (approximately 55 %) 72 h after polymer-siRNA conjugates administration (**Figure 4.18**). RNA activity was not observed in any other organ in though a significant amount distributes to the spleen. RNA isolation for the alveolar macrophages was unsuccessful, presumably due to inadequate numbers of alveolar macrophages or to RNA degradation during cell lysis by intrinsic nucleases[140].

No gene silencing was observed in any of the isolated organs (lungs, liver, spleen, kidneys, and heart) with the mannosylated-siRNA conjugates in a bleomyocin-injured model. The polymer concentration was reduced to 60 mg/kg even though the siRNA concentration stayed the same at 4 mg/kg to prevent carrier toxicity in the animals with ALI. However, as we observed the 60 mg/kg polymer dose was insufficient to cause RNA silencing in the liver. RNA isolation was also unsuccessful from cells in the BAL. The amount of neutrophils that permeate the injured lungs may increase the nuclease activity when the cells are lyzed, and the amount and quality of the RNA from these samples was insufficient to perform quantitative PCR, even though a large cell pellet was observed from the BAL.

We evaluated the effective of delivery 2 mg/kg siRNA and 120 mg/kg polymer for three consecutive days in non-injured mice with both the mannosylated polymer and the non-targeted polymer conjugated to either GAPDH or anti-TGF-β1 siRNA. As expected, RNA knockdown was observed in the liver for both the mannosylated and non-targeting polymer-GAPDH conjugates (**Figure 4.19**). The RNA isolation protocol was then modified, and we were successfully able to isolate RNA from the alveolar macrophages to perform quantitative PCR.

No knockdown activity was observed for the mannosylated or non-targeting polymer for either TGF-β1 or GAPDH siRNA sequence (**Figures 4.20**).

4.4 CONCLUSIONS

In this chapter we evaluated a neutral, pH-responsive polymeric carrier for siRNA delivery via intranasal, intratrachael, and intravenous administrations. Based on polymer associated toxicity profiles, intravenous administrations via retro-orbital injections were well tolerated up to 120 mg polymer/kg mouse healthy mice. Animals with bleomycin injury were more susceptible to polymer toxicity and it was limited to 60 mg polymer/kg mouse. A mannose-targeted version of the polymer was successfully synthesized and demonstrated similar properties and *in vitro* efficacy in Hela cells as the non-targeted polymer. Both the non-targeted and mannose-targeted polymers primarily distributed to the liver and spleen 24 h after intravenous injection. We compared alveolar, circulating, and splenic macrophage uptake with the mannosylated polymer and non-targeted polymer; however, mannose incorporation in the polymer system did not significantly increased uptake *in vivo* either in healthy on bleomyocin-injured mice. In addition, we evaluated efficacy of our siRNA conjugates in both healthy mice and bleomyocin-injured mice at the maximum polymer dose tolerated. No mRNA knockdown was observed in the alveolar macrophages with either GAPDH or the therapeutic TGF-B siRNA-polymer conjugates after 72 h. However, GAPDH gene expression in the liver was significantly knocked-down by the polymer-siRNA conjugates 72 h after a single 4 mg siRNA/kg dose or 3 consecutive 2 mg siRNA/kg doses.

Table 4.1 Mean pharmacokinetics parameters of polymer via non-compartmental analysis.

Dosage (mg/kg)	*$t_{1/2}$-Early (h)*	*$t_{1/2}$-Late (h)*	*$AUC_{o-\infty}$ (mg•h/mL)*	*CL (mL/h/kg)*	*Vd_{ss} (mL/kg)*
90	0.511	2.15	124.4	0.724	1.52

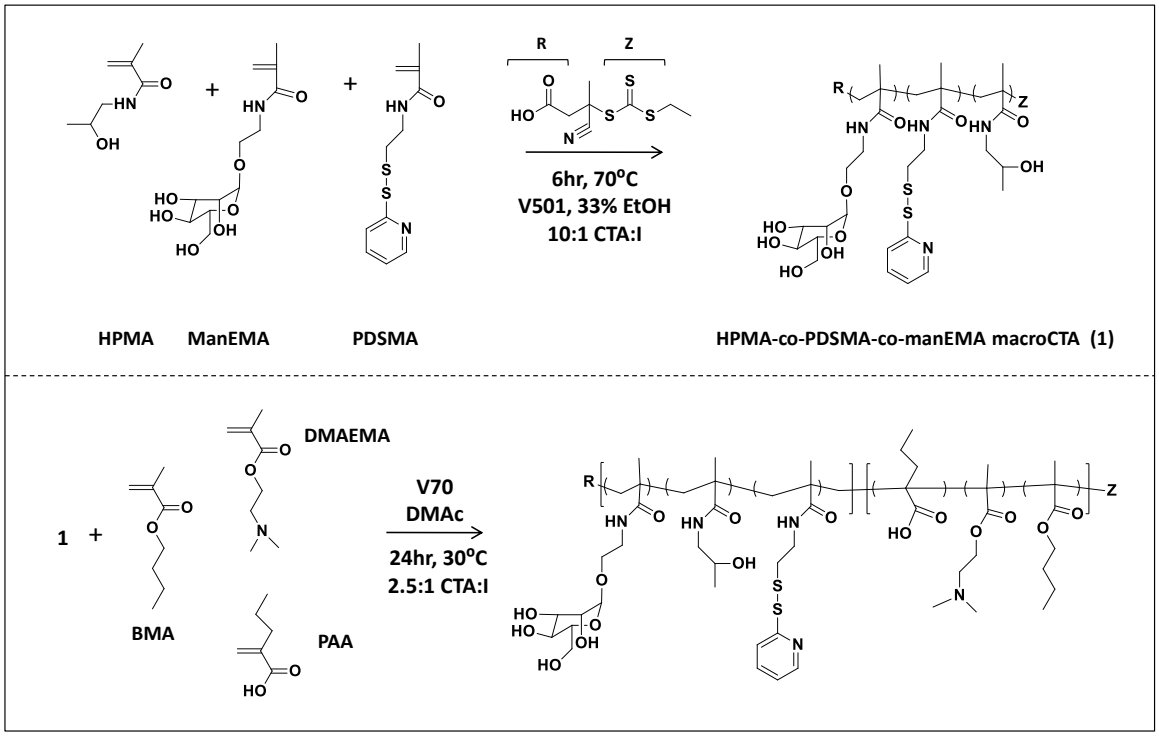

Scheme 4.1 Mannosylated polymer synthesis strategy.

RAFT conditions of poly[(HPMA-*co*-PDSMA-*co*-ManEMA)-*b*-(PAA-DMAEMA-BMA)] synthesis developed by Salka Keller. Polymer is synthesized via a reversible addition fragmentation chain transfer (RAFT) agent to produce a poly(HPMA-co-PDSMA-co-ManEMA) block that reversibly conjugates small interfering RNA (siRNA) and binds mannose-binding lectin Concanavalin A. A subsequent pH-responsive block of DMAEMA, PAA, and BMA subunits is chain extended via RAFT polymerization. BMA, butylmethacrylate; DMAEMA, dimethylaminoethyl methacrylate; HPMA, N-(2-hydroxypropyl) methacrylamide; ManEMA, 2-*O*-(α-D-mannosyl)hydroxyethyl methacrylamide); PAA, polyacrylic acid; PDSMA, pyridyl disulfide methacrylate; siRNA, small interfering RNA.

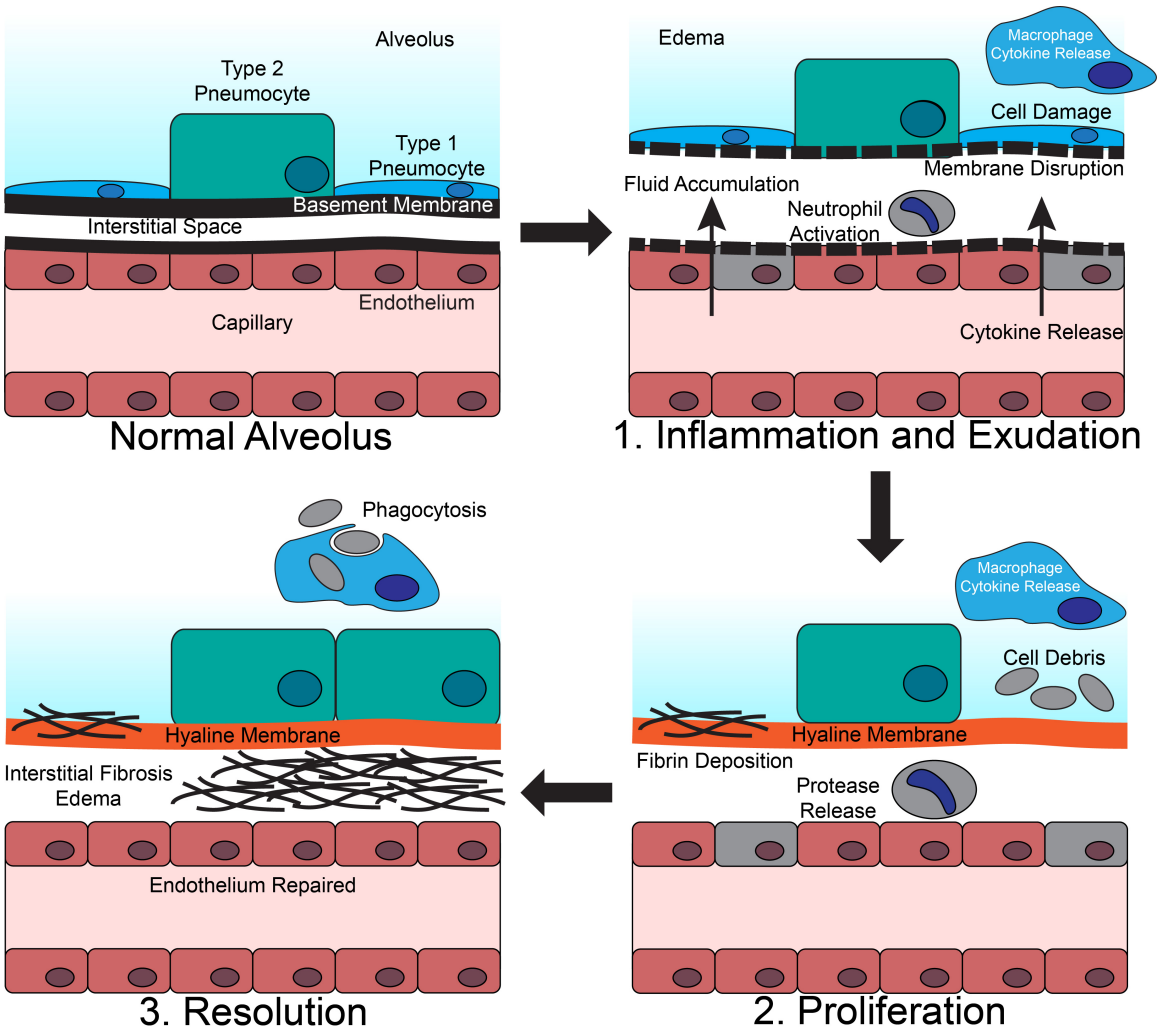

Figure 4.1 Illustration of the three-stage pathophysiology of acute lung injury.

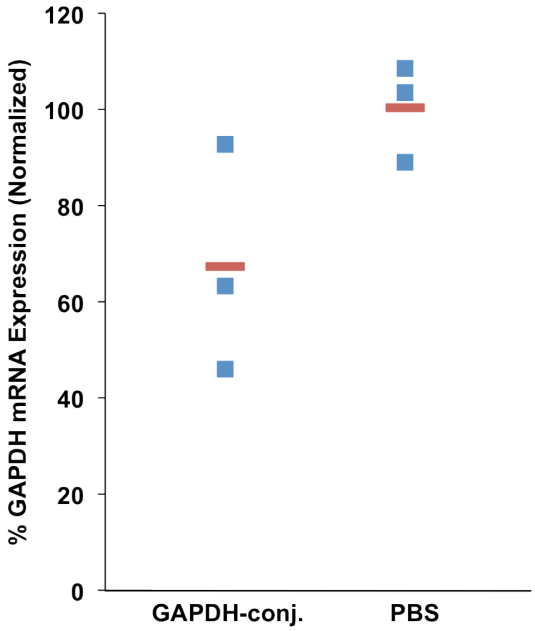

Figure 4.2 GAPDH gene silencing after IN administration.

GAPDH suppression by GAPDH-polymer conjugate in BALB/c mice. GAPDH mRNA levels were assayed by quantitative reverse transcription (qRT)-PCR 72 hours after intranasal delivery of polymeric micelles conjugated with GAPDH siRNA. Values were normalized to the housekeeping gene B-actin and are relative to GAPDH expression in untreated cells. Blue markers represent individual mice while the red bar represents the mean of the sample group.

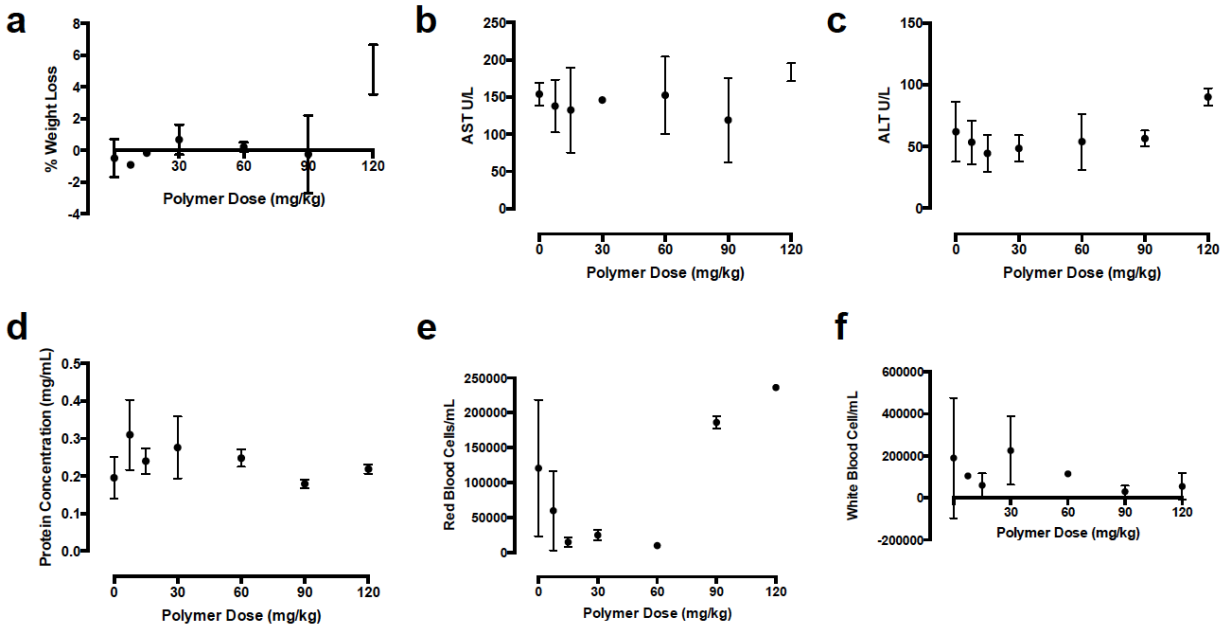

Figure 4.3 Toxicity analysis after IV administration in healthy mice.

Parameters to evaluate polymer toxicity in healthy mice determined 72 h after IV administration as a function of p[(HPMA-co-PDMSA)-b-(PAA-co-DMAEMA-co-BMA)] dose. (a) Weight loss (b) Levels of aspartate aminotransferase (AST) liver enzyme (c) Levels of analine aminotransferase (ALT) liver enzyme (d) Total protein levels in brochoalveolar lavage (e) Red Blood Cells in brochoalveolar lavage (f) White Blood Cells in brochoalveolar lavage.

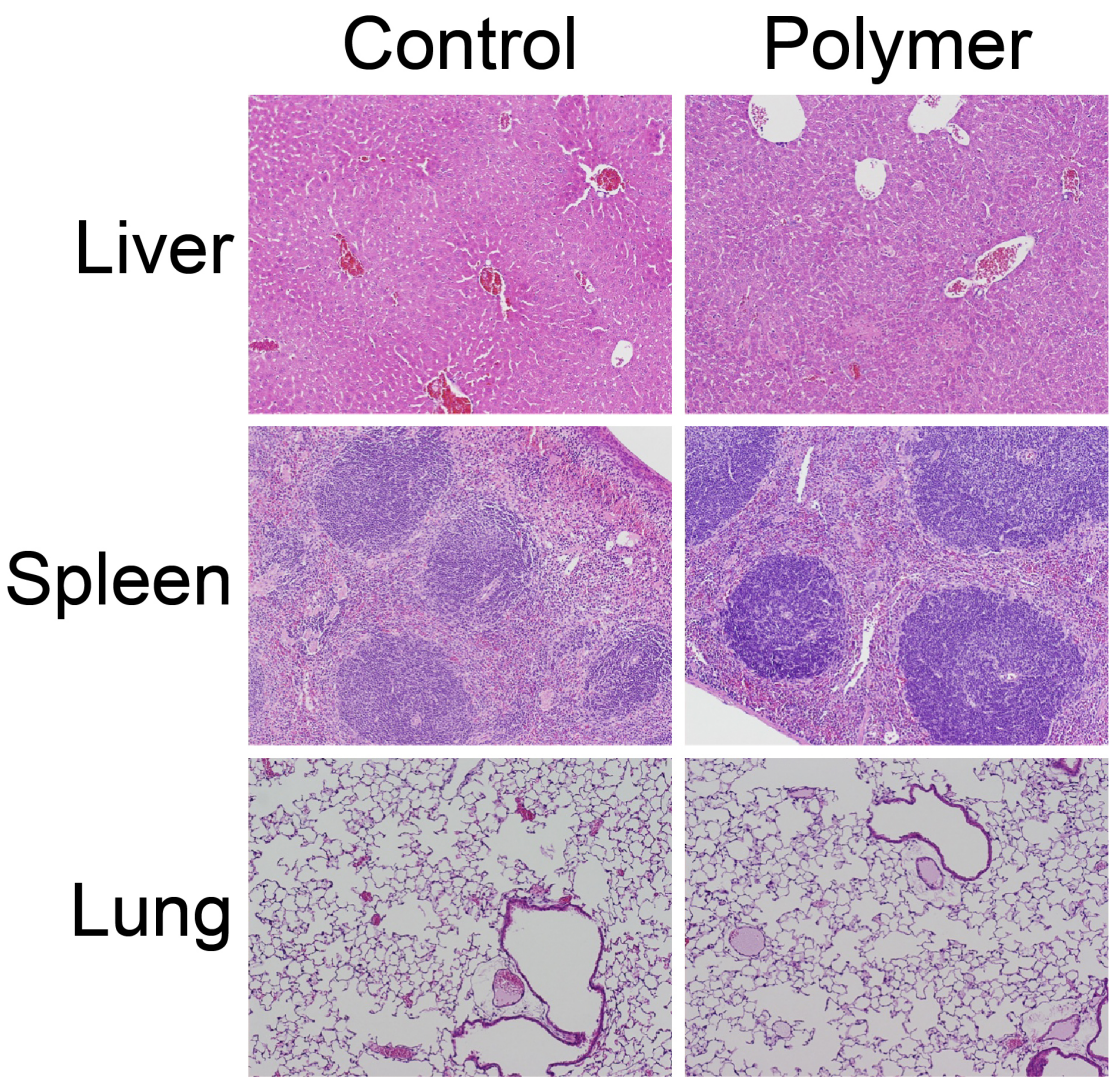

Figure 4.4 Organ histology to evaluate polymer toxicity.

Light microscopy images of H & E stained lung tissue sections both with and without polymer treatment after 24 hours.

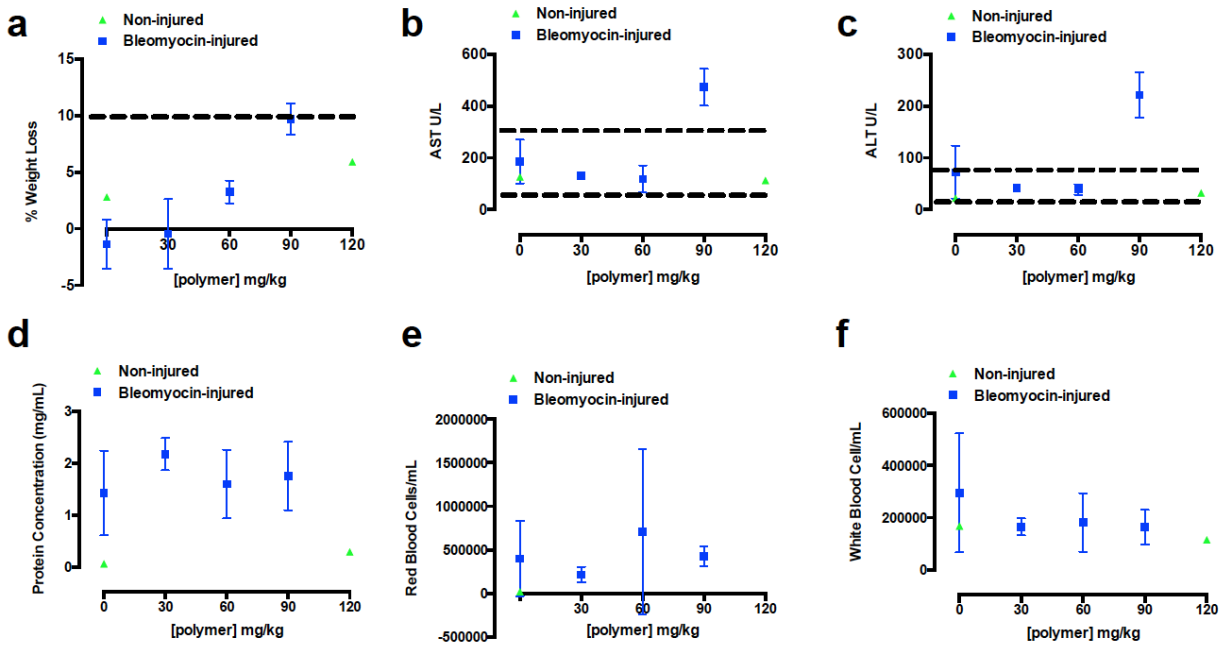

Figure 4.5 Toxicity analysis after IV administration in ALI mice model.

Parameters to evaluate polymer toxicity in bleomycin-injured mice determined 24 h after IV administration as a function of p[(HPMA-co-PDMSA)-b-(PAA-co-DMAEMA-co-BMA)] dose. (a) Weight loss normalized to IV administration (b) Levels of aspartate aminotransferase (AST) liver enzyme (c) Levels of analine aminotransferase (ALT) liver enzyme (d) Total protein levels in brochoalveolar lavage (e) Red Blood Cells in brochoalveolar lavage (f) White Blood Cells in brochoalveolar lavage.

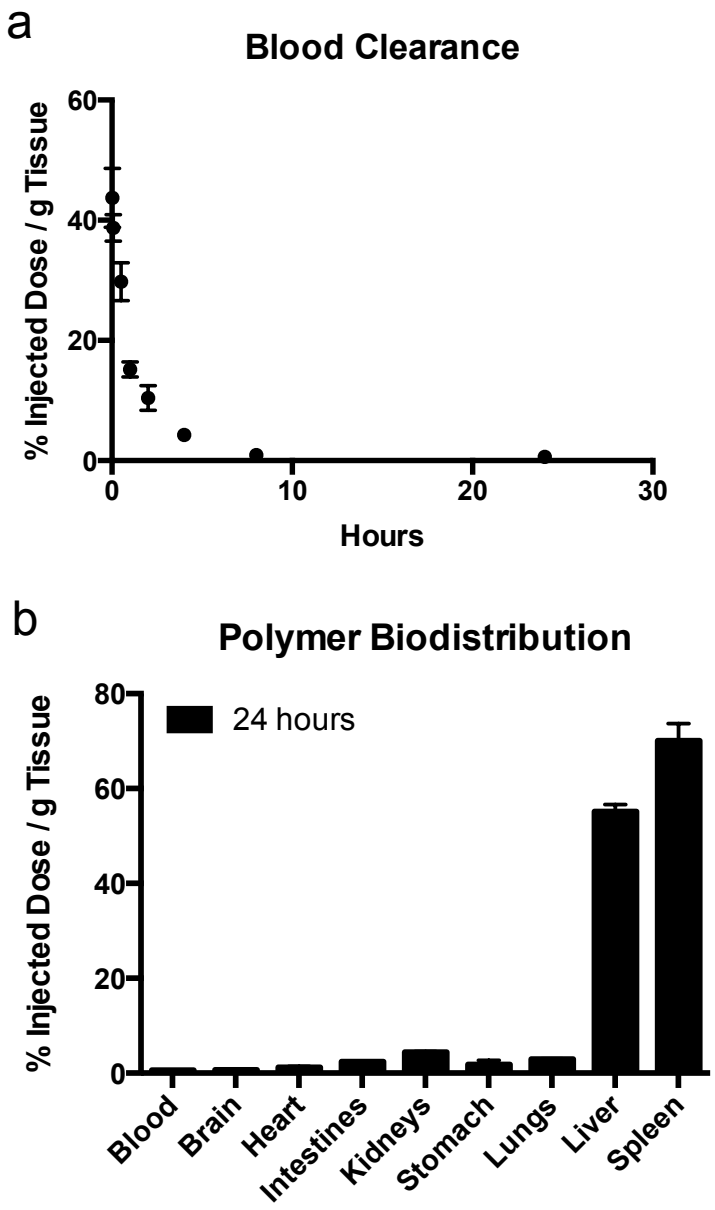

Figure 4.6 Polymer circulation in blood and organ accumulation.

(a) Blood concentrations of radiolabeled p[(HPMA-co-PDMSA)-b-(PAA-co-DMAEMA-co-BMA)] over time after IV administration in healthy mice. (b) Biodistribution of radiolabeled p[(HPMA-co-PDMSA)-b-(PAA-co-DMAEMA-co-BMA)] after 24 h after IV administration in healthy mice. Values are mean ± standard deviation (N=5).

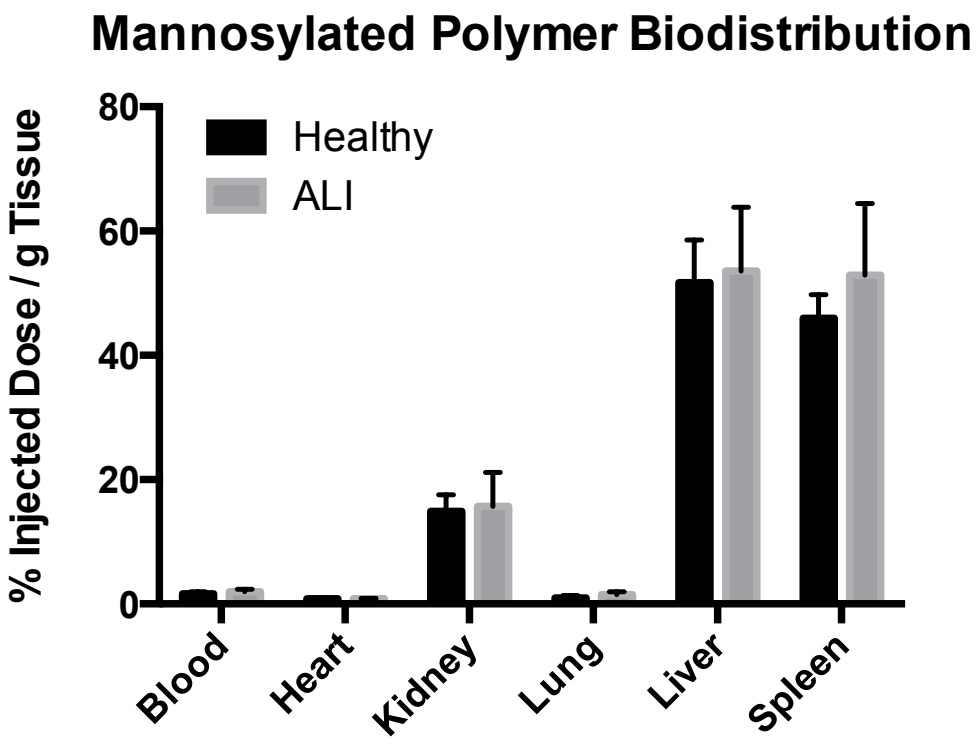

Figure 4.7 Polymer organ biodistribution in healthy vs ALI mice.

Biodistribution of fluorescently labeled p[(HPMA-co-PDMSA)-b-(PAA-co-DMAEMA-co-BMA)] at 24 h following IV administration and 72 h post bleomyocin-induced injury. Values are mean ± standard deviation (N=4).

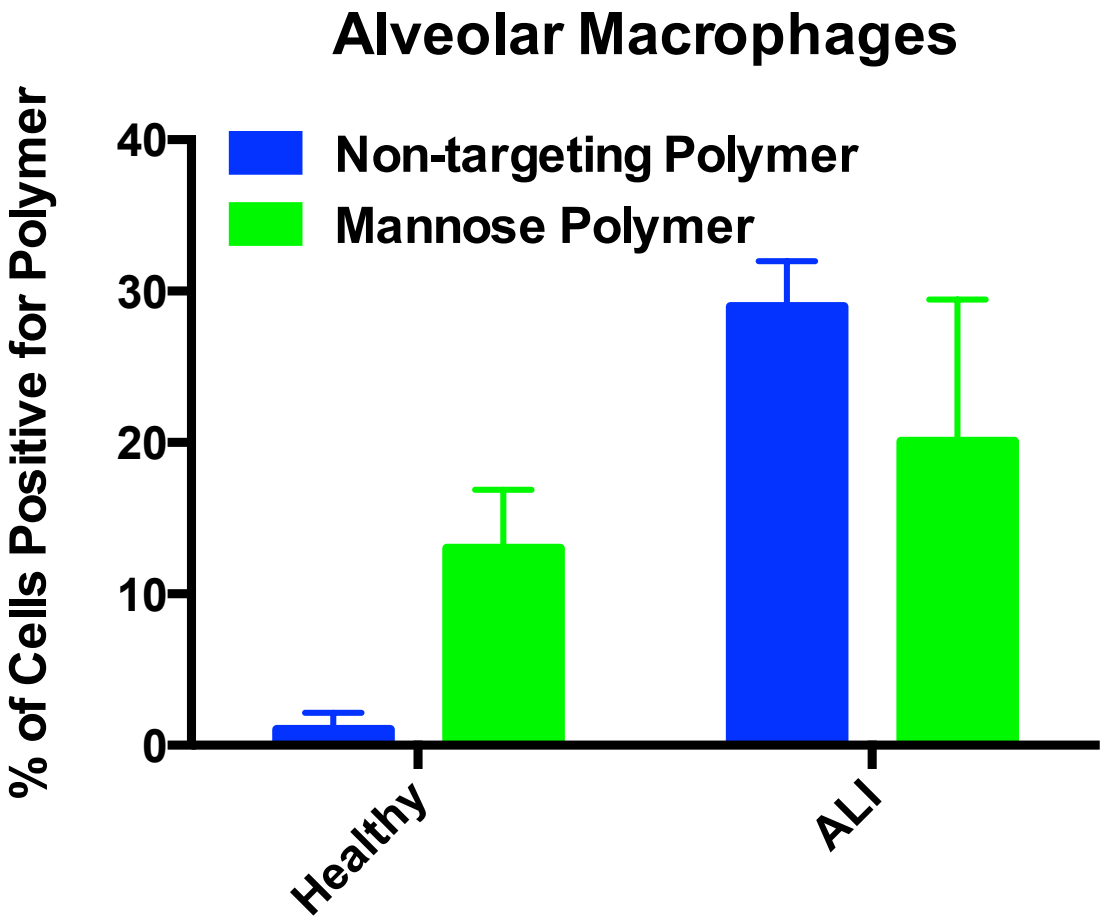

Figure 4.8 Polymer uptake by alveolar macrophages in healthy and ALI mice.

Internalization of Alexa 488-labeled poly[(HPMA-co-PDSMA)-b-(PAA-co-DMAEMA-co-BMA) in Alveolar Macrophages 24 h after 60 mg/kg polymer dose via IV administration in C57Bl/6 mice measured by flow cytometry. Vertical axis is the percent positive alveolar macrophages for polymer ± standard deviation (N=4) over baseline (PBS treated animals).

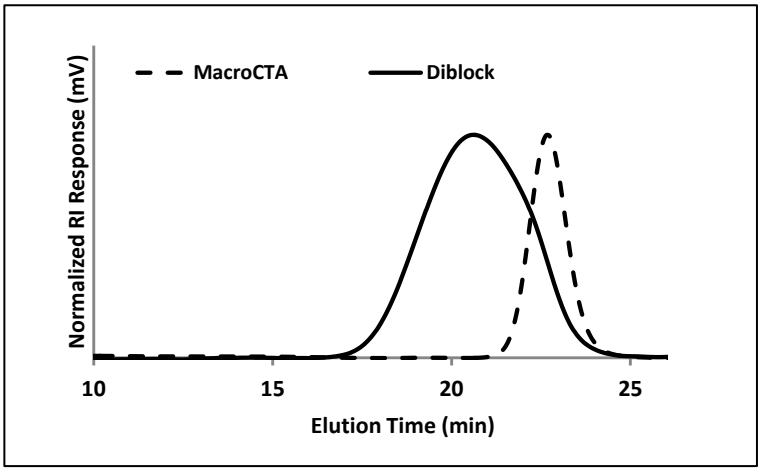

Figure 4.9 Mannosylated polymer characterization by SEC.

Size exclusion chromatograms of poly(HPMA-*co*-PDSMA-*co*-ManEMA) macroCTA and poly[(HPMA-*co*-PDSMA-*co*-ManEMA)-*b*-(PAA-DMAEMA-BMA)] diblock glycopolymer depicting successful chain extension via Reversible Addition Fragmentation Chain Transfer. Figure courtesy of Salka Keller.

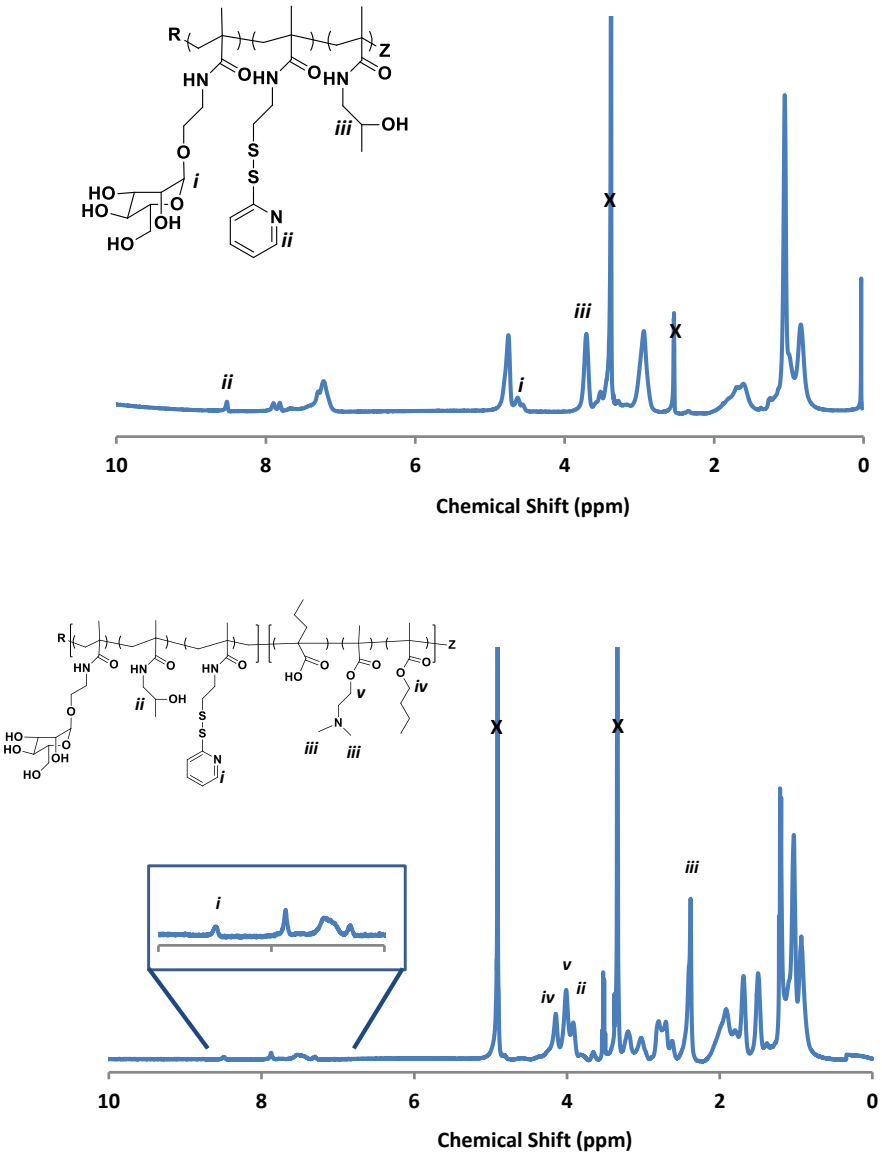

Figure 4.10 Mannosylated polymer characterization by ^{1}H NMR.

^{1}H-NMR spectra of poly(HPMA-*co*-PDSMA-*co*-ManEMA) macroCTA (DMSO) and poly[(HPMA-*co*-PDSMA-*co*-ManEMA)-*b*-(PAA-DMAEMA-BMA)] (MeOD) at 500 MHz. Indicated peaks were used for determining block compositions. Figure courtesy of Salka Keller.

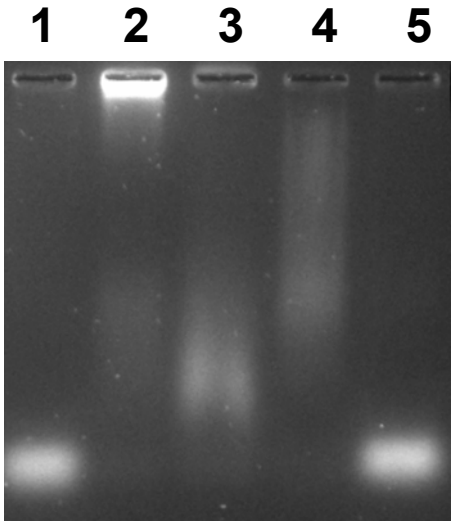

Figure 4.11 Mannosylated polymer-siRNA conjugates validation.

Gel Retardation Assay validating poly[(HPMA-co-PDSMA-ManEMA)-b-(PAA-DMAEMA-co-BMA)-siRNA conjugation via a reducible disulfide bond. 1 μg siRNA/lane. Lane: Free thiolated siRNA (1), 1:10 (siRNA to polymer) polymer-siRNA conjugate (2), polymer-siRNA conjugate and 0.1 M DTT to reduce disulfide linkages (3), polymer-siRNA conjugate and 1 % SDS to disrupt micelle formation and electrostatic interactions (4), polymer-siRNA conjugate, 0.1 M DTT and 1 % SDS (5).

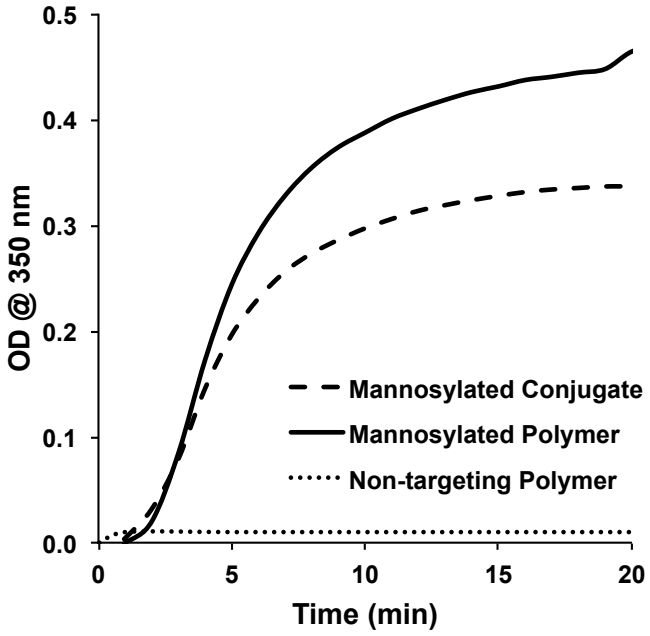

Figure 4.12 Mannose targeting is retained in siRNA conjugates.

Validation of mannose-binding of p[(HPMA-co-PDSMA-ManEMA)-b-(PAA-co-DMAEMA-co-BMA)]- siRNA conjugates via agglutination assay. Mannosylated polymer was conjugated to thiolated siRNA at a 1:10 siRNA to polymer ratio and incubated with mannose binding lectin Concanavalin A. Positive binding is indicated via an increase on optical density at 350 nm. The p[(HPMA-co-PDSMA-ManEMA)-b-(PAA-co-DMAEMA-co-BMA)] and p[(HPMA-co-PDSMA)-b-(PAA-co-DMAEMA-co-BMA)], were shown as a positive and negative control, respectively.

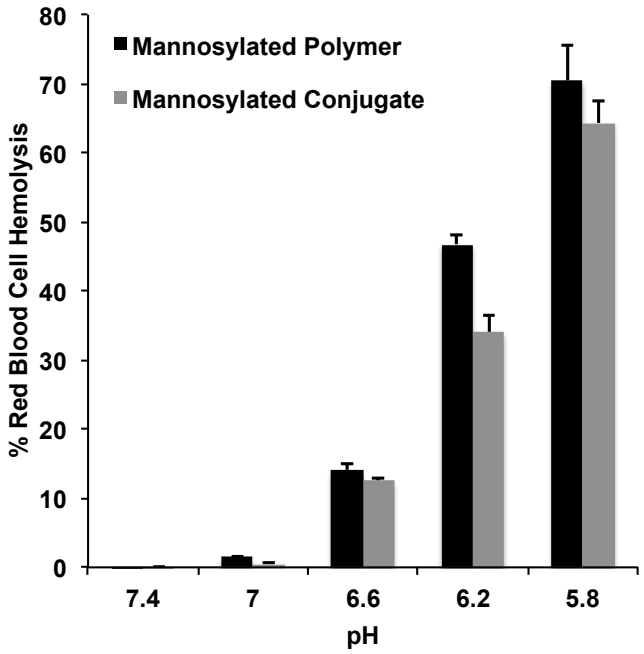

Figure 4.13 Membrane destabilizing profile of mannosylated siRNA conjugates.

Hemolysis of the poly [(HPMA-co-PDSMA-co-ManEMA)-b-(PAA-co-DMAEMA-co-BMA)] diblock copolymer and poly [(HPMA-co-PDSMA-co-ManEMA)-b-(PAA-co-DMAEMA-co-BMA)] diblock copolymer-siRNA conjugates both at a 10:1 polymer to thiolated siRNA at pH concentrations of 5.8, 6.2, 6.6 and 7.4 of 40 μg polymer/mL. Hemolytic activity is normalized relative to a positive control, 1 % v/v Triton X-100, and the data represent a single experiment conducted in triplicate ± standard deviation.

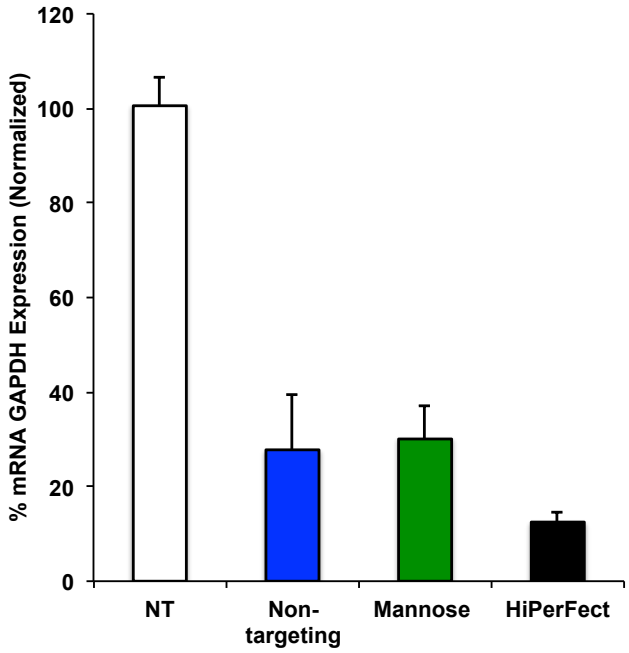

Figure 4.14 GAPDH gene silencing validation of mannose conjugates *in vitro*.

Reduction of Glyceraldehyde-3-phosphate dehydrogenase (GAPDH) gene expression in HeLa cells. GAPDH mRNA levels were assayed by quantitative reverse transcription (qRT)-PCR after a 48 hr incubation with siRNA-polymer conjugates. The poly [(HPMA-co-PDSMA)-b-(PAA-co-DMAEMA-co-BMA)] diblock copolymer (Blue) and the poly [(HPMA-co-PDSMA-co-ManEMA)-b-(PAA-co-DMAEMA-co-BMA)] diblock copolymer (Green) was conjugated with thiolated siRNA at 1:10 siRNA to polymer ratio and cells were dosed with 50 nmol/L siRNA directed against GAPDH. GAPDH HiPerFect was used a positive control at 25 nmol/L. Values are normalized to the housekeeping gene PPIA (Cyclophilin A) and relative to GAPDH expression in untreated cells. Error bars represent the mean GAPDH expression ± standard error of triplicate samples.

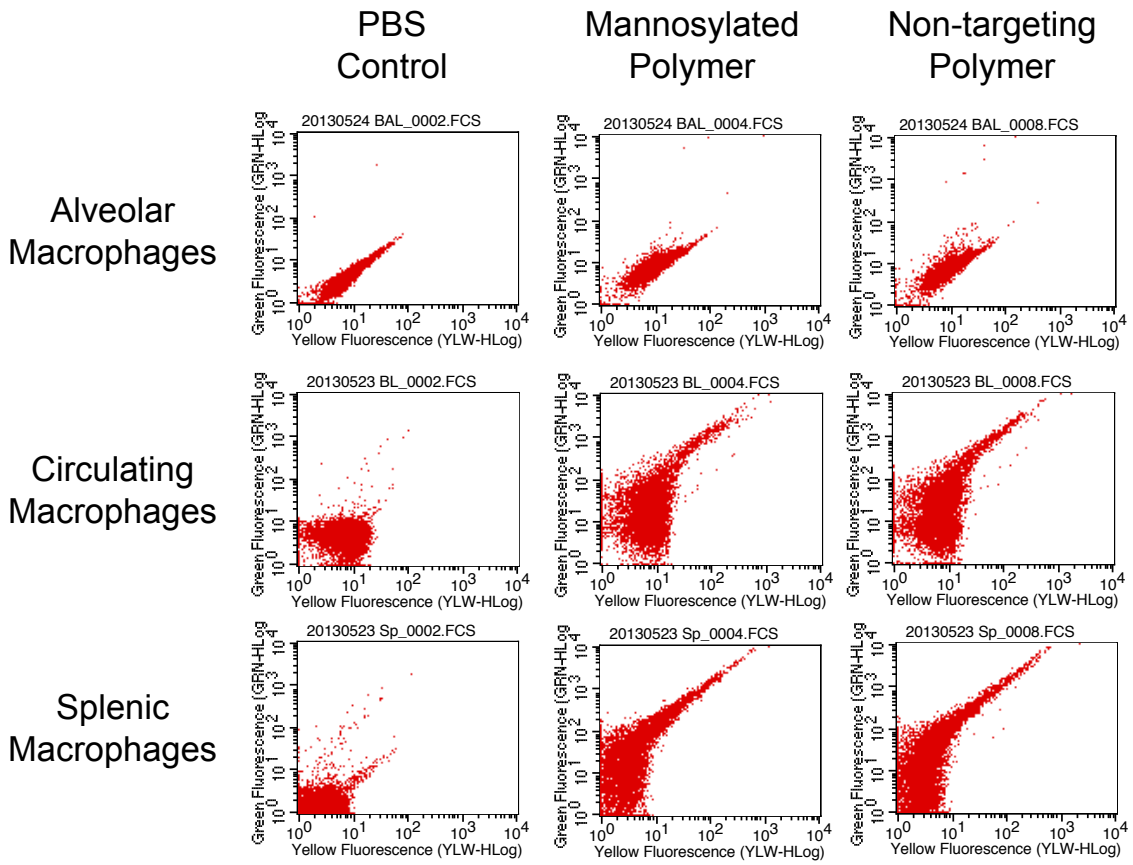

Figure 4.15 Macrophage uptake of mannose and nontargeted polymer *in vivo*.

Mannose-targeted macrophage uptake evaluation with flow cytometry. Representative flow cytometry plots depict green fluorescence intensity (vertical axis) of Alveolar Macrophages, Circulating Macrophages, or Splenic Macrophages vs. yellow fluorescence intensity (horizontal axis). poly [(HPMA-co-PDSMA-co-ManEMA)-b-(PAA-co-DMAEMA-co-BMA)] diblock copolymer and the poly [(HPMA-co-PDSMA)-b-(PAA-co-DMAEMA-co-BMA)] diblock copolymer labeled with Oregon Green 488 and were IV administered. After 24 h, the macrophages were harvest from the lungs, blood and spleen then analyzed for fluorescent polymer internalization by flow cytometry.

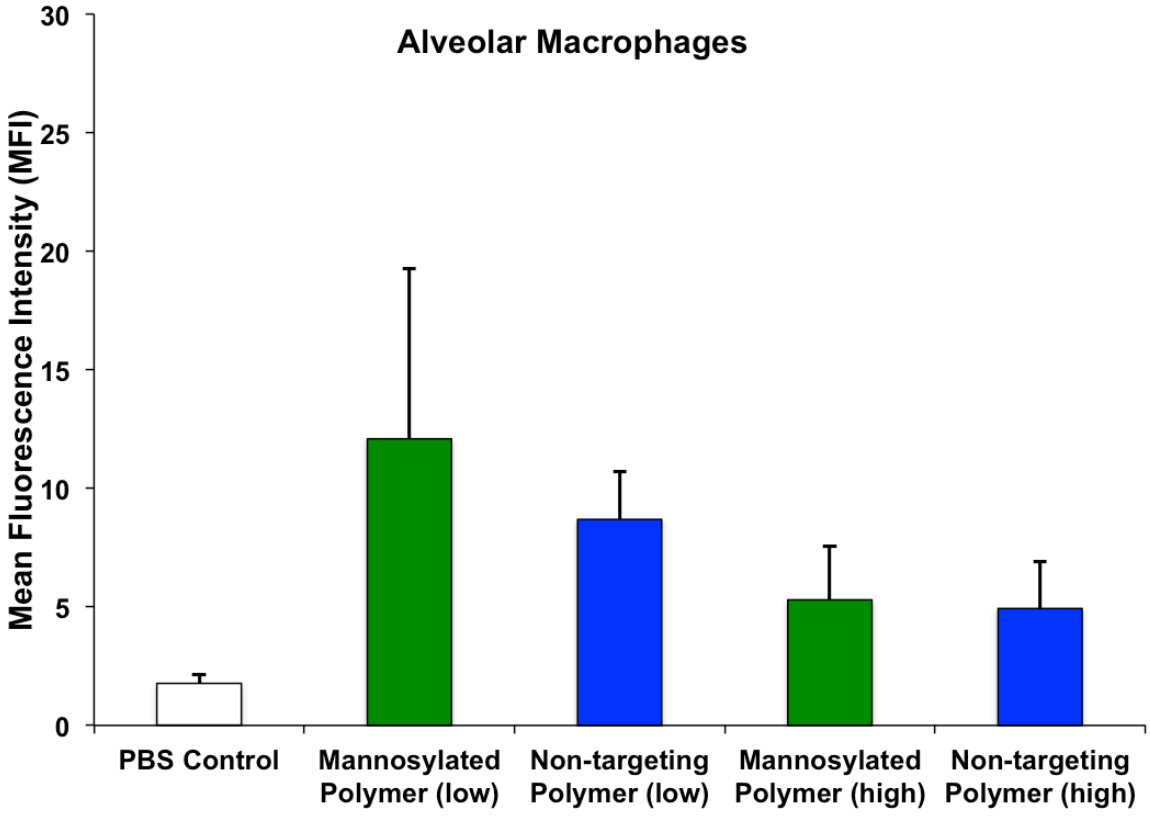

Figure 4.16 Alveolar macrophage uptake of mannose and nontargeted polymer *in vivo*.

Mannose-targeted alveolar macrophage uptake evaluation with flow cytometry. poly [(HPMA-co-PDSMA-co-ManEMA)-b-(PAA-co-DMAEMA-co-BMA)] diblock copolymer and the poly [(HPMA-co-PDSMA)-b-(PAA-co-DMAEMA-co-BMA)] diblock copolymer labeled with Oregon Green 488 and were IV administered at a 60 mg/kg and 120 mg/kg polymer doses. After 24 h, the alveolar macrophages were isolated and stained with CD11 and F40/80 macrophage markers, then analyzed for fluorescent polymer internalization by flow cytometry. Median relative fluorescence intensity (RFI) ± standard deviation (N=4).

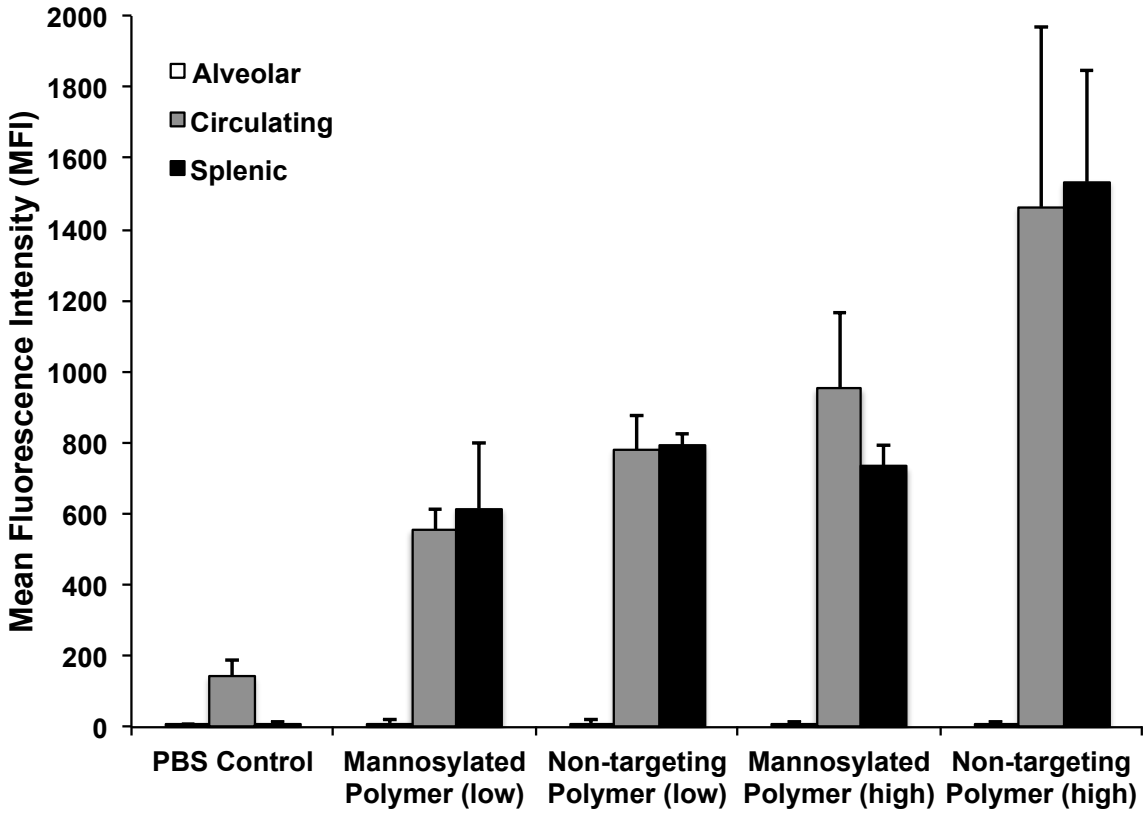

Figure 4.17 Relative macrophage uptake of polymers *in vivo*.

Mannose-targeted macrophage uptake evaluation with flow cytometry. poly[(HPMA-co-PDSMA-co-ManEMA)-b-(PAA-co-DMAEMA-co-BMA)] diblock copolymer and the poly [(HPMA-co-PDSMA)-b-(PAA-co-DMAEMA-co-BMA)] diblock copolymer labeled with Oregon Green 488 and were IV administered at 60 mg/kg and 120 mg/kg polymer doses. After 24 h, the alveolar, circulating, and splenic macrophages were isolated and stained with CD11 and F40/80 macrophage markers, then analyzed for fluorescent polymer internalization by flow cytometry. Median relative fluorescence intensity (RFI) ± standard deviation (N=4).

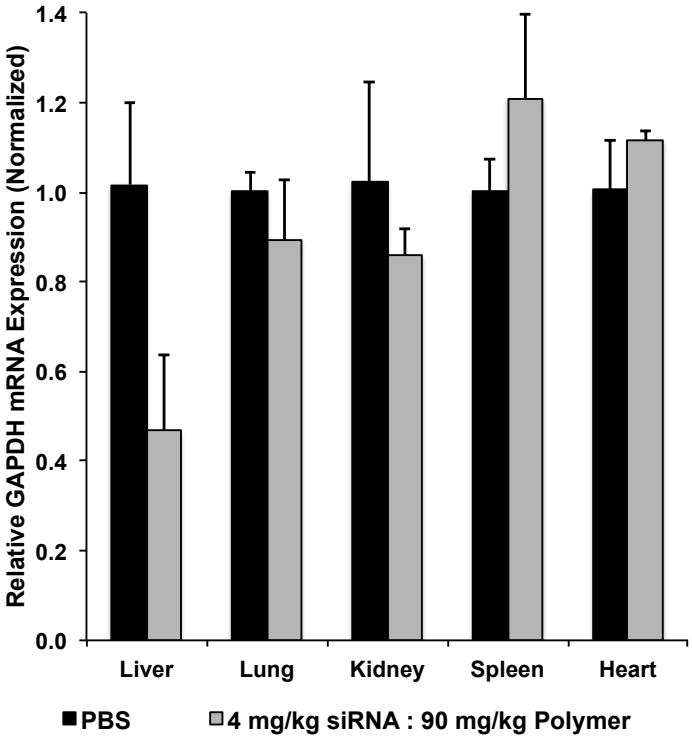

Figure 4.18 RNA silencing in organs after IV administration of siRNA-polymer conjugates.

Reduction of Glyceraldehyde-3-phosphate dehydrogenase (GAPDH) gene expression in C57Bl/6 mice. GAPDH mRNA levels were assayed by quantitative reverse transcription (qRT)-PCR 72 h after IV administration of siRNA-polymer conjugates. The poly [(HPMA-co-PDSMA)-b-(PAA-co-DMAEMA-co-BMA)] diblock copolymer was conjugated with thiolated GAPDH siRNA at 4 mg/kg siRNA and a 90 mg/kg polymer dose. Values are normalized to the housekeeping gene B-actin and relative to GAPDH expression in PBS treated mice. Error bars represent the mean GAPDH expression ± standard deviation (N=2).

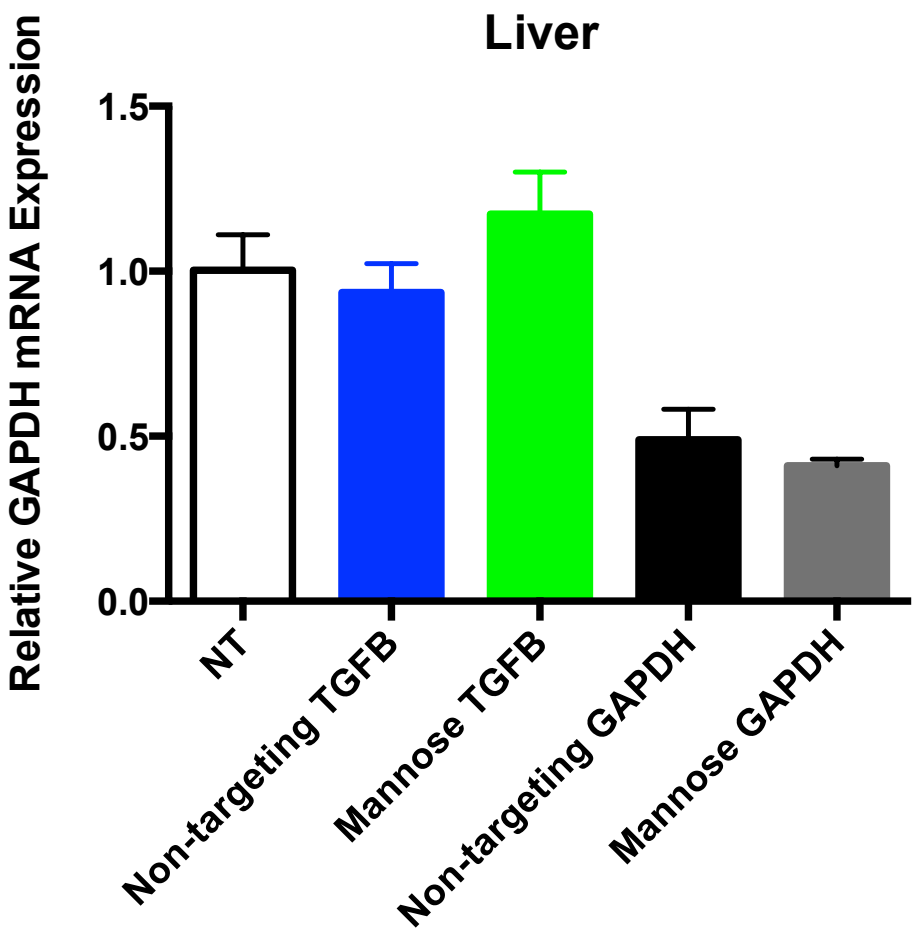

Figure 4.19 RNA silencing by both non-targeted and mannosylated conjugates in the liver.

Reduction of Glyceraldehyde-3-phosphate dehydrogenase (GAPDH) gene expression in the liver of C57Bl/6 mice after 3 daily doses of siRNA-polymer conjugates. GAPDH mRNA levels were assayed by quantitative reverse transcription (qRT)-PCR 72 h after IV administration of siRNA-polymer conjugates. The poly [(HPMA-co-PDSMA)-b-(PAA-co-DMAEMA-co-BMA)] diblock copolymer (blue) and the poly [(HPMA-co-PDSMA-co-ManEMA)-b-(PAA-co-DMAEMA-co-BMA)] diblock copolymer (Green) were conjugated with thiolated GAPDH or TGF-β1 siRNA at 2 mg/kg siRNA and a 120 mg/kg polymer dose. Values are normalized to the housekeeping gene B-actin and relative to GAPDH expression in PBS treated mice. Error bars represent the mean GAPDH expression ± standard error (N=4).

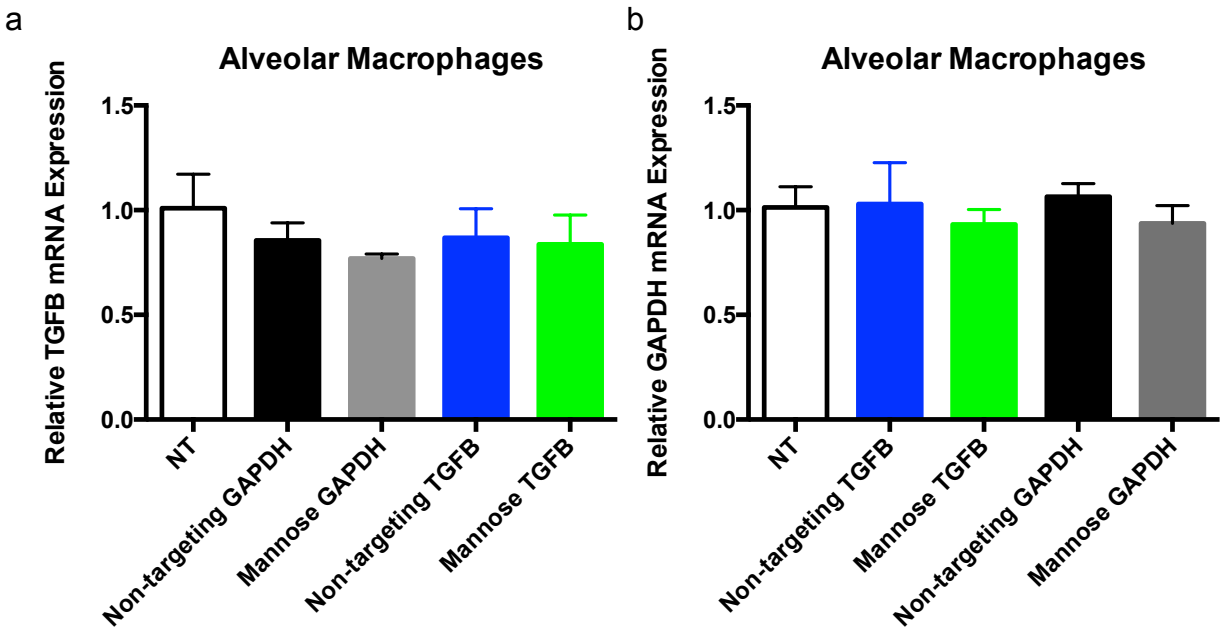

Figure 4.20 Evaluation TGFβ-1 silencing in alveolar macrophages.

Reduction of Transforming Growth Factor Beta (TGF-β1) gene expression (a) and Glyceraldehyde-3-phosphate dehydrogenase (GAPDH) gene expression (b) in the Alveolar Macrophages of C57Bl/6 mice after 3 daily doses of siRNA-polymer conjugates. mRNA levels were assayed by quantitative reverse transcription (qRT)-PCR 72 h after IV administration of siRNA-polymer conjugates. The poly [(HPMA-co-PDSMA)-b-(PAA-co-DMAEMA-co-BMA)] diblock copolymer and the poly [(HPMA-co-PDSMA-co-ManEMA)-b-(PAA-co-DMAEMA-co-BMA)] diblock copolymer were conjugated with thiolated GAPDH or TGF-β1 siRNA at 2 mg/kg siRNA and a 120 mg/kg polymer dose. Values are normalized to the housekeeping gene B-actin and relative to GAPDH expression in PBS treated mice. Error bars represent the mean GAPDH expression ± standard error (N=4).

Chapter 5. CONCLUSIONS AND FUTURE DIRECTIONS

5.1 SUMMARY OF MAJOR FINDINGS

5.1.1 Design and validation of new siRNA delivery carriers

Effective siRNA delivery relies strongly on a delivery platform capable of overcoming the barriers associated with effective cytosolic delivery. In chapter 2 we discussed the rationale design of a biocompatible, siRNA polymer conjugate system to facilitate escape from the endosomal pathway. We employed reversible addition fragmentation chain transfer (RAFT) technology in a mixed aqueous solvent system to successfully synthesize a well controlled pH-responsive diblock copolymer for the direct conjugation of siRNA. Polymers self-assembled into 25-30 nm micelles as shown with dynamic light scattering and transmission electron microscopy. We characterized core-shell morphology via ^{1}H NMR in both organic and aqueous solvents. The corona was composed of a hydrophilic monomer N-(2-hydroxypropyl)methacrylamide (HPMA) with approximately 2 pyridyl disulfide functionalities per polymer chain, based on ^{1}H NMR. The micelle core was composed propylacrylic acid (PAA), dimethylaminoethyl methacrylate (DMAEMA), and butyl methacrylate (BMA), which formed the pH-responsive block that facilitated endosomal escape. The 30:30:40 PAA:DMAEMA:BMA composition of the terblock allowed for charge neutrality at physiological pH and the 40 % hydrophobic BMA in particular is responsible for driving the self-assembly of micelle in order to sequester the hydrophobic region from an aqueous environment. When the PAA and DMAEMA encounter acidic pHs, the carboxyl and amino groups became protonated, resulting in a more cationic and hydrophobic polymer. This

ultimately results in a conformational change from micelles to unimers, which are able to interact with the vesicular membrane and cause membrane destabilization. Thiolated siRNA was reversibly bound to the polymer and the siRNA-polymer conjugates retained membrane-destabilizing behavior. The neutral polymer-siRNA conjugates showed minimal toxicity in HeLas up to 500 μg/mL. We confirmed efficacy in HeLa cervical cancer cells at a 50 nmol/L siRNA dose. RNA interference activity was dependent on polymer concentration; as the polymer to siRNA ratio was increased the more gene silencing was observed. Furthermore, only polymer-siRNA conjugates were able to successfully silence gene expression, and a physical mixture of the two components failed to reduce gene expression.

5.1.2 Trastuzumab targeting enhances conjugate efficacy and works in synergy with carboplatin in ovarian cancer cells

In chapter 3, we evaluated the need for extracellular targeting capabilities of the siRNA-polymer conjugates to deliver a therapeutic siRNA in combination with chemotherapy to ovarian cancer cells. We first incorporated trastuzumab targeting using a trastuzumab-streptavidin conjugate, which bound free biotins from the chain transfer agent on the micelle surface. We then measured HER2/neu receptor mediated endocytosis of the targeted conjugates in two different HER2/neu expressing cancer cell lines, SKOV3 (ovarian cancer) and SKBR3 (breast cancer). Binding to the cell surface and internalization is a known barrier of siRNA delivery, and trastuzumab significantly enhanced micelle uptake above controls. Targeted siRNA-polymer conjugates were successful at reducing GAPDH gene expression in both cell lines at a 50 nmol/L siRNA dose. We optimized RNA knockdown by the addition of more diblock copolymer and shorter transfection times in SKOV3. The efficacy of trastuzumab Bcl-xL-polymer conjugates

was further confirmed with a 5'-RLM-RACE assay and sequencing the cleavage product. The trastuzumab Bcl-xL-polymer conjugates sensitized ovarian cancer cells to carboplatin, and exhibited a synergistic effect by significantly lowering the IC(50) of carboplatin with the targeted conjugated treatment.

5.1.3 siRNA conjugates are biocompatible in vivo after IV administration

In chapter 4, our goal was to demonstrate the clinical relevance of a neutral diblock copolymer siRNA conjugate as a therapeutic delivery system. We first showed that the polymer system was relatively non-toxic up to doses of 120 mg/kg in healthy mice and 60 mg/kg in mice suffering from an acute lung injury (ALI), as noted by percent weight loss, elevation of AST/ALT liver enzymes, markers with the bronchoalveolar lavage fluid, and histology. Polymer batches with more equal block ratios appeared to be better tolerated *in vivo*. After intravenous administration, the polymers distributed primarily to the liver and the spleen in both healthy and bleomyocin-injured mice. Furthermore, we showed that macrophage populations successfully internalize the polymer system with both mannose targeting and the non-targeting control polymer. Unfortunately, we were unable to demonstrate efficacy in healthy or ALI mice with siRNA polymer conjugates (mannosylated or non-targeted) in alveolar macrophages, the cell population of interest to delivery the anti-inflammatory siRNA TGF-β1. We believe that this was due to insufficient drug reaching the alveolar macrophages, base on flow cytometry results, and that isolating other populations of macrophages may provide more insight on the efficacy of this system.

In conclusion, the siRNA-polymer conjugates may be a viable therapy, but the careful selection of target cells and disease process appears to be critical. For example, we were able to deliver functional RNA to cells with the liver to demonstrate over 50 % GAPDH RNA silencing 72 hours after an intravenous administration of 4 mg/kg GAPDH siRNA and 90 mg/kg polymer or after 3 consecutive doses of 2 mg/kg GAPDH siRNA with 120 mg/kg polymer.

5.2 IMPLICATIONS

To treat a majority of cancers and other disseminated diseases with siRNA, systemic delivery is essential for adequate delivery to the target cells and tissues. However, the systemic administration of siRNA *in vivo* has many additional challenges prior to cytosolic delivery to a target cell, including kidney filtration, uptake by phagocytes, aggregation with serum proteins, and enzymatic degradation by endogenous nucleases [121,141]. siRNA molecules alone are unable to overcome these barriers and thus the formulations of siRNA that have translated into a clinical setting has been divided into three subcategories: (1) nanoparticles composed of lipid and lipid-like materials, (2) polymer-based nanocarriers, and (3) siRNA conjugates[142].

Here we report a polymer-based siRNA conjugate delivery system which addresses the drawbacks associated with each the individual platforms and overcomes many barriers to systemic siRNA delivery. To date, the most successful polymer based siRNA delivery carrier for systemic delivery *in vivo* is CALAA-01, a 3 component system composed of cyclodextrin-containing polymer (CDP), an adamantine-polythethylene glycol (AD-PEG) steric stabilization agent, and human transferrin (Tf) as a targeting ligand[55,142]. CDP is a short polycation that minimizes toxicity, permits renal clearance, and condenses siRNA. CDP was capped with

imidazole functional groups that facilitate endosomal escape via the proton sponge effect[143]. AD-PEG interacts with the CDP-siRNA to confer serum stability and prevent nanoparticle disassembly upon dilution in the blood stream[122,142]. However, it prevents interaction with cell surfaces and thus requires targeting via the Tf ligand. Rahman and colleagues demonstrated systemic administration of targeted siRNA nanoparticles for the treatment of head and neck cancers with 4 separate administrations of 10 mg siRNA/kg in mice[141]. Nonhuman primate safety studies show that the nanoparticle is well tolerated up to 27 mg siRNA/kg[123,124,144,145]. The delivery of RRM2 siRNA via CALAA-01 and is currently in phase 1 escalating dose clinical trials for patients with solid tumors[146].

A second approach is a siRNA conjugate system called Dynamic PolyConjugates (DPCs), which is an emerging platform that has completed preclinical trials for the targeted delivery of siRNA to heptacytes. DPCs contain a "reversibly masked" amphipathic endosomolytic polymer composed of poly(butyl amino vinyl ether) modified with carboxylated dimethyl maleic acid chemistry derivatives of PEG and N-acetylgalactosoamice (NAG)[142]. NAG imparts imparted hepatocyte-specific delivery via the highly expressed asialoglycoprotein receptor present on hepatocytes. First generation solutions directly conjugated the siRNA to the polymer backbone via bio-cleavable disulfide linkages and showed efficacy at 2.5 mg ApoB siRNA/kg in mice with 80-90 % gene silencing and 40 % lowering serum cholesterol 48 hours after intravenous injection[36]. Despite this initial success, more recent formulations simply coinject the NAG targeted, reversibly masked polymer with siRNA cholesterol conjugates[147].

In comparison to these two polymer and conjugate based siRNA delivery systems currently in clinical testing, the neutral pH-responsive siRNA conjugate system described here has several unique advantages to address the challenges associated with systemic *in vivo* delivery. Both CALAA-01 and DPCs are formulated with multiple components physically interacting and work under the assumption that the complex will reach target cells intact. In contrast, we directly link to the polymer chain all the major delivery components: cell specific targeting moieties, membrane-lytic capabilities, a neutral, hydrophilic corona to impact biocompatibility, and therapeutic siRNA. Although, we did not intentionally target the liver, we did get significant GAPDH gene silencing with a similar siRNA dose without the presence of NAG-based targeting. With a few modifications, we could synthesize the diblock copolymer with NAG targeting and perhaps have more potent system than DPCs. Furthermore, the siRNA doses we administered were significantly lower than those of the CALAA-01 system. Overall, the future success of siRNA delivery platforms rests upon better understanding the biological barriers as a well as rationally designing a system that can address these barriers.

5.3 Future Directions

5.3.1 Trastuzumab-targeted siRNA polymer conjugates in vivo

Ultimately, *in vivo* evaluation of tumor response to drugs is necessary to recapitulate fundamental aspects of the disease progression, but to date the development of an appropriate animal model for preclinical testing of ovarian targeting drugs has been an ongoing challenge[148]. In 2007, Lin, *et al*. addressed some of the challenges with a more stable and reproducible animal model based upon the SKOV3 human ovarian papillary serous adenocarcinoma cell line. We

propose to use this model as the basis for future *in vivo* evaluation of our targeted siRNA delivery system in ovarian cancer.

Our collaborators in the Press laboratory have been evaluating the effect of Trastuzumab targeted cationic polymer-based siRNA delivery systems *in vivo*. Here we propose the addition of a targeting system capable of preferentially delivering siRNA to a specific pathologic cell population such as tumor cells. Specifically, we hypothesize that functionality of the system described in Chapter 3 will facilitate cell-specific uptake and allow for systemic administration with targeted action. The difference in *in vitro* mRNA knockdown between Trastuzumab targeted and a non-targeted antibody siRNA-polymer conjugate has already demonstrated the importance of targeting in human ovarian adenocarcimoma cells, which overexpress the HER2/neu oncoprotein. To extend this work to an *in vivo* model, we will establish an intraperitoneal xenograft model using human ovarian cancer cells overexpressing firefly luciferase for imaging and detection of tumors. Targeted and control siRNA-polymer conjugates will be intravenously administered and the carrier efficacy will be evaluated with quantitative PCR to determine mRNA knockdown from harvested tumors. Furthermore, upon successful silencing of Bcl-xL mRNA *in vivo*, studies with pretreatment of siRNA conjugates and combined carboplatin treatment should be conducted to determine sensitization with trastuzumab-Bcl-xL siRNA conjugates by a reduction in tumor size and increase mice survival.

5.3.2 Substitution of PDB, pH-responsive block with EB-based technology

Manganiello, *et al*. reported on a family of diblock copolymer (EB) with tunable pH transition for gene delivery that has a diethylaminoethyl methacrylate (DEAEMA) and butyl methacrylate

(BMA) pH-responsive micelle core[149]. This family of polymers exhibited greater pH-responsive behavior by a red blood cell hemolysis assay than compared to the corresponding PAA-DMAEMA-BMA (PDB) based polymers. In collaboration with Matthew Manganiello, we tested these cationic polymers as siRNA delivery carriers. We determined that there was a minimum polymer concentration in order to achieve efficacy, but to avoid significant toxicity a N:P ratio of 4:1 was necessary. Thus, the overall amount of siRNA was 50 nmol/L to achieve these parameters. An interesting finding based on these studies was that a 1:4 and 1:2 (GAPDH:scrambled) mixture of siRNA reduced GAPDH mRNA expression in HeLa cancer cells to 40 % and 30 %, respectively, while an overall 25 nmol/L GAPDH dose had negligible RNA silencing (data unpublished). We propose the investigation of EB-based siRNA conjugates, due to their potent pH-responsive behaviors; however, we acknowledge that the overall polymer dose for the conjugates may be higher than the PDB-based conjugates.

5.3.3 Polymer redesign to increase biocompatibility and siRNA protection in vivo

One potential limitation with our siRNA-polymer conjugates is the lack of siRNA shielding and protection by the neutral corona of the micellar system[150]. We hypothesize the replacement of the hydrophilic monomer HPMA with poly (ethylene glycol) methyl ether methacrylate (PEGMA) in the micelle corona could provide a better protective shield from nucleases[36]. Initial investigations with siRNA conjugation to a $PEGMA_{900}$-co-PDMSA polymer micelle did not show significant siRNA conjugation at a 40:1 polymer to siRNA ratio. However, our laboratory has recently made both PDB and EB based micelles incorporation $PEGMA_{300}$ into the corona for the delivery of therapeutic peptides. We propose the exploration of siRNA conjugates with the PEGMA modification in order to increase siRNA protection of exonuclease *in vivo*.

5.4 CONCLUSIONS

The work presented in this dissertation demonstrates an improved siRNA delivery approach via systemic administration with siRNA-polymer based conjugates. This research was prompted by the *in vitro* success of the cationic, pH-responsive siRNA complexion delivery carrier, but due to its associate toxicity when administered intravenously, the need to develop a more biocompatible carrier arose. By determining that biocompatibility, cell specific targeting, and escape from the endosomal pathway were the major barriers to a robust systemic *in vivo* siRNA delivery we designed a neutral, pH-responsive micellular system with targeting and siRNA conjugation functionalities. Employing RAFT-based controlled radical polymerization technology, we developed synthetic conditions to generate a highly controlled neutral based polymer micelle, with pH-responsive membrane destabilizing behavior for the direct conjugation of siRNA. The development of this polymer has been the foundation of other carriers evaluated in our laboratory including vaccine and peptide delivery polymer conjugate systems. The well-defined diblock copolymer were successfully synthesized, self assembled into micelles, and conjugated thiolated siRNA while retaining their pH-responsive profiles. The siRNA-polymer conjugates were highly effective *in vitro* and were optimized with trastuzumab or mannose targeting to improve efficacy in a desired cell populations. The therapeutic Bcl-xL siRNA-polymer conjugates that had HER2+ targeting sensitized ovarian cancer cells to carboplatin. Most importantly, siRNA-polymer conjugates were well tolerated after systemic administration *in vivo*. This system holds great promise to become the first generation of therapeutic siRNA-polymer conjugates for effective gene silencing following systemic administration *in vivo*.

Chapter 6. REFERENCES

(1) Dollery, C. T. Intracellular Drug Concentrations. *Clin Pharmacol Ther* **2012**, *93*, 263–266.

(2) Sawyer, T. K. AILERON Therapeutics. *Chemical Biology & Drug Design* **2009**, *73*, 3–6.

(3) Fire, A.; Xu, S.; Montgomery, M. K.; Kostas, S. A.; Driver, S. E.; Mello, C. C. Potent and specific genetic interference by double-stranded RNA in Caenorhabditis elegans. *Nature* **1998**, *391*, 806–811.

(4) Elbashir, S. M.; Harborth, J.; Lendeckel, W.; Yalcin, A.; Weber, K.; Tuschl, T. Duplexes of 21-nucleotide RNAs mediate RNA interference in cultured mammalian cells. *Nature* **2001**, *411*, 494–498.

(5) Brummelkamp, T. R.; Bernards, R.; Agami, R. A system for stable expression of short interfering RNAs in mammalian cells. *Science* **2002**, *296*, 550–553.

(6) Akhtar, S.; Benter, I. F. Nonviral delivery of synthetic siRNAs in vivo. *J. Clin. Invest.* **2007**, *117*, 3623–3632.

(7) Tijsterman, M.; Plasterk, R. H. A. Dicers at RISC; the mechanism of RNAi. *Cell* **2004**, *117*, 1–3.

(8) Meister, G.; Landthaler, M.; Peters, L.; Chen, P. Y.; Urlaub, H.; Lührmann, R.; Tuschl, T. Identification of Novel Argonaute-Associated Proteins. *Current Biology* **2005**, *15*, 2149–2155.

(9) Kim, D. H.; Rossi, J. J. Strategies for silencing human disease using RNA interference. *Nat. Rev. Genet.* **2007**, *8*, 173–184.

(10) Shim, M. S.; Kwon, Y. J. Efficient and targeted delivery of siRNA in vivo. *FEBS Journal* **2010**, *277*, 4814–4827.

(11) Bumcrot, D.; Manoharan, M.; Koteliansky, V.; Sah, D. W. Y. RNAi therapeutics: a potential new class of pharmaceutical drugs. *Nat. Chem. Biol.* **2006**, *2*, 711–719.

(12) Judge, A. D.; Sood, V.; Shaw, J. R.; Fang, D.; McClintock, K.; MacLachlan, I. Sequence-dependent stimulation of the mammalian innate immune response by synthetic siRNA. *Nat Biotechnol* **2005**, *23*, 457–462.

(13) Qixin Leng, M. C. W. P. Y. L. A. J. M. Advances in Systemic siRNA Delivery. *Drugs of the future* **2009**, *34*, 721.

(14) Shim, M. S.; Kwon, Y. J. Efficient and targeted delivery of siRNA in vivo. *FEBS Journal* **2010**, *227*, 4817–4827.

(15) Elsabahy, M.; Nazarali, A.; Foldvari, M. Non-viral nucleic acid delivery: key challenges and future directions. *Curr Drug Deliv* **2011**, *8*, 235–244.

(16) Gilmore, I. R.; Fox, S. P.; Hollins, A. J.; Sohail, M.; Akhtar, S. The design and exogenous delivery of siRNA for post-transcriptional gene silencing. *Journal of Drug Targeting* **2004**, *12*, 315–340.

(17) Sato, A.; Choi, S.; Hirai, M.; Yamayoshi, A. ScienceDirect - Journal of Controlled Release : Polymer brush-stabilized polyplex for a siRNA carrier with long circulatory half-life. *Journal of Controlled …* **2007**.

(18) Tokatlian, T.; Segura, T. siRNA applications in nanomedicine. *Wiley Interdiscip Rev Nanomed Nanobiotechnol* **2010**, *2*, 305–315.

(19) Musacchio, T.; Vaze, O.; D'Souza, G.; Torchilin, V. P. Effective stabilization and delivery of siRNA: reversible siRNA-phospholipid conjugate in nanosized mixed polymeric micelles. *Bioconjug Chem* **2010**, *21*, 1530–1536.
(20) Jiang, G.; Park, K.; Kim, J.; Kim, K. S.; Hahn, S. K. Target Specific Intracellular Delivery of siRNA/PEI–HA Complex by Receptor Mediated Endocytosis. *Mol Pharmaceut* **2009**, *6*, 727–737.
(21) Jang, S. H.; Wientjes, M. G.; Lu, D.; Au, J. L.-S. SpringerLink - Pharmaceutical Research, Volume 20, Number 9. *Pharm Res* **2003**, *20*, 1337–1350.
(22) Cho, Y. W.; Kim, J.-D.; Park, K. Polycation gene delivery systems: escape from endosomes to cytosol. *J. Pharm. Pharmacol.* **2003**, *55*, 721–734.
(23) Palanca-Wessels, M. C.; Convertine, A. J.; Cutler-Strom, R.; Booth, G. C.; Lee, F.; Berguig, G. Y.; Stayton, P. S.; Press, O. W. Anti-CD22 Antibody Targeting of pH-responsive Micelles Enhances Small Interfering RNA Delivery and Gene Silencing in Lymphoma Cells. *Mol. Ther.* **2011**, *19*, 1529–1537.
(24) Du, F.-S.; Wang, Y.; Zhang, R.; Li, Z.-C. Intelligent nucleic acid delivery systems based on stimuli-responsive polymers. *Soft Matter* **2010**, *6*, 835.
(25) Breunig, M.; Hozsa, C.; Lungwitz, U.; Watanabe, K.; Umeda, I.; Kato, H.; Goepferich, A. Mechanistic investigation of poly(ethylene imine)-based siRNA delivery: Disulfide bonds boost intracellular release of the cargo. *Journal of Controlled Release* **2008**, *130*, 57–63.
(26) Cheung, C. Y.; Murthy, N.; Stayton, P. S.; Hoffman, A. S. A pH-sensitive polymer that enhances cationic lipid-mediated gene transfer. *Bioconjug Chem* **2001**, *12*, 906–910.
(27) Wadia, J.; Stan, R.; Dowdy, S. Transducible TAT-HA fusogenic peptide enhances escape of TAT-fusion proteins after lipid raft macropinocytosis. *Nat Med* **2004**.
(28) Murthy, N.; Robichaud, J.; Tirrell, D. ScienceDirect - Journal of Controlled Release : The design and synthesis of polymers for eukaryotic membrane disruption. *Journal of Controlled …* **1999**.
(29) Lackey, C. A.; Press, O. W.; Hoffman, A. S.; Stayton, P. S. A Biomimetic pH-Responsive Polymer Directs Endosomal Release and Intracellular Delivery of an Endocytosed Antibody Complex. *Bioconjug Chem* **2002**, *13*, 996–1001.
(30) El-Sayed, M. E.; Hoffman, A. S.; Stayton, P. S. Smart polymeric carriers for enhanced intracellular delivery of therapeutic macromolecules. *Expert Opin. Biol. Ther.* **2005**, *5*, 23–32.
(31) Kim, W. J.; Kim, S. W. Efficient siRNA Delivery with Non-viral Polymeric Vehicles. *Pharm Res* **2008**, *26*, 657–666.
(32) Godbey, W. T.; Barry, M. A.; Saggau, P.; Wu, K. K.; Mikos, A. G. Poly(ethylenimine)-mediated transfection: a new paradigm for gene delivery. *J. Biomed. Mater. Res.* **2000**, *51*, 321–328.
(33) Oishi, M.; Nagasaki, Y.; Itaka, K.; Nishiyama, N.; Kataoka, K. Lactosylated poly(ethylene glycol)-siRNA conjugate through acid-labile beta-thiopropionate linkage to construct pH-sensitive polyion complex micelles achieving enhanced gene silencing in hepatoma cells. *J. Am. Chem. Soc.* **2005**, *127*, 1624–1625.
(34) Heredia, K. L.; Nguyen, T. H.; Chang, C.-W.; Bulmus, V.; Davis, T. P.; Maynard, H. D. Reversible siRNA-polymer conjugates by RAFT polymerization. *Chem. Commun. (Camb.)* **2008**, 3245–3247.
(35) Choi, S. W.; Lee, S. H.; Mok, H.; Park, T. G. Multifunctional siRNA delivery system:

polyelectrolyte complex micelles of six-arm PEG conjugate of siRNA and cell penetrating peptide with crosslinked fusogenic peptide. *Biotechnol. Prog.* **2010**, *26*, 57–63.

(36) Rozema, D. B.; Lewis, D. L.; Wakefield, D. H.; Wong, S. C.; Klein, J. J.; Roesch, P. L.; Bertin, S. L.; Reppen, T. W.; Chu, Q.; Blokhin, A. V.; Hagstrom, J. E.; Wolff, J. A. Dynamic PolyConjugates for targeted in vivo delivery of siRNA to hepatocytes. *Proc Natl Acad Sci USA* **2007**, *104*, 12982–12987.

(37) York, A. W.; Huang, F.; McCormick, C. L. Rational Design of Targeted Cancer Therapeutics through the Multiconjugation of Folate and Cleavable siRNA to RAFT-Synthesized (HPMA- s-APMA) Copolymers †. *Biomacromolecules* **2010**, *11*, 505–514.

(38) Chiefari, J.; Chong, Y. K. B.; Ercole, F.; Krstina, J.; Jeffery, J.; Le, T. P. T.; Mayadunne, R. T. A.; Meijs, G. F.; Moad, C. L.; Moad, G.; Rizzardo, E.; Thang, S. H. Living Free-Radical Polymerization by Reversible Addition–Fragmentation Chain Transfer: The RAFT Process. *Macromolecules* **1998**, *31*, 5559–5562.

(39) Bernard, J.; Hao, X.; Davis, T. P.; Barner-Kowollik, C.; Stenzel, M. H. Synthesis of various glycopolymer architectures via RAFT polymerization: from block copolymers to stars. *Biomacromolecules* **2006**, *7*, 232–238.

(40) Barner-Kowollik, C.; Buback, M.; Charleux, B.; Coote, M. L.; Drache, M.; Fukuda, T.; Goto, A.; Klumperman, B.; Lowe, A. B.; Mcleary, J. B.; Moad, G.; Monteiro, M. J.; Sanderson, R. D.; Tonge, M. P.; Vana, P. Mechanism and kinetics of dithiobenzoate-mediated RAFT polymerization. I. The current situation. *J. Polym. Sci. A Polym. Chem.* **2006**, *44*, 5809–5831.

(41) Boyer, C.; Granville, A.; Davis, T. Modification of RAFT-polymers via thiol-ene reactions: A general route to functional polymers and new architectures. *Journal of Polymer …* **2009**.

(42) Xu, X.; McCormick, C. Stimuli-responsive amphiphilic (co) polymers via RAFT polymerization. *Progress in Polymer Science* **2010**.

(43) Zhu, J.; Zhou, Z.; Yang, C.; Kong, D.; Wan, Y.; Wang, Z. Folate-conjugated amphiphilic star-shaped block copolymers as targeted nanocarriers. *J Biomed Mater Res A* **2011**, *97*, 498–508.

(44) YOKOYAMA, M. Polymeric micelles for the targeting of hydrophobic drugs. *Polymeric Drug Delivery Systems*.

(45) Benoit, D. S. W.; Henry, S. M.; Shubin, A. D.; Hoffman, A. S.; Stayton, P. S. pH-responsive polymeric sirna carriers sensitize multidrug resistant ovarian cancer cells to doxorubicin via knockdown of polo-like kinase 1. *Mol Pharmaceut* **2010**, *7*, 442–455.

(46) Convertine, A. J.; Diab, C.; Prieve, M.; Paschal, A.; Hoffman, A. S.; Johnson, P. H.; Stayton, P. S. pH-Responsive Polymeric Micelle Carriers for siRNA Drugs. *Biomacromolecules* **2010**.

(47) Yu, B.; Zhao, X.; Lee, L. J.; Lee, R. J. Targeted delivery systems for oligonucleotide therapeutics. *AAPS J* **2009**, *11*, 195–203.

(48) York, A. W.; Zhang, Y.; Holley, A. C.; Guo, Y.; Huang, F.; McCormick, C. L. Facile synthesis of multivalent folate-block copolymer conjugates via aqueous RAFT polymerization: targeted delivery of siRNA and subsequent gene suppression. *Biomacromolecules* **2009**, *10*, 936–943.

(49) Tietze, N.; Pelisek, J.; Philipp, A.; Roedl, W.; Merdan, T.; Tarcha, P.; Ogris, M.;

Wagner, E. Induction of apoptosis in murine neuroblastoma by systemic delivery of transferrin-shielded siRNA polyplexes for downregulation of Ran. *Oligonucleotides* **2008**, *18*, 161–174.

(50) Xia, C.-F.; Boado, R. J.; Pardridge, W. M. Antibody-mediated targeting of siRNA via the human insulin receptor using avidin-biotin technology. *Mol Pharmaceut* **2009**, *6*, 747–751.

(51) Oishi, M.; Nagasaki, Y.; Nishiyama, N.; Itaka, K.; Takagi, M.; Shimamoto, A.; Furuichi, Y.; Kataoka, K. Enhanced growth inhibition of hepatic multicellular tumor spheroids by lactosylated poly(ethylene glycol)-siRNA conjugate formulated in PEGylated polyplexes. *ChemMedChem* **2007**, *2*, 1290–1297.

(52) Yang, R.; Meng, F.; Ma, S.; Huang, F.; Liu, H.; Zhong, Z. Galactose-Decorated Cross-Linked Biodegradable Poly(ethylene glycol)- b-poly(ε-caprolactone) Block Copolymer Micelles for Enhanced Hepatoma-Targeting Delivery of Paclitaxel. *Biomacromolecules* **2011**, *12*, 3047–3055.

(53) Vázquez-Dorbatt, V.; Tolstyka, Z. P.; Chang, C.-W.; Maynard, H. D. Synthesis of a Pyridyl Disulfide End-Functionalized Glycopolymer for Conjugation to Biomolecules and Patterning on Gold Surfaces. *Biomacromolecules* **2009**, *10*, 2207–2212.

(54) Zielinski, R.; Lyakhov, I.; Hassan, M.; Kuban, M.; Shafer-Weaver, K.; Gandjbakhche, A.; Capala, J. HER2-Affitoxin: A Potent Therapeutic Agent for the Treatment of HER2-Overexpressing Tumors. *Clin Cancer Res* **2011**, *17*, 5071–5081.

(55) Tai, W.; Mahato, R.; Cheng, K. The role of HER2 in cancer therapy and targeted drug delivery. *J Control Release* **2010**, *146*, 264–275.

(56) DESANTES, K.; SLAMON, D.; ANDERSON, S.; SHEPARD, M.; FENDLY, B.; MANEVAL, D.; PRESS, O. Radiolabeled Antibody Targeting of the Her-2/Neu Oncoprotein. *Cancer Res*. **1992**, *52*, 1916–1923.

(57) Pegram, M.; Konecny, G.; Slamon, D. The molecular and cellular biology of HER2/neu gene amplification/overexpression and the clinical development of herceptin (trastuzumab) therapy for breast cancer. *Advances in Breast Cancer …* **2000**.

(58) Niehans, G.; Singleton, T. Stability of HER-2/neu expression over time and at multiple metastatic sites. *Journal of the …* **1993**.

(59) Tiwari, S.; Chaturvedi, A. P.; Tripathi, Y. B.; Mishra, B. Macrophage-specific targeting of isoniazid through mannosylated gelatin microspheres. *AAPS PharmSciTech* **2011**, *12*, 900–908.

(60) Liang, W. W.; Shi, X.; Deshpande, D.; Malanga, C. J.; Rojanasakul, Y. Oligonucleotide targeting to alveolar macrophages by mannose receptor-mediated endocytosis. *Biochim Biophys Acta* **1996**, *1279*, 227–234.

(61) Dong, L.; Xia, S.; Luo, Y.; Diao, H.; Zhang, J. Targeting delivery oligonucleotide into macrophages by cationic polysaccharide from Bletilla striata successfully inhibited the expression of TNF-[alpha]. *Journal of Controlled …* **2009**.

(62) Singodia, D.; Verma, A.; Verma, R. K.; Mishra, P. R. Investigations into an alternate approach to target mannose receptors on macrophages using 4-sulfated N-acetyl galactosamine more efficiently in comparison with mannose-decorated liposomes: An application in drug delivery. *Nanomedicine* **2011**.

(63) Nimje, N.; Agarwal, A.; Saraogi, G. K.; Lariya, N.; Rai, G.; Agrawal, H.; Agrawal, G. P. Mannosylated nanoparticulate carriers of rifabutin for alveolar targeting. *http://dx.doi.org.offcampus.lib.washington.edu/10.3109/10611860903115308* **2009**.

(64) Aliabadi, H. M.; Landry, B.; Sun, C.; Tang, T.; Uludağ, H. Supramolecular assemblies in functional siRNA delivery: Where do we stand? *Biomaterials* **2012**, *33*, 2546–2569.
(65) Whitehead, K. A.; Langer, R.; Anderson, D. G. Knocking down barriers: advances in siRNA delivery. *Nat Rev Drug Discov* **2009**, *8*, 129–138.
(66) Guo, P.; Coban, O.; Snead, N. M.; Trebley, J.; Hoeprich, S.; Guo, S.; Shu, Y. Engineering RNA for Targeted siRNA Delivery and Medical Application. *Adv Drug Deliv Rev* **2010**, *62*, 650–666.
(67) Landen, C.; Chavez-Reyes, A.; Bucana, C.; Schmandt, R.; Deavers, M.; Lopez-Berestein, G.; Sood, A. Therapeutic EphA2 gene targeting in vivo using neutral liposomal small interfering RNA delivery. *Cancer Res*. **2005**, *65*, 6910–6918.
(68) Tran, M. A.; Watts, R. J.; Robertson, G. P. Use of liposomes as drug delivery vehicles for treatment of melanoma. *Pigm Cell Melanoma R* **2009**, *22*, 388–399.
(69) Villares, G. J. G.; Zigler, M. M.; Wang, H. H.; Melnikova, V. O. V.; Wu, H. H.; Friedman, R. R.; Leslie, M. C. M.; Vivas-Mejia, P. E. P.; Lopez-Berestein, G. G.; Sood, A. K. A.; Bar-Eli, M. M. Targeting melanoma growth and metastasis with systemic delivery of liposome-incorporated protease-activated receptor-1 small interfering RNA. *CORD Conference Proceedings* **2008**, *68*, 9078–9086.
(70) Halder, J. J.; Kamat, A. A. A.; Landen, C. N. C.; Han, L. Y. L.; Lutgendorf, S. K. S.; Lin, Y. G. Y.; Merritt, W. M. W.; Jennings, N. B. N.; Chavez-Reyes, A. A.; Coleman, R. L. R.; Gershenson, D. M. D.; Schmandt, R. R.; Cole, S. W. S.; Lopez-Berestein, G. G.; Sood, A. K. A. Focal adhesion kinase targeting using in vivo short interfering RNA delivery in neutral liposomes for ovarian carcinoma therapy. *Clin Cancer Res* **2006**, *12*, 4916–4924.
(71) Sato, A.; Takagi, M.; Shimamoto, A.; Kawakami, S.; Hashida, M. Small interfering RNA delivery to the liver by intravenous administration of galactosylated cationic liposomes in mice. *Biomaterials* **2007**, *28*, 1434–1442.
(72) Chien, P.-Y. P.; Wang, J. J.; Carbonaro, D. D.; Lei, S. S.; Miller, B. B.; Sheikh, S. S.; Ali, S. M. S.; Ahmad, M. U. M.; Ahmad, I. I. Novel cationic cardiolipin analogue-based liposome for efficient DNA and small interfering RNA delivery in vitro and in vivo. *Cancer Gene Ther* **2005**, *12*, 321–328.
(73) Pal, A. A.; Ahmad, A. A.; Khan, S. S.; Sakabe, I. I.; Zhang, C. C.; Kasid, U. N. U.; Ahmad, I. I. Systemic delivery of RafsiRNA using cationic cardiolipin liposomes silences Raf-1 expression and inhibits tumor growth in xenograft model of human prostate cancer. *Int J Oncol* **2005**, *26*, 1087–1091.
(74) Basha, G.; Novobrantseva, T. I.; Rosin, N.; Tam, Y. Y. C.; Hafez, I. M.; Wong, M. K.; Sugo, T.; Ruda, V. M.; Qin, J.; Klebanov, B.; Ciufolini, M.; Akinc, A.; Tam, Y. K.; Hope, M. J.; Cullis, P. R. Influence of Cationic Lipid Composition on Gene Silencing Properties of Lipid Nanoparticle Formulations of siRNA in Antigen-Presenting Cells. *Mol. Ther.* **2011**, *19*, 2186–2200.
(75) Semple, S. C.; Akinc, A.; Chen, J.; Sandhu, A. P.; Mui, B. L.; Cho, C. K.; Sah, D. W. Y.; Stebbing, D.; Crosley, E. J.; Yaworski, E.; Hafez, I. M.; Dorkin, J. R.; Qin, J.; Lam, K.; Rajeev, K. G.; Wong, K. F.; Jeffs, L. B.; Nechev, L.; Eisenhardt, M. L.; Jayaraman, M.; Kazem, M.; Maier, M. A.; Srinivasulu, M.; Weinstein, M. J.; Chen, Q.; Alvarez, R.; Barros, S. A.; De, S.; Klimuk, S. K.; Borland, T.; Kosovrasti, V.; Cantley, W. L.; Tam, Y. K.; Manoharan, M.; Ciufolini, M. A.; Tracy, M. A.; de Fougerolles, A.; MacLachlan, I.; Cullis, P. R.; Madden, T. D.; Hope, M. J. Rational design of cationic

lipids for siRNA delivery. *Nat Biotechnol* **2010**, *28*, 172–176.
(76) Huang, Y.-H.; Bao, Y.; Peng, W.; Goldberg, M.; Love, K.; Bumcrot, D. A.; Cole, G.; Langer, R.; Anderson, D. G.; Sawicki, J. A. Claudin-3 gene silencing with siRNA suppresses ovarian tumor growth and metastasis. *Proc Natl Acad Sci USA* **2009**, *106*, 3426–3430.
(77) Leuschner, F. F.; Dutta, P. P.; Gorbatov, R. R.; Novobrantseva, T. I. T.; Donahoe, J. S. J.; Courties, G. G.; Lee, K. M. K.; Kim, J. I. J.; Markmann, J. F. J.; Marinelli, B. B.; Panizzi, P. P.; Lee, W. W. W.; Iwamoto, Y. Y.; Milstein, S. S.; Epstein-Barash, H. H.; Cantley, W. W.; Wong, J. J.; Cortez-Retamozo, V. V.; Newton, A. A.; Love, K. K.; Libby, P. P.; Pittet, M. J. M.; Swirski, F. K. F.; Koteliansky, V. V.; Langer, R. R.; Weissleder, R. R.; Anderson, D. G. D.; Nahrendorf, M. M. Therapeutic siRNA silencing in inflammatory monocytes in mice. *Nat Biotechnol* **2011**, *29*, 1005–1010.
(78) Hashida, M.; Kawakami, S.; Yamashita, F. Lipid carrier systems for targeted drug and gene delivery. *Chem Pharm Bull (Tokyo)* **2005**, *53*, 871–880.
(79) Mahon, K. P.; Love, K. T.; Whitehead, K. A.; Qin, J.; Akinc, A.; Leshchiner, E.; Leshchiner, I.; Langer, R.; Anderson, D. G. Combinatorial approach to determine functional group effects on lipidoid-mediated siRNA delivery. *Bioconjug Chem* **2010**, *21*, 1448–1454.
(80) Howard, K. A.; Rahbek, U. L.; Liu, X.; Damgaard, C. K.; Glud, S. Z.; Andersen, M. O.; Hovgaard, M. B.; Schmitz, A.; Nyengaard, J. R.; Besenbacher, F.; Kjems, J. RNA interference in vitro and in vivo using a chitosan/siRNA nanoparticle system. *Mol. Ther.* **2006**, *14*, 476–484.
(81) Howard, K. A.; Paludan, S. R.; Behlke, M. A.; Besenbacher, F.; Deleuran, B.; Kjems, J. Chitosan/siRNA Nanoparticle-mediated TNF-alpha Knockdown in Peritoneal Macrophages for Anti-inflammatory Treatment in a Murine Arthritis Model. *CORD Conference Proceedings* **2009**, *17*, 162–168.
(82) Sarmento, B.; Neves, das, J. *Chitosan-Based Systems for Biopharmaceuticals*; Delivery, Targeting and Polymer Therapeutics; Wiley, 2012; p. 592.
(83) Pillé, J.-Y. J.; Li, H. H.; Blot, E. E.; Bertrand, J.-R. J.; Pritchard, L.-L. L.; Opolon, P. P.; Maksimenko, A. A.; Lu, H. H.; Vannier, J.-P. J.; Soria, J. J.; Malvy, C. C.; Soria, C. C. Intravenous delivery of anti-RhoA small interfering RNA loaded in nanoparticles of chitosan in mice: safety and efficacy in xenografted aggressive breast cancer. *Hum Gene Ther* **2006**, *17*, 1019–1026.
(84) Heidel, J. D.; Yu, Z.; Liu, J. Y.-C.; Rele, S. M.; Liang, Y.; Zeidan, R. K.; Kornbrust, D. J.; Davis, M. E. Administration in non-human primates of escalating intravenous doses of targeted nanoparticles containing ribonucleotide reductase subunit M2 siRNA. *Proc Natl Acad Sci USA* **2007**, *104*, 5715–5721.
(85) Wightman, L. L.; Kircheis, R. R.; Rössler, V. V.; Carotta, S. S.; Ruzicka, R. R.; Kursa, M. M.; Wagner, E. E. Different behavior of branched and linear polyethylenimine for gene delivery in vitro and in vivo. *J Gene Med* **2001**, *3*, 362–372.
(86) Wang, Y.; Li, Z.; Han, Y.; Liang, L. H.; Ji, A. Nanoparticle-based delivery system for application of siRNA in vivo. *Curr Drug Metab* **2010**, *11*, 182–196.
(87) Kim, I.-D.; Lim, C.-M.; Kim, J.-B.; Nam, H. Y.; Nam, K.; Kim, S.-W.; Park, J.-S.; Lee, J.-K. Neuroprotection by biodegradable PAMAM ester (e-PAM-R)-mediated HMGB1 siRNA delivery in primary cortical cultures and in the postischemic brain. *Journal of Controlled Release* **2010**, *142*, 422–430.

(88) Watanabe, K.; Harada-Shiba, M.; Suzuki, A.; Gokuden, R.; Kurihara, R.; Sugao, Y.; Mori, T.; Katayama, Y.; Niidome, T. In vivo siRNA delivery with dendritic poly(L-lysine) for the treatment of hypercholesterolemia. *Mol Biosyst* **2009**, *5*, 1306–1310.
(89) Khan, A.; Benboubetra, M.; Sayyed, P. Z.; Ng, K. W.; Fox, S.; Beck, G.; Benter, I. F.; Akhtar, S. Sustained polymeric delivery of gene silencing antisense ODNs, siRNA, DNAzymes and ribozymes: in vitro and in vivo studies. *Journal of Drug Targeting* **2004**, *12*, 393–404.
(90) Soutschek, J.; Akinc, A.; Bramlage, B.; Charisse, K. Therapeutic silencing of an endogenous gene by systemic administration of modified siRNAs. *Nature* **2004**.
(91) Wolfrum, C.; Shi, S.; Jayaprakash, K. Mechanisms and optimization of in vivo delivery of lipophilic siRNAs. *Nature* **2007**.
(92) Lorenz, C.; Hadwiger, P.; John, M. Steroid and lipid conjugates of siRNAs to enhance cellular uptake and gene silencing in liver cells. *Bioorganic & medicinal …* **2004**.
(93) Nishina, K.; Unno, T.; Uno, Y.; Kubodera, T. Efficient in vivo delivery of siRNA to the liver by conjugation of α-tocopherol. *Molecular …* **2008**.
(94) Chiu, Y.-L.; Ali, A.; Chu, C.-Y.; Cao, H.; Rana, T. M. Visualizing a Correlation between siRNA Localization, Cellular Uptake, and RNAi in Living Cells. *Chemistry & Biology* **2004**, *11*, 1165–1175.
(95) Moschos, S. A. S.; Jones, S. W. S.; Perry, M. M. M.; Williams, A. E. A.; Erjefalt, J. S. J.; Turner, J. J. J.; Barnes, P. J. P.; Sproat, B. S. B.; Gait, M. J. M.; Lindsay, M. A. M. Lung delivery studies using siRNA conjugated to TAT(48-60) and penetratin reveal peptide induced reduction in gene expression and induction of innate immunity. *Bioconjug Chem* **2007**, *18*, 1450–1459.
(96) Muratovska, A.; Eccles, M. R. Conjugate for efficient delivery of short interfering RNA (siRNA) into mammalian cells. *FEBS Letters* **2004**, *558*, 63–68.
(97) Gunasekaran, K.; Nguyen, T. H.; Maynard, H. D.; Davis, T. P.; Bulmus, V. Conjugation of siRNA with Comb-Type PEG Enhances Serum Stability and Gene Silencing Efficiency. *Macromol Rapid Commun* **2011**, *32*, 654–659.
(98) Kim, S. H.; Jeong, J. H.; Lee, S. H.; Kim, S. W.; Park, T. G. PEG conjugated VEGF siRNA for anti-angiogenic gene therapy. *Journal of Controlled Release* **2006**, *116*, 123–129.
(99) Lee, S. H.; Mok, H.; Park, T. G. Di- and Triblock siRNA-PEG Copolymers: PEG Density Effect of Polyelectrolyte Complexes on Cellular Uptake and Gene Silencing Efficiency. *Macromol. Biosci.* **2010**, *11*, 410–418.
(100) Xu, J.; Boyer, C.; Bulmus, V.; Davis, T. P. Synthesis of dendritic carbohydrate end-functional polymers via RAFT: Versatile multi-functional precursors for bioconjugations. *J. Polym. Sci. A Polym. Chem.* **2009**, *47*, 4302–4313.
(101) Convertine, A. J.; Benoit, D. S. W.; Duvall, C. L.; Hoffman, A. S.; Stayton, P. S. Development of a novel endosomolytic diblock copolymer for siRNA delivery. *Journal of Controlled Release* **2009**, *133*, 221–229.
(102) Crownover, E.; Duvall, C. L.; Convertine, A.; Hoffman, A. S.; Stayton, P. S. RAFT-synthesized graft copolymers that enhance pH-dependent membrane destabilization and protein circulation times. *J Control Release* **2011**.
(103) Crownover, E. F.; Convertine, A. J.; Stayton, P. S. pH-responsive polymer-antigen vaccine bioconjugates. *Polym. Chem.* **2011**, *2*, 1499–1504.
(104) Scales, C.; Vasilieva, Y.; Convertine, A.; Lowe, A.; McCormick, C. Direct, controlled

synthesis of the nonimmunogenic, hydrophilic polymer, poly(N-(2-hydroxypropyl)methacrylamide) via RAFT in aqueous media. *Biomacromolecules* **2005**, *6*, 1846–1850.

(105) Scales, C. W.; Huang, F.; Li, N.; Vasilieva, Y. A.; Ray, J.; Convertine, A. J.; McCormick, C. L. Corona-Stabilized Interpolyelectrolyte Complexes of SiRNA with Nonimmunogenic, Hydrophilic/Cationic Block Copolymers Prepared by Aqueous RAFT Polymerization †. *Macromolecules* **2006**, *39*, 6871–6881.

(106) Xie, F. Y.; Woodle, M. C.; Lu, P. Y. Harnessing in vivo siRNA delivery for drug discovery and therapeutic development. *Drug Discov Today* **2006**, *11*, 67–73.

(107) Torchilin, V. Recent advances with liposomes as pharmaceutical carriers. *Nat Rev Drug Discov* **2005**, *4*, 145–160.

(108) Puri, A.; Loomis, K.; Smith, B.; Lee, J.-H.; Yavlovich, A.; Heldman, E.; Blumenthal, R. Lipid-Based Nanoparticles as Pharmaceutical Drug Carriers: From Concepts to Clinic. *Crit Rev Ther Drug* **2009**, *26*, 523–580.

(109) Siegel, R.; Naishadham, D. Cancer statistics, 2013 - Siegel - 2013 - CA: A Cancer Journal for Clinicians - Wiley Online Library. … *cancer journal for clinicians* **2013**.

(110) Witham, J.; Valenti, M. R.; De-Haven-Brandon, A. K.; Vidot, S.; Eccles, S. A.; Kaye, S. B.; Richardson, A. The Bcl-2/Bcl-XL Family Inhibitor ABT-737 Sensitizes Ovarian Cancer Cells to Carboplatin. *Clinical Cancer Research* **2007**, *13*, 7191–7198.

(111) Boise, L.; González-Garcia, M.; Postema, C.; Ding, L. bcl-x, a bcl-2-related gene that functions as a dominant regulator of apoptotic cell death. *Cell* **1993**.

(112) Castle, V. P.; Heidelberger, K. P.; Bromberg, J.; Ou, X.; Dole, M.; Nunez, G. Expression of the apoptosis-suppressing protein bcl-2, in neuroblastoma is associated with unfavorable histology and N-myc amplification. *Am. J. Pathol.* **1993**, *143*, 1543–1550.

(113) Dole, M.; Nunez, G.; Merchant, A. K.; Maybaum, J.; Rode, C. K.; Bloch, C. A.; Castle, V. P. Bcl-2 inhibits chemotherapy-induced apoptosis in neuroblastoma. *Cancer Res.* **1994**, *54*, 3253–3259.

(114) Williams, J.; Lucas, P. C.; Griffith, K. A.; Choi, M.; Fogoros, S.; Hu, Y. Y.; Liu, J. R. Expression of Bcl-xL in ovarian carcinoma is associated with chemoresistance and recurrent disease. *Gynecologic Oncology* **2005**, *96*, 287–295.

(115) Liu, J. R.; Fletcher, B.; Page, C.; Hu, C.; Nunez, G.; Baker, V. Bcl-xL is expressed in ovarian carcinoma and modulates chemotherapy-induced apoptosis. *Gynecologic Oncology* **1998**, *70*, 398–403.

(116) Vidot, S.; Witham, J.; Agarwal, R.; Greenhough, S.; Bamrah, H. S.; Tigyi, G. J.; Kaye, S. B.; Richardson, A. Autotaxin delays apoptosis induced by carboplatin in ovarian cancer cells. *Cell Signal* **2010**, *22*, 926–935.

(117) Yang, J.; Sun, M.; Zhang, A.; Lv, C.; De, W.; Wang, Z. Adenovirus-mediated siRNA targeting Bcl-xL inhibits proliferation, reduces invasion and enhances radiosensitivity of human colorectal cancer cells. *World Journal of Surgical Oncology* **2011**, *9*, 117.

(118) Kunigal, S.; Lakka, S. S.; Sodadasu, P. K.; Estes, N.; Rao, J. S. Stat3-siRNA induces Fas-mediated apoptosis in vitro and in vivo in breast cancer. *Int J Oncol* **2009**, *34*, 1209–1220.

(119) Jagani, H. V.; Josyula, V. R.; Palanimuthu, V. R.; Hariharapura, R. C.; Gang, S. S. Improvement of therapeutic efficacy of PLGA nanoformulation of siRNA targeting anti-apoptotic Bcl-2 through chitosan coating. *EUROPEAN JOURNAL OF*

PHARMACEUTICAL SCIENCES **2013**, *48*, 611–618.
(120) Allen, T. Ligand-targeted therapeutics in anticancer therapy. *Nature Reviews Cancer* **2002**.
(121) Yu, B.; Mao, Y.; Bai, L.; Herman, S. Targeted nanoparticle delivery overcomes off-target immunostimulatory effects of oligonucleotides and improves therapeutic efficacy in chronic lymphocytic leukemia. … **2013**.
(122) Wilken, J. A.; Webster, K. T.; Maihle, N. J. Trastuzumab Sensitizes Ovarian Cancer Cells to EGFR-targeted Therapeutics. *J Ovarian Res* **2010**, *3*, 7.
(123) Koganti, S.; Jagani, H. V.; Palanimuthu, V. R.; Mathew, J. A.; Rao, M. C.; Rao, J. V. In vitro and in vivo evaluation of the efficacy of nanoformulation of siRNA as an adjuvant to improve the anticancer potential of cisplatin. *Experimental and Molecular Pathology* **2013**, *94*, 137–147.
(124) Liu, J.-L.; Wang, Y.; Jiang, J.; Kong, R.; Yang, Y.-M.; Ji, H.-F.; Shi, Y.-Z. Inhibition of survivin expression and mechanisms of reversing drug-resistance of human lung adenocarcinoma cells by siRNA. *Chin. Med. J.* **2010**, *123*, 2901–2907.
(125) Lundy, B. B.; Convertine, A.; Miteva, M.; Stayton, P. S. Neutral Polymeric Micelles for RNA Delivery. *Bioconjug Chem* **2013**, *24*, 398–407.
(126) Hylarides, M. D.; Mallett, R. W.; Meyer, D. L. A robust method for the preparation and purification of antibody/streptavidin conjugates. *Bioconjug Chem* **2001**, *12*, 421–427.
(127) Pagel, J.; Hedin, N.; Subbiah, K.; Meyer, D. Comparison of anti-CD20 and anti-CD45 antibodies for conventional and pretargeted radioimmunotherapy of B-cell lymphomas. … **2003**.
(128) Sahlin, S.; Hed, J.; Runfquist, I. Differentiation between attached and ingested immune complexes by a fluorescence quenching cytofluorometric assay. *J Immunol Methods* **1983**.
(129) Lasham, A.; Herbert, M. A rapid and sensitive method to detect siRNA-mediated mRNA cleavage in vivo using 5′ RACE and a molecular beacon probe. *Nucleic acids* … **2010**.
(130) DeFazio-Eli, L.; Strommen, K.; Dao-Pick, T.; Parry, G.; Goodman, L.; Winslow, J. Quantitative assays for the measurement of HER1-HER2 heterodimerization and phosphorylation in cell lines and breast tumors: applications for diagnostics and targeted drug mechanism of action. *Breast Cancer Research* **2011**, *13*, R44.
(131) Inoue, S.; Ding, H.; Portilla-Arias, J.; Hu, J.; Konda, B.; Fujita, M.; Espinoza, A.; Suhane, S.; Riley, M.; Gates, M.; Patil, R.; Penichet, M. L.; Ljubimov, A. V.; Black, K. L.; Holler, E.; Ljubimova, J. Y. Polymalic Acid-Based Nanobiopolymer Provides Efficient Systemic Breast Cancer Treatment by Inhibiting both HER2/neu Receptor Synthesis and Activity. *Cancer Res.* **2011**, *71*, 1454–1464.
(132) Rubenfeld, G. D.; Herridge, M. S. Epidemiology and Outcomes of Acute Lung Injury. *Chest* **2007**, *131*, 554–562.
(133) Tsushima, K.; King, L. S.; Aggarwal, N. R.; De Gorordo, A.; D'Alessio, F. R.; Kubo, K. Acute Lung Injury Review. *Intern. Med.* **2009**, *48*, 621–630.
(134) Hoshino, T.; Okamoto, M.; Sakazaki, Y.; Kato, S.; Young, H. A.; Aizawa, H. Role of Proinflammatory Cytokines IL-18 and IL-1 in Bleomycin-Induced Lung Injury in Humans and Mice. *American Journal of Respiratory Cell and Molecular Biology* **2009**, *41*, 661–670.

(135) Martin, T.; Hagimoto, N. Cell Death and Acute Lung Injury. *Mechanisms of Sepsis-Induced …* **2007**.
(136) Perl, M.; Chung, C.-S.; Perl, U.; Thakkar, R.; Lomas-Neira, J.; Ayala, A. Therapeutic accessibility of caspase-mediated cell death as a key pathomechanism in indirect acute lung injury. *Critical Care Medicine* **2010**, *38*, 1179–1186.
(137) Kass, D.; Bridges, R. S.; Borczuk, A.; Greenberg, S. Methionine aminopeptidase-2 as a selective target of myofibroblasts in pulmonary fibrosis. *American Journal of Respiratory Cell and Molecular Biology* **2007**, *37*, 193–201.
(138) Hay, J.; Haslam, P.; Dewar, A.; Addis, B. Development of acute lung injury after the combination of intravenous bleomycin and exposure to hyperoxia in rats. *Thorax* **1987**.
(139) Yu, S. S.; Lau, C. M.; Barham, W. J.; Onishko, H. M.; Nelson, C. E.; Li, H.; Smith, C. A.; Yull, F. E.; Duvall, C. L.; Giorgio, T. D. Macrophage-Specific RNA Interference Targeting via "Click," Mannosylated Polymeric Micelles. *Mol Pharmaceut* **2013**, *10*, 975–987.
(140) Stacey, K.; Ross, I.; Hume, D. Electroporation and DNA-dependent cell death in murine macrophages. *Immunology and cell biology* **1993**.
(141) Rahman, M. A.; Amin, A. R. M. R.; Wang, X.; Zuckerman, J. E.; Choi, C. H. J.; Zhou, B.; Wang, D.; Nannapaneni, S.; Koenig, L.; Chen, Z.; Chen, Z. G.; Yen, Y.; Davis, M. E.; Shin, D. M. Systemic delivery of siRNA nanoparticles targeting RRM2 suppresses head and neck tumor growth. *Journal of Controlled Release* **2012**, *159*, 384–392.
(142) Alabi, C.; Vegas, A.; Anderson, D. Attacking the genome: emerging siRNA nanocarriers from concept to clinic. *Current Opinion in Pharmacology* **2012**, *12*, 427–433.
(143) Kulkarni, R. P.; Mishra, S.; Fraser, S. E.; Davis, M. E. Single cell kinetics of intracellular, nonviral, nucleic acid delivery vehicle acidification and trafficking. *Bioconjug Chem* **2005**, *16*, 986–994.
(144) Bartlett, D. W.; Su, H.; Hildebrandt, I. J.; Weber, W. A.; Davis, M. E. Impact of tumor-specific targeting on the biodistribution and efficacy of siRNA nanoparticles measured by multimodality in vivo imaging. *Proc Natl Acad Sci USA* **2007**, *104*, 15549–15554.
(145) Bartlett, D. W.; Davis, M. E. Impact of tumor-specific targeting and dosing schedule on tumor growth inhibition after intravenous administration of siRNA-containing nanoparticles. *Biotechnol. Bioeng.* **2008**, *99*, 975–985.
(146) Davis, M. E.; Zuckerman, J. E.; Choi, C. H. J.; Seligson, D.; Tolcher, A.; Alabi, C. A.; Yen, Y.; Heidel, J. D.; Ribas, A. Evidence of RNAi in humans from systemically administered siRNA via targeted nanoparticles. *Nature* **2010**, *464*, 1067–1070.
(147) Wooddell, C. I.; Rozema, D. B.; Hossbach, M.; John, M.; Hamilton, H. L.; Chu, Q.; Hegge, J. O.; Klein, J. J.; Wakefield, D. H.; Oropeza, C. E.; Deckert, J.; Roehl, I.; Jahn-Hofmann, K.; Hadwiger, P.; Vornlocher, H.-P.; McLachlan, A.; Lewis, D. L. Hepatocyte-targeted RNAi Therapeutics for the Treatment of Chronic Hepatitis B Virus Infection. *Mol. Ther.* **2013**, *21*, 973–985.
(148) Lin, X. J.; Chen, X. C.; Wang, L.; Wei, Y. Q.; Kan, B.; Wen, Y. J.; He, X.; Zhao, X. Dynamic progression of an intraperitoneal xenograft model of human ovarian cancer and its potential for preclinical trials. *J. Exp. Clin. Cancer Res.* **2007**, *26*, 467–474.
(149) Manganiello, M. J.; Cheng, C.; Convertine, A. J.; Bryers, J. D.; Stayton, P. S. Diblock copolymers with tunable pH transitions for gene delivery. *Biomaterials* **2012**, *33*,

2301–2309.
(150) Jeong, J. H.; Mok, H.; Oh, Y.-K.; Park, T. G. siRNA Conjugate Delivery Systems. *Bioconjug Chem* **2009**, *20*, 5–14.